Zeeman effect in simple molecules by beam maser spectroscopy

Ton Ellenbroek

ZEEMAN EFFECT IN SIMPLE MOLECULES BY BEAM MASER SPECTROSCOPY

PROMOTOR:

PROF. DR. A. DYMANUS

ZEEMAN EFFECT IN SIMPLE MOLECULES BY BEAM MASER SPECTROSCOPY

PROEFSCHRIFT

TER VERKRIJGING VAN DE GRAAD VAN DOCTOR
IN DE WISKUNDE EN NATUURWETENSCHAPPEN
AAN DE KATHOLIEKE UNIVERSITEIT TE NIJMEGEN,
OP GEZAG VAN DE RECTOR MAGNIFICUS
PROF. DR. A.J.H. VENDRIK
VOLGENS BESLUIT VAN HET COLLEGE VAN DECANEN
IN HET OPENBAAR TE VERDEDIGEN
OP DONDERDAG 6 OKTOBER 1977
DES NAMIDDAGS TE 2 UUR PRECIES

DOOR

ANTONIUS WILHELMUS ELLENBROEK

geboren te Apeldoorn

1977
Druk: Krips Repro Meppel

Allen die hebben bijgedragen aan de totstandkoming van dit proefschrift wil ik bedanken. In het bijzonder wil ik vermelden:

De leden van de afdeling Atoom- en Molecuulfysica met wie ik de afgelopen jaren zo prettig heb samengewerkt.

Dr. Jan Heuvel, die mij onder andere heeft ingewijd in de theoretische en experimentele aspecten van de beam maser spectroscopie.

Drs. Jacques Reijnders, met wie ik in de beginfase van het onderzoek veel heb samengewerkt.

De heer John Holtkamp voor het repareren van defecte electronische apparatuur en het mij wakker houden tijdens nachtelijke experimenten.

De heer Eugène van Leeuwen voor zijn hulp bij de opbouw van de machine en bij de reparatie van de supergeleidende magneet.

Prof. J. Reuss voor het kritisch lezen van het manuscript.

De dienstverlenende afdelingen wil ik graag bedanken in de personen van de heren H. Verschoor, P. Walraven en J. van Langen.

Mevr. Lies Remers voor het typen van het manuscript.

De afdelingen Illustratie en Fotografie voor het vervaardigen van de figuren.

De Offsetdrukkerij van de faculteit der wiskunde en natuurwetenschappen onder leiding van de heer J. Geertsen voor het verlenen van de faciliteiten ter realisering van de druk van dit proefschrift.

Aan mijn ouders
Aan Thea

C O N T E N T S

CHAPTER 5 RESULTS AND DISCUSSION

C H A P T E R 1

INTRODUCTION

1.1 HISTORICAL NOTE

The splitting of atomic spectral lines by a magnetic field was discovered by the Dutch physicist Pieter Zeeman in 1896 on the D-lines of sodium (Na). It was quite soon realized that this splitting is due to the interaction of the magnetic moment associated with the valence electron in Na with the applied magnetic field. The effect of splitting of spectral lines by a magnetic field is called after him "Zeeman effect".

The existence of a rotationally induced magnetic moment in molecules was recognized in the late twenties. It was believed that in $^1\Sigma$-molecules this moment is produced by the rotating nuclear charges in the molecule. Already in 1927 Condon (CON 27) calculated this magnetic moment. The first experimental observations by Frisch and Stern (FRI 33) indicated, however, that in addition to the nuclear magnetic moment there exists a non neglegible rotationally induced electronic magnetic moment in spite of the fact that the net electronic angular momentum is zero in $^1\Sigma$-molecules. In fact both moments are of the same order of magnitude and the observed magnetic moment is the result of the near cancellation of these moments as pointed out by Wick (WIC 33). A more general theory for the molecular magnetic moment was developed by Eshbach and Strandberg (ESH 52). The electronic contribution to the magnetic moment originates from the second order contribution of the electronic angular momentum.

A second order Zeeman effect is due to the induced

magnetic moment of a molecule. The applied magnetic field disturbs the molecular charge distribution and gives thereby raise to an induced magnetic moment, which in turn reacts with the applied field. The induced magnetic moment depends linearly on the applied field and can be described as a product of the field $\underline{H}$ and the magnetic susceptibility tensor $\underline{\underline{\chi}}$. Magnetic susceptibilities in gases were already measured at the end of the nineteenth and the beginning of the twentieth century in the so-called bulk experiments. These experiments yield values for the average magnetic susceptibility χ_{av}, a quantity that, generally cannot be measured in molecular transitions because of its independence of the rotational state of the molecule. The anisotropic part of the susceptibility, however, does depend upon the rotational quantum numbers and can be observed in rotational transitions. It is a small effect, about 100-1000 times smaller than the first order effect at fields of about 10 kG, and its observation requires a high field and/or a high resolution.

Another important Zeeman interaction is the interaction of the magnetic field with the magnetic moments of the nuclei. The magnetic moments, however, are shielded from the applied field by the electrons surrounding the nuclei. The shielding $\underline{\underline{\sigma}}$ is usually a very small tensorial effect. The determination of the shielding requires a high magnetic field, combined with a good experimental resolution. In rotational transitions mostly only the anisotropic shielding σ_{an} can be measured in electric dipole transitions, unless there is a strong hyperfine coupling in the molecule (see e.g. Sect.4.1.3), in which case both isotropic and anisotropic shielding can be observed.

The first microwave measurements on molecular Zeeman effect in rotational transitions were performed by Jen (JEN 48). These measurements yielded the magnetic moments for N_2O, NH_3 and OCS. In the following years measurements by microwave spectroscopy yielded magnetic moments of many molecules, but it lasted until 1967 before the first experimental observation of the molecular susceptibility anisotropy was reported by Hüttner et al on formaldehyde (HUT 67). The Zeeman effect for a large number of diamagnetic molecules has been measured by Flygare and his collaborators (for a representative reference see FLY 70). The essential component of their spectrometer is a long absorption cell mounted in a six foot long electromagnet, which can reach a field of 30 kG over the full length. The observations yield rather accurate values for the magnetic moments and, less accurate, values for the susceptibility anisotropies.

The same accuracy at a considerably lower field can also be achieved using molecular beam techniques, for example in a beam maser (VER 69) or in an electric beam resonance machine (LEE 71) at fields of only about 10 kG over a length of 10-20 cm.

The isotropic nuclear shielding has been observed in NMR experiments. The resolution in these experiments is very good (linewidth less than 10 Hz) even compared with the resolution in a beam machine (linewidth from 2-5 kHz), so that at relatively low field (10kG) shieldings can easily be observed to a good accuracy. The experiments, in general, give no information about the anisotropic shielding. In the past the only beam maser measurements have been performed on CF_2H_2 by Kukolich (KUK 72) using a Bitter magnet of the Nat. Magnet. Lab. of M.I.T. at 98 kG. A rather accurate value for the anisotropic fluorine nuclear shielding was obtained.

The primary goal of the present investigation was to obtain detailed information on the weak Zeeman interactions, especially those involving the susceptibility and the nuclear shielding. Although for many molecules the susceptibilities were measured, the values were rather inaccurate to deduce from it the molecular quadrupole moment $\underline{\underline{\Theta}}$. This moment plays an important role in intermolecular interaction in gases and liquids. Moreover it is a property that can be obtained by theorists in ab-inition calculations. As will be shown in Sect. 5.1 the molecular quadrupole moment can be obtained from the molecular susceptibility and the magnetic moment. The nuclear shielding is the sum of a dia- and a paramagnetic term. The paramagnetic term can be calculated from the spin-rotation constant, which can be measured in zero magnetic field. The diamagnetic shielding depends strongly upon the electronic charge distribution in the vicinity of the nucleus. This constant can also be obtained in ab-initio calculations. It is a well-known fact that the molecular properties such as the quadrupole moment and the nuclear diamagnetic susceptibility are much more sensitive to the electronic wavefunction calculated by ab-initio methods than the total energy. Hence these quantities are a much better test upon the reliability of the calculated electronic wavefunctions.

Our experiments were mainly focussed on two important classes of molecules, the symmetric tops of the form XY_3, and the internal rotors. For the latter category no Zeeman measurements were performed until now, although at the moment these molecules are of great interest for theoretists. The reason why the Zeeman effect of these molecules has not been examined is probably due to the complexity of their spectra in absorption

measurements thereby making their interpretation almost impossible.

It has been pointed out that the observation of the weak Zeeman interactions require a high field and/or a high resolution. The latter condition is statisfied in a beam maser. An outline of this spectrometer is given in Sect. 1.2, more details in Chap. 2. To reach the desired magnetic field we had two magnets at our disposal: a polar C-type magnet for the low field measurements (up to 8.7 kG) and an axial superconducting solenoid type magnet for the high fields (up to 70 kG).

1.2 The beam maser

The linewidth of the spectral lines is determined by the resolution of the spectrometer. The most important contribution to the linewidth is the collision and Doppler broadening. In a beam maser this broadening is completely removed by using a molecular beam. The molecular beam is formed in an effuser or nozzle source and is then passed through a region where a transition is induced.

The price one has to pay for the gain in resolution is a considerable loss in signal to noise (S/N) ratio. At a normal pumping speed the beam flux is about 10^{18} particles per second. A higher flux will cause scattering of the beam particles with the dispersed particles. In order to obtain a reasonable S/N-ratio in the spectrometer sketched above a flux of 10^{20} particles per second is required. The reason for this high flux is that, as in gas absorption measurements, the intensity of the microwave signal is determined by the difference in occupation of the levels involved in a transition. If n_1 be the

number of particles in the upper state and n_2 the number of particles in the lower state, then, in thermal equilibrium, the occupation difference is given by

$$n_2 - n_1 = \frac{h\nu}{kT} \; n_1 \qquad (1.1)$$

where h is Planck's constant, k is Boltzmann's constant, T the absolute temperature and ν the level separation in Hz. The power absorbed by the beam is approximately

$$P = (n_1 - n_2)\; h\nu \; P_{12}$$

where P_{12} is the transition probability between the two states. Substituting Eq (1.1) gives

$$P = \frac{h^2\nu^2}{kT} \; n_1 P_{12} \qquad (1.2)$$

For a spectrometer with a minimum detectable power of 10^{-13}W a total molecular flow of 10^{20} mol/s (DYM 76) is required, if the fractional occupation of level one and the beam divergence is taken into account for a temperature of 300°K.

Consequently a way has to be found to increase the relative population difference, or what comes to the same, to obtain a non-thermal population in the beam. The non-thermal population is achieved by passing the molecules through a region, where a strong field gradient perpendicular to the beam exists. In the case of polar molecules a gradient in an electric field is required. If r be the distance to the beam axis and E(r) the electric field at r, then the force acting upon the molecules is

$$F_r = - \frac{\partial W}{\partial E} \quad \frac{\partial E}{\partial r} \qquad (1.3)$$

where W(E) is the Stark energy of the molecule in the field E. In the simplest case the states involved in an electric dipole

transition repell each other. This means that for the upper level $\partial W/\partial E>0$ and for the lower level $\partial W/\partial E<0$. If $\partial E/\partial r>0$ then the molecules in the upper level experience a force towards the beam axis and consequently these molecules are focussed onto the cavity, and the molecules of the lower level are defocussed. If $\partial E/\partial r<0$ the situation is reversed. The different action of the force F upon upper and lower level is called state selection and the device that effects the state selection is called state selector. In Fig. 1.1 the action of the state selector is clearly demonstrated. In the ideal case when all molecules of the upper level are focussed and all molecules of the lower level are defocussed the gain in population difference is $kT/h\nu$ as is immediately seen from Eq (1.2). At room temperature this is about 300 for a frequency of 20 GHz.

The focussed molecules pass through a transition region, usually a microwave cavity. The molecules make a transition if the frequency in the cavity corresponds with the level separation of an allowed transition. In a properly designed spectrometer the linewidth is determined by the transit time of the molecules through the transition region and to some extent by the field distribution in the cavity. For a cavity resonating in the TM_{010} mode the linewidth $\Delta\nu$ for a monochromatic beam is given by

$$\Delta\nu = 0.9 \frac{v}{L} \qquad (1.4)$$

where v is the velocity of the molecule and L the length of the cavity. For a derivation of this formula see e.g. (RAM 56). For a cavity of 16 cm of length and a beam velocity of 600 m/s the linewidth in Eq (1.4) is about 50 times smaller than in gas absorption experiments at pressures of 10^{-3} Torr.

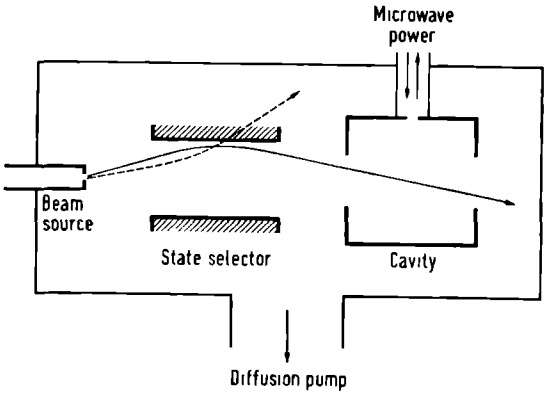

FIG.1.1 Schematic diagram of a beam maser spectrometer. The straight and the dashed curve represent the trajectory of a molecule in the upper and the lower state, respectively.

The apparatus described in this section is known as a molecular beam maser. In the original maser developed by Gordon et al (GOR 54) state selection was achieved by an electrostatic quadrupole. In the present experiment a hexapole is used, its cross section is depicted in Fig. 2.2. The electric field in a hexapole reaches a maximum between the rods, so $\partial E/\partial r>0$. Although until now little state selection is performed using selectors with $\partial E/\partial r<0$, we believe that these selectors are sometimes preferable in case of a poor Stark effect. A schematic diagram of a beam maser showing the principle components of the spectrometer as discussed in this section is given in Fig. 1.1. To observe the molecular Zeeman effect the cavity is placed in a magnetic field.

C H A P T E R 2

EXPERIMENT

2.1 INTRODUCTION

Both zero field and Zeeman measurements were performed in a beam-maser spectrometer. The present machine is a modification of the apparatus described by Verhoeven (VER 69). In this Chapter we discuss only the modifications dictated by the present experiment (Sect. 2.2).

The Zeeman measurements were performed in two different magnets. For the low field experiments a C-type electromagnet (Bruker Physik) was used. Details of this magnet are given by de Leeuw (LEE 71). Its maximum field is about 8.7 kG, the homogeneity is better than 10^{-4} over a length of 20 cm. The determination of weaker effects, such as the molecular susceptibility and the nuclear magnetic shielding, requires often a higher field. To perform these measurements a superconducting magnet was used. It is described in Sect. 2.3. The maximum allowed field is about 70 kG, the homogeneity is, however, only 10^{-3} over a length of 17 cm.

The experiments were usually carried out in two steps. In the first step measurements were performed at low magnetic fields, followed by the high field measurements in the second step. Although high field measurements give more information about the weaker effects, the larger magnetic effects can more accurately be determined in the conventional magnet because of its higher homogeneity. Another reason to perform low field measurements is, that without any knowledge of the Zeeman

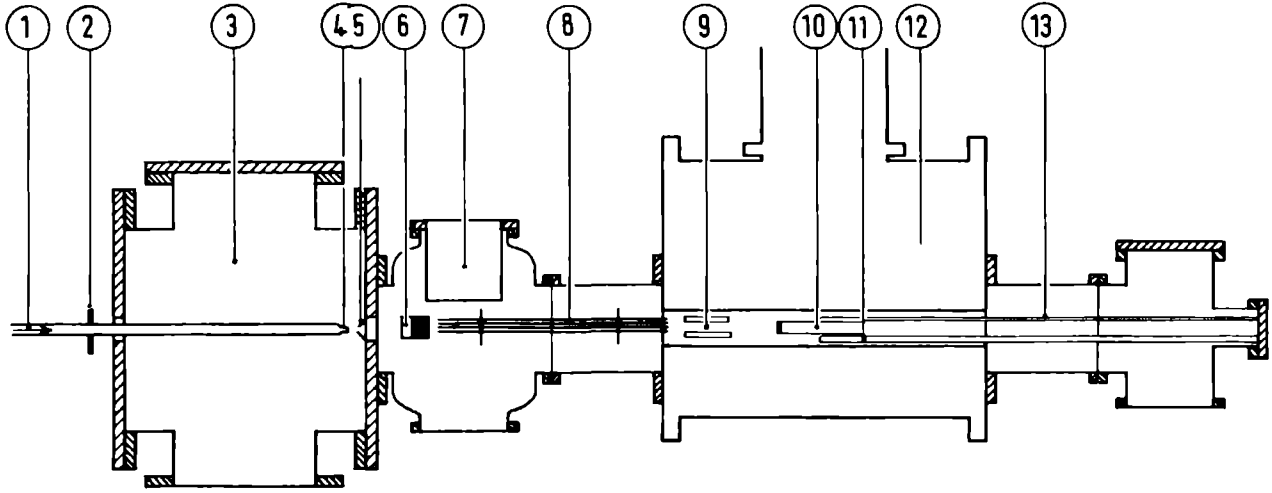

1 gas inlet pipe
2 supply lines for heating or cooling of the inlet pipe
3 source chamber
4 nozzle
5 skimmer
6 chopper
7 liquid nitrogen cooling trap
8 focuser
9 scrambler/crosser
10 cavity
11 probe holder
12 super conducting magnet
13 wave guide

FIG. 2.1 The beam maser Zeeman spectrometer for high field experiments.

spectrum a search for lines at high fields becomes time consuming (high field effects can be large) and consequently expensive, because of a considerable helium consumption.

2.2 THE BEAM-MASER ZEEMAN SPECTROMETER

A cross sectional view of the spectrometer used for high field experiments is shown in Fig. 2.1. The vacuum system is divided into two chambers. The first (nozzle) chamber, housing the nozzle and the skimmer is pumped by a 3000 l/s oil diffusion pump. The bore of the superconducting magnet forms an integral part of the second (main) chamber. This chamber contains the beam chopper, the state selector and the microwave cavity. It is pumped by two baffled 1000 l/s oil diffusion pumps. Additional pumping is achieved by a liquid nitrogen trap.

2.2.1 The source

In most experiments the beam source was a nozzle source. The nozzle itself was a hole in a thin (0.05 mm) brass or aluminium foil. Typical diameters of the hole were from 60 to 150 μm. The backing pressure of the nozzle ranged from about 200 Torr to 1 atm. For liquids this pressure was reached by heating the liquid container and the nozzle feed pipe, which was surrounded by a jacket. Heating was achieved by a water or oil bath thermostat, which could be stabilized in the temperature range from 20 - 200°C. The pressure in the source chamber was between 1 and 5 x 10^{-4} Torr. The molecular beam is formed by the skimmer (opening Ø 1mm) mounted on the flange separating the source and the main chamber. The nozzle-skimmer distance

could be varied from 0 to 20 mm.

The advantages of nozzle beams compared to effusive beams have been discussed by Reinartz (REI 76). An extension of this technique is the use of seeded beams. The principle of seeding is, that the sample gas is mixed with a gas with low number of internal degrees of freedom, usually a noble gas. Due to the few internal degrees of freedom of the foreign gas the rotational cooling in the expansion at the nozzle can be very large. If in the mixture an overdose (90% or more) of the foreign gas is used, the rotational temperature in the molecular beam will be determined by the foreign gas temperature. In our laboratory experiments with this technique were performed by ter Horst (HOR 76) on OCS-Ar mixtures. The observed rotational temperature due to the argon cooling was 4^{o} K. The advantage of low rotational temperatures is that the lower J-states become much better populated. The seeded beam method has been used in the present work for the $J_K = 2_1 \rightarrow 1_1$ transition in fluoroform. Using a mixture of 10% fluoroform and 90% argon an increase in (S/N)-ratio by a factor of three was obtained as compared to a pure fluoroform beam under the same conditions. More details about the seeded beam technique can be found in the reference cited.

For the measurements on hydrogen peroxide the gas feed had to be made out of glass, because metal surfaces act as a catalyzer for the reaction $H_2O_2 \rightarrow H_2O + O$. The pressure in the feed line of 2 Torr was equal to the vapour pressure of hydrogen peroxyde at room temperature. At such low pressures nozzling is not possible. The molecules entered the source chamber via a hole (Ø 1 mm) at the end of the feed line. The observed S/N-ratio appeared to be sufficient for our purposes. More details can be found in (ELL 75).

2.2.2 The state selector

As discussed in Sect. 1.2 state selection of the beam molecules is the basic condition for the operation of a beam-maser. In all experiments it was achieved by means of an electrostatic hexapole. Its cross section is depicted in Fig. 2.2. The distance between the rods is 4 mm., their length is 40 cm.

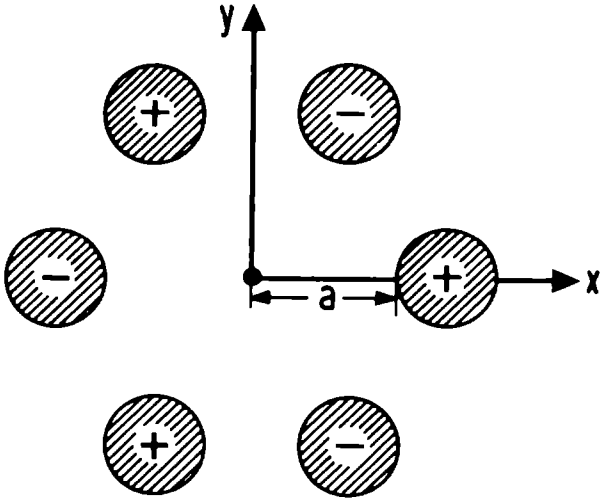

FIG. 2.2 Cross section of the state selector z-axis out of paper a = 4 mm.

The action of the state selector is described in Sect. 1.2 in the case of an "ideal" Stark effect. A good example is OH (MEU 76), where Λ-doublet states have a Stark effect making a complete state selection feasible. In many case, however, the Stark effect is not so favourable. In Fig. 2.3 the Stark effect is

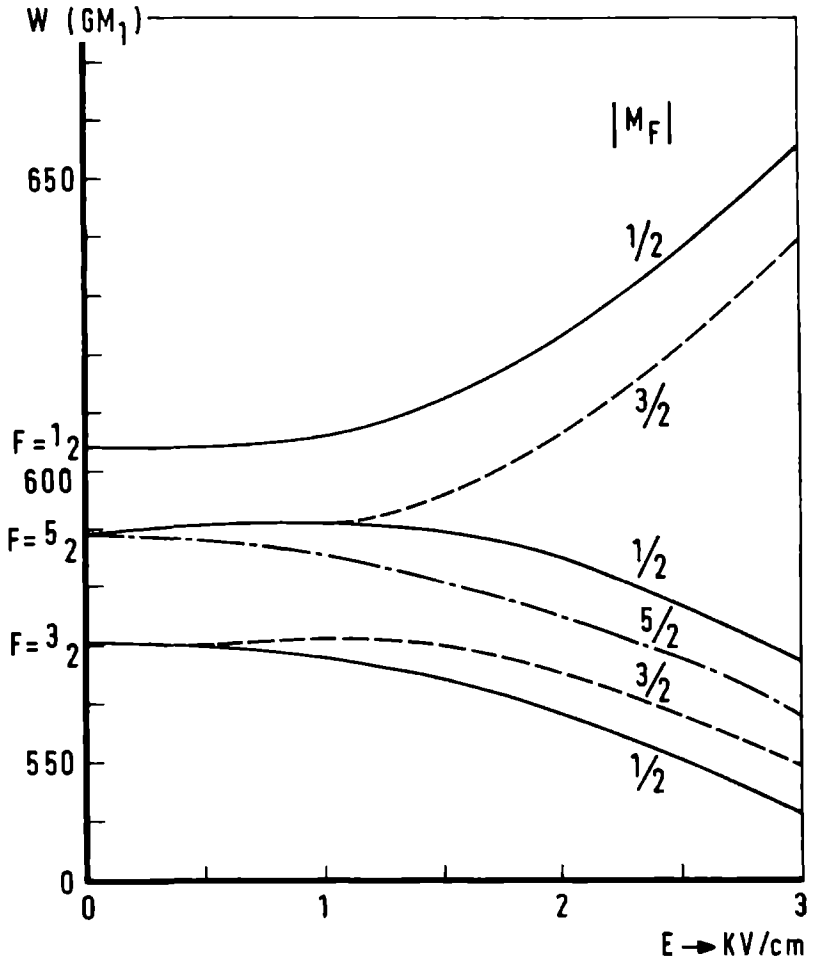

FIG. 2.3 Stark effect in CH_3Cl for the $J_K=1_o$ state. The energy is given in GHz relative to 26000 MHz.

shown of the (upper) $J_K=1_o$ rotational state of CH_3Cl. It is seen that the $(F,|M_F|) = (1/2,1/2)$ and $(5/2,3/2)$ hyperfine levels are focussed, because they have positive Stark effect. All other levels of the $J_K=1_o$ state are defocussed. A similar

behaviour shows the Stark effect of the $J_\tau = 4_{-4}$ level of SO_2, where the states with $M_J=0$ and ±1 are focussed, while all others M_J states are defocussed.

A poor Stark effect may cause irregularities in the population of the hyperfine sublevels of a focussed state. In a simple picture one might assume that the population of the hyperfine levels can easily be found by following the levels from their position in the state selector field adiabatically to zero field. However, it has already been pointed out by Majorana (MAJ 32) that in the rapidly decreasing field experienced by the molecules on leaving the selector transitions between the hyperfine levels can be induced. These transitions are called the Majorana transitions. Because the electric dipole moment of the molecule in the absence of magnetic fields is always directed along the electric field only $\Delta M_F=0$ transitions will occur.

A good example for the experimental evidence of Majorana transitions is the $J_K = 1_o \rightarrow 0_o$ transition in fluoroform. The Stark effect is, just as in the case of methyl chloride, such that certain hyperfine sublevels are depopulated by the action of the selector. Measurements by Reijnders et al (REY 74), however, show unambiguously that all sublevels are occupied, thereby clearly illustrating that Majorana transitions occurred. In the case of methyl chloride however, the depopulated levels were not observed, evidently no Majorana transitions happened. The reason is that in fluoroform the distance between the hyperfine levels is about 30 kHz, while in methyl chloride this distance is about 30 MHz, making Majorana transitions quite improbable. In CH_3Cl also the protons contribute to the hyperfine structure, but this effect is rather small. For the F=5/2

sublevel the splitting due to the total proton spin $\underline{I}_H$ is about 15 kHz. Yet within this sublevel no transitions from the focussed $M_F = \pm 3/2$ to the defocussed $M_F = \pm 5/2$ or $\pm 1/2$ can occur, since these transitions would violate the selection rule $\Delta M_F = 0$. So the $(F, M_F) = (5/2, \pm 3/2)$ levels must adiabatically pass in to the zero field hyperfine levels. It appears that in this way only two of the four possible hyperfine levels become occupied. This explains, why in Table 4.8 the other two levels are not occupied in spite of the small distance to occupied levels.

The maximum frequency the Majorana transitions can bridge, depends upon the rate at which the state selector field falls off when the molecules leave the selector. This field gradient depends upon the geometry of the apparatus. For a state selector in free space the decay is almost exponential. In our case the distance between the state selector and the cavity was very large (15 to 20 cm) compared to the radius of the selector (4 mm). When this distance approaches the selector radius, the decay of the electrostatic field is much sharper. In that case the fourier transform of the decreasing field contains higher frequencies. This is probably the reason why Kukolich (KUK 72a) did observe a maser signal from the F = 3/2 sublevel.

In SO_2 the "hyperfine" structure originates from the Zeeman effect. Only the highest M_J levels of the upper $J_\tau = 4_{-4}$ state are populated by adiabatic passage from the high field to the low field levels. Here again the other levels cannot be occupied by Majorana transitions because of selection rules. This is the reason, why in the experiment of Reijnders these lines were not observed in spite of the small distance between cavity and state selector (see REY 71).

2.2.3 The state "scrambler" and state "crosser"

The determination of all the coupling constants that describe the hyperfine structure of a rotational transition makes it prerequisite that transitions are observed from all the hyperfine sublevels allowed from the upper rotational state. In the previous section we saw that in certain molecules state selection depopulates some of these levels and so a way must be found to repopulate them.

Repopulation can be achieved by simply shortening the distance between the selector and the cavity as was pointed out in the previous section in the case of methyl chloride. This method however fails in several cases as discussed for SO_2. Another way is to induce transitions between the hyperfine levels. These transitions are usually in the RF region and only allowed in an external (static) electric field. Therefore a setup was made as shown in Fig. 2.4. It consists of two parallel conducting plates, the upper one of them is cut into two parts. The slit between the parts is in the direction of the molecular beam; the two parts are connected by a resistor R, and one of the parts is connected with the lower plate via a condensor C. Between the two plates exists a dc voltage, which gives an electric field between the plates perpendicular to the molecular beam. One of the parts of the upper plate is connected to an RF power supply. The field lines of the RF-electric field are rather complicated, they make various angles with the dc field, such that both $\Delta M=0$ and $\Delta M=\pm 1$ transitions can occur. The setup will be referred to as the scrambler. The scrambler was used in several cases and proved to work statisfactory if the RF frequency did not approach the intermediate frequency of

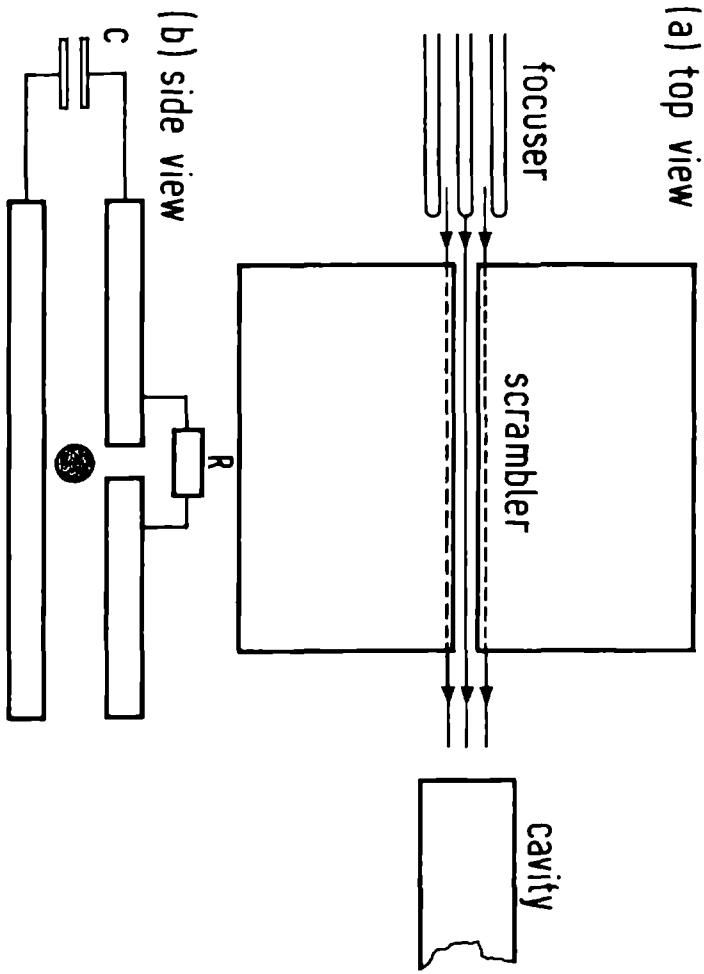

FIG. 2.4 Scheme of the state scrambler.

the superheterodyne detector, which was 30 MHz. A good example is the $J_K = 1_o \rightarrow 0_o$ transition in fluoroform in a magnetic field of 8kG. The upper part of the spectrum could be measured directly on the recorder, while the lower part required a repopulation by the scrambler (see Fig. 4.1).

In the case of SO_2 repopulation of the Zeeman levels was achieved by applying a dc electric field parallel to the applied magnetic field. By the state selection only the M_J = -4, -3 and -2 levels of the rotational $J_\tau = 4_{-4}$ state are populated as can be seen from adiabatic passage for this state in a similar way as shown in Fig. 2.3 for CH_3Cl. A repopulation of the depleted levels can be achieved by varying the electric field. This is due to the fact that in case that electric and magnetic field are parallel the projection of the angular momentum $\underline{J}$ on this axis is conserved. The 4_{-4}-state has linear Zeeman and quadratic Stark effect. In Fig. 2.5 the Stark effect of this state in a (constant) magnetic field of 4 kG is shown. It is seen from this figure that several crossings between the M_J-sublevels appear. In the selected beam only the three highest M_J-sublevels are occupied. By adjusting the electric field these levels can be made to cross a depleted level. In such a crossing both M_J levels are indistinguishable, so that if the time the molecule remains in this situation is sufficiently long, both M_J levels have the same probability. In our experiment the length over which the electric field exists was 8 cm and appeared to be long enough to observe the crossings indicated by a square in Fig. 2.5.

2.2.4 The cavity

In most experiments cylindrical TM_{010}-cavities were used.

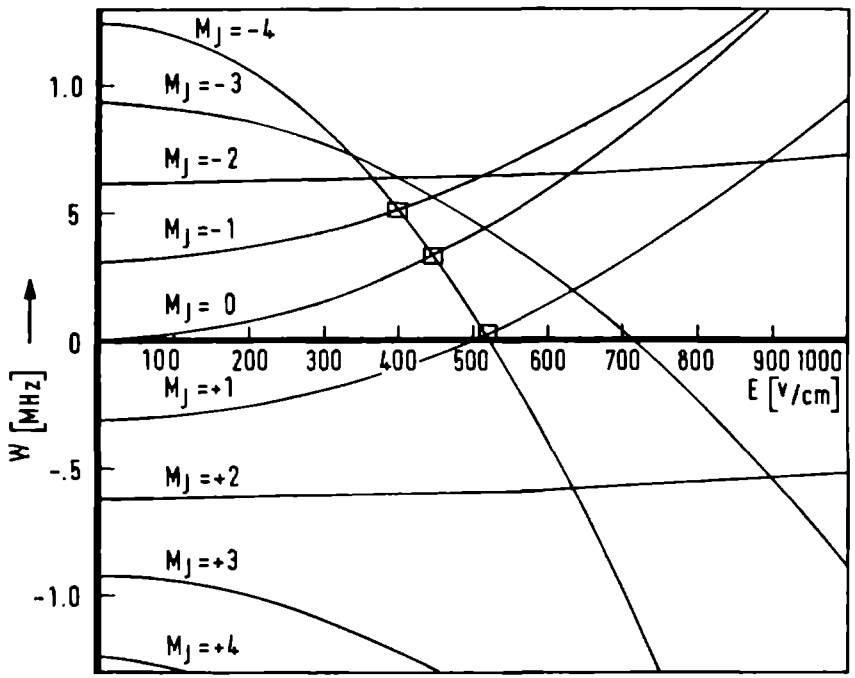

FIG. 2.5 Stark effect of the 4_{-4} level of SO_2 in a magnetic field of 4 kG. The electric field is parallel to the magnetic field.

The M_J= -4, -3 and -2 levels are populated by the State-selector;a square denotes an observed crossing in the state scrambler;all frequencies are in MHz relative to ν_o.

Tuning was achieved thermally by means of oil or water flowing through a jacket surrounding the cavity. Because of the limited space in the region of the magnetic field of the superconducting magnet (only 65 mm) coupling of the waveguide to the cavity could not be done in the usual way (BLU 68). The coupling arrangements are shown in Fig. 2.6. The waveguide is parallel to the cavity axis and its broad side is soldered onto the cavity. At the end the waveguide makes a so called "mitered" corner of 90^{o}.

This manner of coupling was statisfactory for frequencies between 10 and 30 GHz. In many cases this coupling was even stronger than the coupling in the old way (ELL 73). For high frequencies, for instance the $J_K = 2_1 \rightarrow 1_1$ transition in CF_3H at 41 GHz, an adjustable plunger had to be put into the waveguide to achieve optimum coupling*.

For TM-modes the electric field is parallel to the cavity axis and hence parallel to the field of the superconducting magnet. In this case only $\Delta M_F=0$ transitions can be observed. In some cases it is necessary to measure $\Delta M_F= \pm 1$ transitions as well. Then use must be made of TE-cavities, in which the electric field is perpendicular to the d.c. magnetic field. The cavity used for the $J_K= 2_{2+} \rightarrow 2_{2-}$ transition in NH_3 was a TE_{01} type cavity. Its construction is shown in Fig. 2.6.

2.3 THE SUPERCONDUCTING MAGNET

2.3.1 Technical properties

The superconducting magnet was constructed by the British

* In fact the waveguide ends in a T. The cavity is mounted in one arm of the T, while the adjustable plunger is in the other arm of the T.

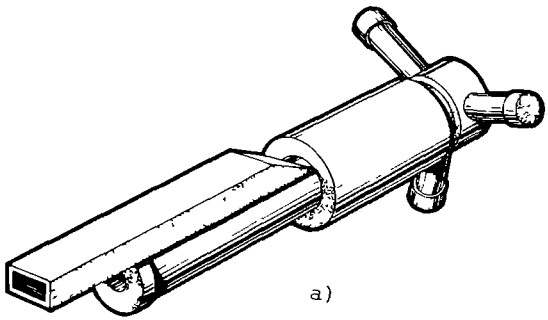

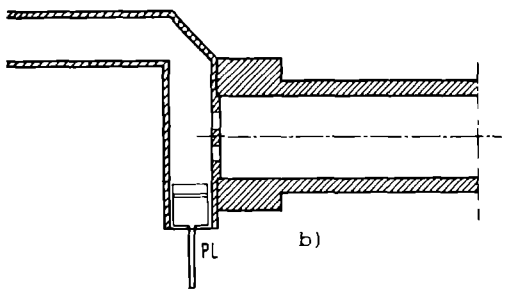

FIG. 2.6a) Coupling to TM cavity.

b) Coupling to TE cavity. PL is an adjustable plunger.

Oxygen Company. It is a niobium-titanium solenoid, which becomes superconducting at temperatures below $9^{o}K$. The superconducting wire consists of a copper matrix with more than 60 Nb-Ti filaments each less than 25 μm in diameter. A cross sectional view of the magnet is depicted in Fig. 2.7. The solenoid is mounted in a liquid helium cryostat, which can contain 25 l of liquid helium. The cryostat is placed in a vacuum chamber, which is at a pressure of 10^{-4} Torr. To minimize radiation losses, the cryostat is surrounded by copper shields cooled by liquid nitrogen. These shields are in turn surrounded by the so-called super insulation foil to reduce radiation losses to the room temperature wall.

The magnet can operate in the so-called persistent current mode. The switching circuit for this mode is depicted in Fig. 2.8. When the magnet is cooled down the whole system is superconducting. The magnet cannot be charged, because all current fed to the magnet will flow through the line A-B; the large self inductance of the coil (18 H) resists charging at any reasonable rate. When the heater is switched on, the temperature in the line AB becomes higher than $9^{o}K$ making AB resistive. Now the current will flow through the coil, because this has zero resistance. A part of the current, however, will still flow through AB, because a charge current I(t) will cause a voltage across the magnet equal to L.dI/dt, where L is the self inductance of the coil. This voltage should be kept low because of a possible damage of the AB resistive line. In practice dI/dt = 83 mA/s. When the desired current is reached, the heater is turned off and AB becomes superconducting again. If now the current through the leads is decreased the current through AB will increase because the coil itself resists against

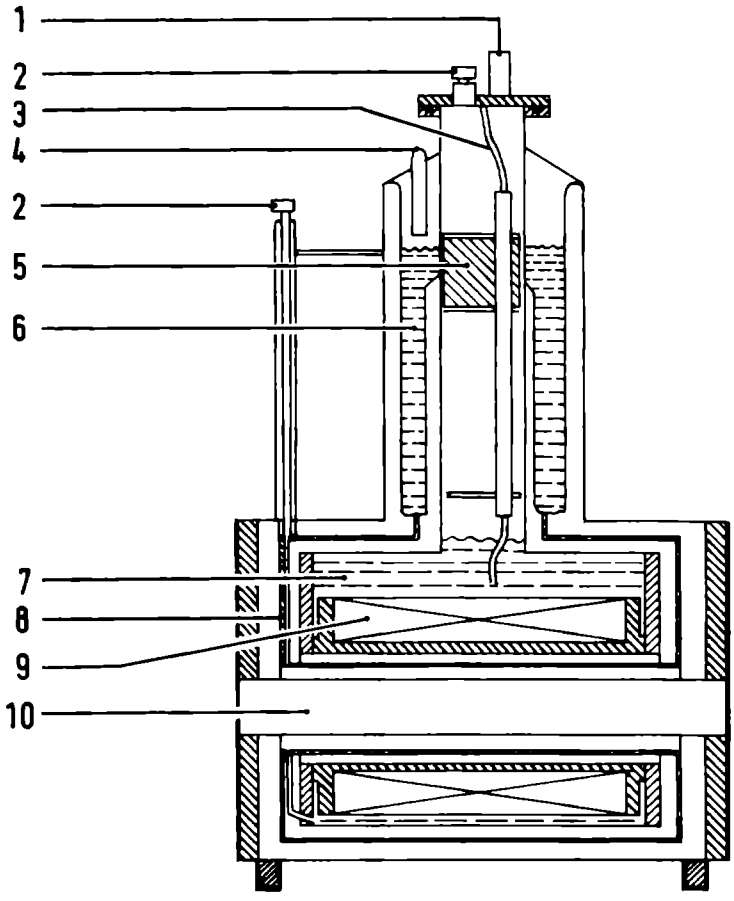

1	helium vent	7	liquid helium
2	syphon access	8	radiation shield
3	current lead	9	super conducting coil
4	nitrogen fill and vent	10	room temperature bore
5	plastic foam		
6	liquid nitrogen		

FIG. 2.7 Cross sectional view of the superconducting magnet.

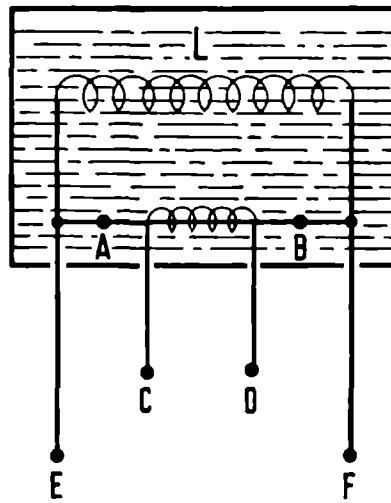

FIG. 2.8 Principle of the thermoswitch.

A-B switch

C-D heater

E-F magnet terminals

L inductance of magnet coil

a change in current. Finally the current through the leads reaches zero and the current through AB is equal to the current through the coil and the magnet is said to be in the persistent current mode. The line AB is called thermoswitch.

The maximum current in the coil is 100 A. The stored energy in the magnet is then 90 kJ. In case of a quench or a disconnection of the current leads while the magnet is charging or discharging, very large voltages will suddenly be developed destroying the superconducting switch. Moreover these voltages are very dangerous. To dissipate the freecoming energy and to decrease the voltages a thyristor controlled safety circuit constructed in our laboratory was mounted on the top of the

dewar. The electronic diagram is shown in Fig. 2.9. If the voltage between the magnet terminals increases above 10 V, the thyristors become conducting and all energy is dissipated in them. The thyristors used are the 71 RC 60 A thyristors which can stand a continuous current of 110 A at a voltage of 2 V. The peak current of the thyristors is 1000 A.

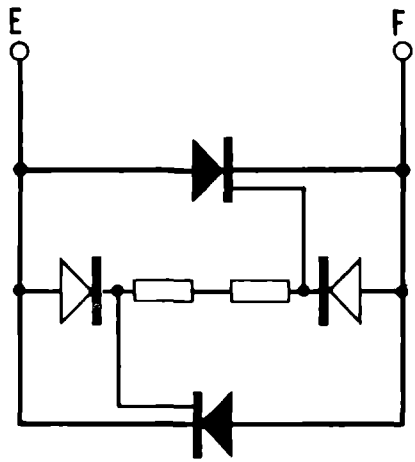

FIG. 2.9 Thyristor safety circuit; E and F are magnet terminals.

2.3.2 Measurement of the magnetic field

The maximum field on the axis of the superconducting magnet is 70 kG at a current of 102.2 A. The quench field is not known exactly because the magnet has not been tested for a quench. It is expected that the quench field is between 72 and 74 kG. The homogeneity of the field is better than 10^{-3} in the axial direction over a length of 17 cm. The radial homogeity is better than 10^{-4} over 6 mm radial distance. A plot of the

magnetic field at 70 kG along the axis of the magnet bore as measured by means of a Hall probe is shown in Fig. 2.10. This plot is measured by the manufacturers at the B.O.C. factory.

The cheapest and yet very accurate way to measure the field is by means of a flux meter. If a probe coil with n turns and an effective diameter ρ is placed in a variable magnetic field H(t), the voltage between the terminals is given by

$$v_i(t) = n\pi\rho^2 \frac{dH}{dt}\perp \qquad (2\text{-}1)$$

where $H_\perp$ is the component of $\underline{H}$ perpendicular to the cross sectional surface of the coil. Integrating this voltage with an RC-time integrator gives

$$V_o(t) = \int_0^t \frac{1}{RC} v_i(\tau)d\tau = \frac{n\pi\rho^2}{RC} (H(t)-H(0)) \qquad (2\text{-}2)$$

If we move the probe from a place where the magnetic field is zero and start the integrator when moving the probe to the center of the magnet, then the output voltage of the integrator is proportional to the magnetic field. However since the integrator integrates all voltages, special care must be taken with respect to thermo voltages, which are usually in the order of microvolts. The thermo voltages can be reduced by making the number of solderings and contact points as small as possible. The other possibility is to make v_i large with respect to these voltages by increasing ρ or n. The maximum value of ρ and n, however, depends upon the given geometry; in our case n = 500 and ρ = 8mm;therewith field measurements with an accuracy of 1 part in 10^4 at a measuring time of approximately three minutes could readily be performed. This accuracy is 10 times better than the homogeneity of the magnetic field. The probe was calibrated against an NMR probe at a field of 10 kG.

2.3.3 *The homogeneity*

The homogeneity of the magnetic field was measured by the manufacturer (B.O.C.) of the magnet using a Hall probe (Fig.2.10). However a more direct test is provided by measuring the line broadening of the Zeeman transitions due to the inhomogeneous field. Calculations on time dependent wavefunctions show, that the line broadening due to the magnetic field does not depend upon the position of the energy levels, but only upon the frequency shift of the Zeeman line with respect to the corresponding hyperfine line. For second order effect the relative

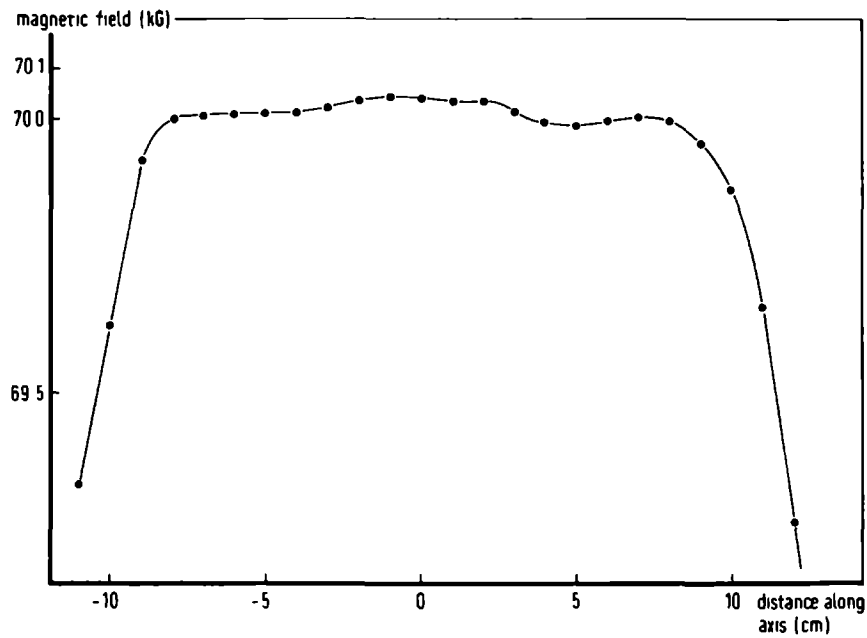

FIG. 2.10 The homogeneity of the magnetic field at 70 kG. The distance along the axis is measured with respect to the center of the magnet.

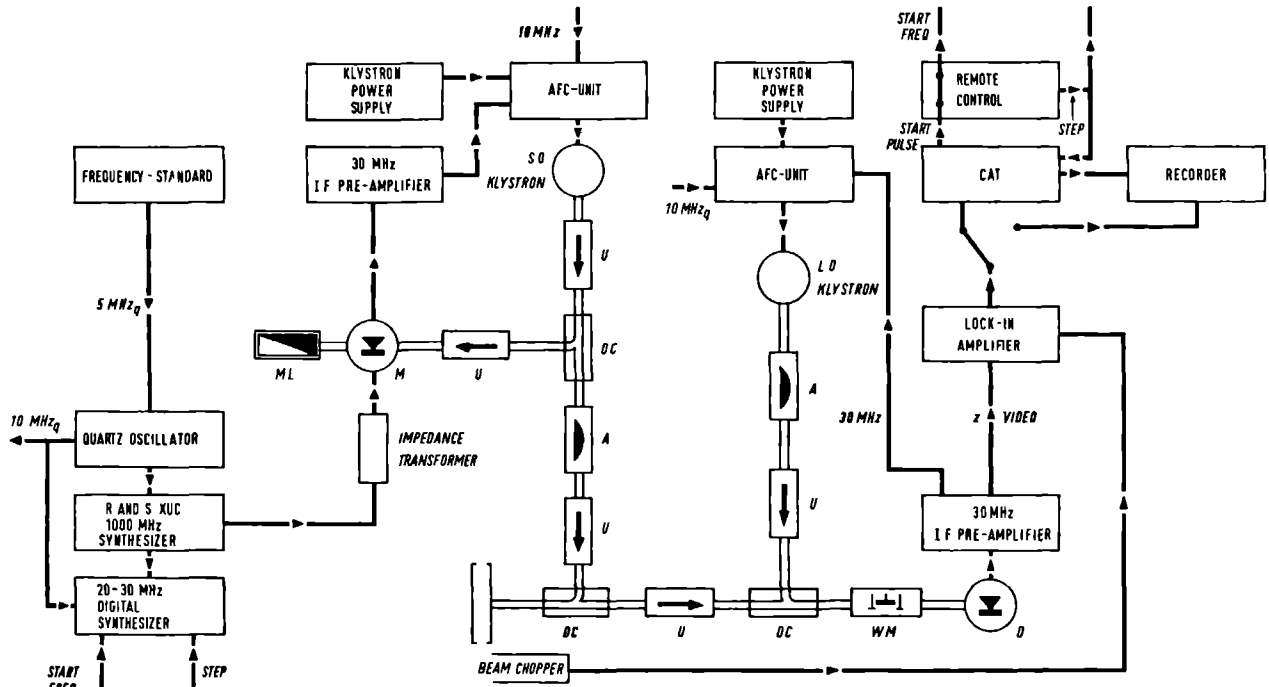

FIG. 2.11 The superheterodyne detection scheme.

effect of the inhomogeneity is twice as large as the relative effect for linear Zeeman terms. Most of the present experiments were done using TM_{010} cavities. In such cavities the stimulating electric field is parallel to the axis of the cavity. Also the dc magnetic field is parallel to this axis, such that only $\Delta M_F=0$ transitions can occur. In the case that the molecular g-factor of upper and lower level are comparable the Zeeman splittings are rather small. For the molecules studied in TM_{010} cavities the line shift due to the Zeeman effect was usually not more than about 200 kHz. So the increase in linewidth due to the inhomogeneity of the magnetic field is about 200 Hz for linear effects and 400 Hz for quadratic effects, provided the full shift is caused by these effects; these increase in linewidth is negligible compared to the experimental linewidth.

For the $2_{2+} \rightarrow 2_{2-}$ transition of ammonia a TE cavity was used to observe $\Delta M_F= \pm 1$ transitions. The splittings were in the order of 30 MHz so a considerable line broadening might be expected. The observed single lines of that spectrum were about 35 kHz wide as compared to a field free linewidth of 7-8 kHz.

2.4 THE SIGNAL DETECTOR

The signal emitted by the molecules making a microwave transition is in the order of 10^{-12}W. The stimulating power is in the order of 10^{-9}W. At these power levels a good signal to noise ratio can only be achieved by using superheterodyne detection. In all experiments a two klystron superheterodyne detection system was employed. The scheme is depicted in Fig. 2.11. The output power of a frequency stabilized signal oscillator (S.O.) is sent to the microwave cavity, where it produces

a stimulating field. The reflected power is transmitted to a crystal diode and mixed with the output of the local oscillator (L.O.), which is kept at a frequency 30 MHz higher than the S.O.-signal. The 30 MHz component at the mixer crystal is amplified, demodulated and applied to a lock-in amplifier. The output of the lock-in is fed to a recorder or a computer of average transients (C.A.T.). In some measurements only one klystron at the desired frequency was available. This klystron was then used as local oscillator. The signal power was emitted by the second or third harmonic of a klystron with lower frequency produced in a harmonic generator. The power in these harmonics (at 200mW fundamental power) was sufficient to saturate the transitions.

CHAPTER 3

THEORY

This chapter is divided in three sections. In the first section we apply the method developed by Anderson and Ramsey (AND 66) for the symmetrization of the hyperfine and Zeeman hamiltonian to symmetric rotors of the XY_3-type. The second section contains the discussion of the Zeeman effect of the asymmetric rotor. In the last section the Zeeman hamiltonian for an internal rotor is derived.

3.1 Symmetric top molecules

The advantage of symmetrization of the hyperfine hamiltonian has first been recognized by Anderson and Ramsey (AND 66) for tetrahedral molecules. This theory has been extended and generalized by Yi, Ozier and Anderson (YI 68) and by Ozier Crapo and Lee (OZI 68). The method however was only applied to spherical top molecules. In some special cases the theory was used for C_{3v} molecules (WOF 70).

In this section the method of symmetrization of the hyperfine and Zeeman hamiltonian is applied to general C_{3v} type molecules of the form XY_3 or XAY_3, where A denotes a nucleus with zero magnetic moment on the symmetry axis.

The geometry of the XAY_3-molecule is given in Fig. 3.1. The AX-axis is a threefold symmetry axis and each XAY plane is a plane of symmetry. We call the AX axis the c-axis and choose the b-axis perpendicular to the c-axis in one of the symmetry planes. The a-axis is chosen such that the abc-reference system

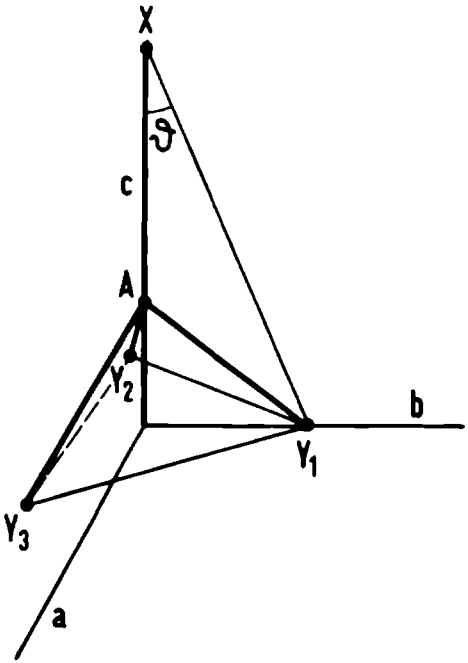

FIG. 3.1 The XAY_3 symmetric top molecule. For clarity the origin of the molecule fixed reference system is translated to the plane of the Y atoms.

is a right handed one. We call this system the molecule fixed reference system.

The invariance group of the molecule is now

$$C_{3v} = \{1, C_{3c}, C_{3c}^2, \sigma_a, \sigma_a C_{3c}, \sigma_a C_{3c}^2\} \tag{3.1}$$

where C_{3c} is an (active) rotation about the c-axis over $2\pi/3$, and σ_a a reflection in the bc-plane. It is easy to see that

the elements of the C_{3v} set constitute a group.

The symmetry operations of the C_{3v} group permute the identical Y-nuclei. There is a one to one correspondence between the permutations of the Y-nuclei and the symmetry operations. For the situation of Fig. 3.1 we have

$$\begin{aligned} C_{3c}&: Y_1 \rightarrow Y_3;\ Y_2 \rightarrow Y_1;\ Y_3 \rightarrow Y_2 \\ &\quad \text{in short } (132) \\ \sigma_a &: (23) \end{aligned} \tag{3.2}$$

The group of permutations of the three Y-nuclei is called the symmetric group of order three S_3. In total

$$S_3 = \{1,(132),(123),(23),(13),(12)\} \tag{3.3}$$

3.1.1 The wavefunction

The molecular wavefunction u is a function of the electronic and nuclear spatial and spin coordinates. In the Born-Oppenheimer approximation the function u can be written as

$$u = \Psi_{el}\,\Psi_{nucl}, \tag{3.4}$$

where Ψ_{el} and Ψ_{nucl} is the electronic and nuclear part of the total wavefunction respectively. We assume that the electronic function is known. The nuclear wavefunction can be written as

$$\Psi_{nucl} = \Psi_{vib}\,\Psi_{rot}\chi\ , \tag{3.5}$$

where Ψ_{rot} is the rotational, Ψ_{vib} the vibrational and χ is the nuclear spin wavefunction. This decoupling into a vibrational and rotational part of the nuclear function is only valid in the absence of vibration rotation coupling. Assuming that the molecule is in the vibrational ground state we only consider the function

$$\Psi = \Psi_{rot}\chi \tag{3.6}$$

(a) The rotational wavefunction

Symmetry shows that the moments of inertia for the XAY_3-molecule about the a and b-axes are equal. Consequently the rotational hamiltonian is

$$\mathcal{H}_{rot} = A\, J^2 + (C-A)\, J_c^2 \tag{3.7}$$

where $\underline{J}=\underline{N}+\underline{L}$ is the total angular momentum of the molecule, $\underline{N}$ is the nuclear and $\underline{L}$ the electronic contribution to it; A and C is the rotational constant about the a and c-axis respectively. We assume that the molecule is in the electronic ground state in which case $\langle\underline{L}\rangle = 0$ and hence (in zeroth order) $\langle\underline{N}\rangle = \langle\underline{J}\rangle$.

The hamiltonian of Eq.(3.7) is invariant under any rotation about the molecular symmetry axis and under a rotation over π about an axis perpendicular to the symmetry axis. The invariance group is the D_∞ - group. The solutions of the Schrödinger equation

$$\mathcal{H}_{rot}\,\Psi_{rot} = E_{rot}\Psi_{rot}$$

are the well known symmetric top eigenfunctions. If ψ,ϑ and φ are the Euler angles of the molecule, then we have in the convention of Edmonds (EDM 57)

$$\Psi_{rot}(\psi,\vartheta,\varphi) = \sqrt{\frac{(2J+1)}{8\pi^2}}\,\mathcal{D}^{(J)}_{MK}(\psi,\vartheta,\varphi) \tag{3.8a}$$

$$E_{rot} = AJ(J+1) + (C-A)K^2 \tag{3.8b}$$

$$J = 0,1,2,\ldots$$

$$K = \pm J, \pm(J-1), \ldots, 0 \tag{3.8c}$$

$$M = \pm J, \pm(J-1), \ldots, 0$$

In Eq.(3.8a) the $\mathcal{D}^{(J)}_{MK}$ are the matrix elements of the J-th irreducible representation of the threedimensional rotation group SO(3) on the basis of the spherical harmonic functions. For a given rotational energy E_{rot} we have 2(2J+1) rotational wavefunctions. The hamiltonian of Eq.(3.7) is not only invariant under the D_∞-group but also under inversion at the origen. The inversion operator $\mathcal{J}$, commutes with any rotation, and from the parity of the spherical harmonics follows

$$\mathcal{J}\mathcal{D}^{(J)}_{MK}(\psi\vartheta\varphi) = (-1)^J \mathcal{D}^{(J)}_{MK}(\psi\vartheta\varphi) \tag{3.9}$$

The factor $(-1)^J$ is the parity of the $\mathcal{D}^{(J)}_{MK}$ function.

(b) The spin function

Let $\underline{I}_K$ be the angular momentum associated with the K-th nucleus and

$$\begin{aligned} \underline{I}_{23} &= \underline{I}_2 + \underline{I}_3 \\ \underline{I}_T &= \underline{I}_{23} + \underline{I}_1 \end{aligned} \tag{3.10}$$

then the basisfunctions can be written as

$$\chi_{I_{23}}(I_T, M_T) \equiv |(I_2 I_3) I_{23} I_1 I_T M_T\rangle \tag{3.11}$$

i.e. eigenfunctions of the $I_1^2, I_2^2, I_3^2, I_{23}^2, I_T^2$ and I_{Tz} operators; $I_1=I_2=I_3=I_Y$ is the spin of the Y-nucleus.

For a given I_T and M_T there will in general be a number of possible basis functions depending on I_{23}. Let V be the space spanned by these functions. Under the permutations in Eq.(3.3) the vector $\underline{I}_T$ always transforms into itself. So I_T and M_T are conserved under S_3. The permutations therefore cause a one to one mapping of the space V onto itself. The so formed representation of S_3 is in general reducible. The characters of the

irreducible representations of S_3 are given in Table 3.1, and from the basis functions in Eq. (3.11) linear combinations can be formed, which transform under S_3 as one of the irreducible representations. The new basis functions are defined as

$$\chi_j^{\Gamma\xi}(I_T,M_T) = \sum_{I_{23}} c_{j,I_{23}}^{\Gamma\xi} \chi_{I_{23}}(I_T,M_T) \qquad (j=1, \ldots, n_{\Gamma\xi}) \quad (3.12)$$

Where Γ can be A_1,A_2 or E; ξ is one for the A_1 and A_2 representations and can take the values 1 and 2 for the E-type representation; $n_{\Gamma\xi}$ can be zero.

S_3	1	(123)	(23)
A_1	1	1	1
A_2	1	1	-1
E	2	-1	0

Table 3.1 Character table of S_3.

We note that the coefficients $c_{j,I_{23}}^{\Gamma\xi}$ do not depend upon M_T as can be seen by applying the $I_{T\pm}$ operators. The matrix of the $c_{j,I_{23}}^{\Gamma\xi}$ is unitary.

From Table 3-1 we see that for all $\rho \epsilon S_3$

$$\rho\chi_j^{A_1} = \chi_j^{A_1} \qquad (3.13a)$$

$$\rho\chi_j^{A_2} = (-1)^P \chi_j^{A_2} \qquad (3.13b)$$

where P is zero or one depending on whether ρ is even or odd respectively. On the two dimensional $\{\chi_j^{E,1}, \chi_j^{E,2}\}$

$$(132) \rightarrow \begin{pmatrix} e^{2\pi i/3} & 0 \\ 0 & e^{-2\pi i/3} \end{pmatrix} \qquad (23) \rightarrow \begin{pmatrix} 0 & 1 \\ 1 & 0 \end{pmatrix} \qquad (3.13c)$$

The representation of the other permutations on this basis can be found by expressing them as a product of these two basic operations. The coefficients $c^{\Gamma\xi}_{j,I_{23}}$ are discussed in Appendix I.

(c) The total wavefunction

The total wavefunction must obey the Pauli exclusion principle under an interchange of two identical Y-nuclei. Consider a $(J,\pm K)$ rotational level. First assume $K \neq 0$. Without loss of generality we may take $K > 0$.

The spin function can belong to A_1, A_2 or E symmetry. We shall treat these cases here separately.

I. Spin function of A_1 symmetry

For a given I_T and M_T we have the basis functions

$$\{|JKM\chi_j^{A_1}>,\ |J-KM\chi_j^{A_1}>\} \tag{3.14}$$

where $M = -J, \ldots, J$ and $j=1, \ldots, n_{A_1}$.

The two independent symmetry operations of the C_{3v}-group are C_{3c} and σ_a. Expressed in the Euler angles ψ,ϑ and φ we have

$$C_{3c}: \psi \to \psi, \vartheta \to \vartheta, \varphi \to \varphi + 2\pi/3$$

However σ_a is not a rotation, but a reflection. We have $\sigma_a = \mathcal{J} C_{2a}$ and

$$C_{2a}: \psi \to \psi + \pi, \vartheta \to \pi - \vartheta, \varphi \to 2\pi - \varphi$$

Because of the properties of the $\mathfrak{D}^{(J)}_{MK}(\psi\vartheta\varphi)$ we have

$$C_{3c}\mathfrak{D}^{(J)}_{MK}(\psi\vartheta\varphi) = e^{2\pi iK/3}\mathfrak{D}^{(J)}_{MK}(\psi\vartheta\varphi) \tag{3.15a}$$

$$C_{2a}\mathfrak{D}^{(J)}_{MK}(\psi\vartheta\varphi) = (-1)^J\mathfrak{D}^{(J)}_{M-K}(\psi\vartheta\varphi) \tag{3.15b}$$

So on the basis of (3-14) we get

$$C_{3c} = (132)\begin{pmatrix} e^{2\pi iK/3} & 0 \\ 0 & e^{-2\pi iK/3} \end{pmatrix} \tag{3.16a}$$

$$\sigma_a = \mathfrak{I}C_{2a} = (23):\begin{pmatrix} 0 & 1 \\ 1 & 0 \end{pmatrix} \tag{3.16b}$$

The first operation represents an even permutation of the Y-nuclei. The Pauli principle states that for both bosons and fermions the wavefunction should be invariant. This can only be statisfied if K = 3n, where n is an integer.

The second operation is an odd permutation of the Y-nuclei. The appropriate wavefunction obeying the Pauli principle should be symmetric (antisymmetric) under this operation if the Y-nuclei are bosons (fermions). Consequently the following linear combinations must be taken

$$|\Psi_j^{A_1}\rangle \equiv \frac{1}{\sqrt{2}}\{|JKM\rangle + (-1)^{J+\gamma}\,|J-KM\rangle\}\chi_j^{A_1}(I_T,M_T) \tag{3.17}$$

where γ can take the values zero or one. The factor $(-1)^J$ is introduced for calculation purposes only. Operating with σ_a on this wavefunction yields

$$\sigma_a|\Psi_j^{A_1}\rangle = (-1)^{J+\gamma}|\Psi_j^{A_1}\rangle \tag{3.18}$$

So for bosons $\gamma \equiv J(\text{mod}.2)$ and for fermions $\gamma \equiv J+1 \ (\text{mod}.2)$

II. Spin function of A_2-symmetry

The procedure of deriving the total wavefunction for this case is the same as above. The matrix for C_{3c} is identical with the one of Eq(3.16a) while the matrix of σ_a is the negative of the matrix in Eq(3.17b). Again K must be a multiple of three, and the wavefunctions become

$$|\Psi_j^{A_2}> = \frac{1}{\sqrt{2}} \{|JKM> + (-1)^{J+\gamma}|J-KM>\}\chi_j^{A_2} \tag{3.19}$$

where again γ can be zero or one. Furthermore

$$\sigma_a|\Psi_j^{A_2}> = (-1)^{J+\gamma+1}|\Psi^{A_2}_j> \tag{3.20}$$

So for bosons $\gamma \equiv J+1(\text{mod}.2)$, and for fermions $\gamma \equiv J(\text{mod}.2)$

III. Spin function of E-symmetry

In this case the basisfunctions for a given I_T, M_T and M are

$$\{|\ JKM\chi_j^{E,1}>,\ |JKM\chi_j^{E,2}>\ ,|\ J-KM\chi_j^{E,1}>\ ,\ |J-KM\chi_j^{E,2}>\} \tag{3.21}$$

where $j=1, \ldots, n_E$. On this basis we obtain for the two independent C_{3v}-operators using Eqs(3.16) and (3.13c)

$$C_{3c} \rightarrow \begin{pmatrix} e^{2\pi i(K+1)/3} & 0 & 0 & 0 \\ 0 & e^{2\pi i(K-1)/3} & 0 & 0 \\ 0 & 0 & e^{2\pi i(-K+1)/3} & 0 \\ 0 & 0 & 0 & e^{2\pi i(-K-1)/3} \end{pmatrix} \tag{3.22a}$$

$$\sigma_a \rightarrow \begin{pmatrix} 0 & 0 & 0 & 1 \\ 0 & 0 & 1 & 0 \\ 0 & 1 & 0 & 0 \\ 1 & 0 & 0 & 0 \end{pmatrix} \qquad (3.22b)$$

As for the spin functions of A-symmetry the first operator should leave the wavefunctions invariant, which leads to $K \pm 1 = 3n$, or $K = 3n \pm 1$, where n is an integer. Then the appropriate linear combinations are

$$|\Psi_j^{E,1}\rangle = \frac{1}{\sqrt{2}} \{ |JKM\chi_j^{E,1}\rangle + (-1)^{J+\gamma} |J-KM\chi_j^{E,2}\rangle \} \quad K=3n-1 \qquad (3.23a)$$

$$|\Psi_j^{E,2}\rangle = \frac{1}{\sqrt{2}} \{ |JKM\chi_j^{E,2}\rangle + (-1)^{J+\gamma} |J-KM\chi_j^{E,1}\rangle \} \quad K=3n+1 \qquad (3.23b)$$

Again γ can take the values zero or one. For both functions

$$\sigma_a |\Psi_j^{E,\xi}\rangle = (-1)^{J+\gamma} |\Psi_j^{E,\xi}\rangle \qquad (3.24)$$

So $\gamma \equiv J \pmod 2$ for bosons and $\gamma \equiv J+1 \pmod 2$ for fermions.

So far we assumed the case $K>0$. In case $K=0$ the wavefunctions are simpler because there is no K-degeneracy for the rotational level.

For a spin function of A_1-symmetry the basis functions are the $|JOM\ \chi_j^{A_1}\rangle$,

where M and j can take the same values as the corresponding symbols in Eq(3-14). On this basis both C_{3c} and σ_a are the unit matrix, hence the appropriate function for K=0 is

$$|\Psi_j^{A_1}\rangle = (-1)^{J+\gamma} |JOM\chi_j^{A_1}\rangle$$

where $\gamma \equiv J \pmod 2$ for bosons and $\gamma \equiv J+1 \pmod 2$ for fermions.

Analogously for A_2-type spin functions we get for K=0.

$$|\Psi_j^{A_2}> = (-1)^{J+\gamma}|JOM\chi_j^{A_2}>$$

with now $\gamma \equiv J+1 \pmod 2$ for bosons, and $\gamma \equiv J \pmod 2$ for fermions.

For E-type spin functions it is clear from Eq(3.22a) that for K=0 C_{3c} does not have the eigenvalue one, and hence no valid wavefunction can be constructed.

The results for the total wavefunction, excluding the spin of the X-nucleus, are summarized in Table 3.2.

K	symm. spin f.	Total wavefunction
0	A_1	$(-1)^{J+\gamma}\|JOM\chi_J^{A_1}(I_TM_T)>$
	A_2	$(-1)^{J+\gamma}\|JOM\chi_J^{A_2}(I_TM_T)>$
3n	A_1	$\sqrt{\frac{1}{2}}\{\|JKM> + (-1)^{J+\gamma}\|J-KM>\}\|\chi_J^{A_1}(I_TM_T)>$
	A_2	$\sqrt{\frac{1}{2}}\{\|JKM> + (-1)^{J+\gamma}\|J-KM>\}\|\chi_J^{A_2}(I_TM_T)>$
3n-1	E	$\sqrt{\frac{1}{2}}\{\|JKM\chi_J^{E,1}(I_TM_T)> + (-1)^{J+\gamma}\|J-KM\chi_j^{E,2}(I_TM_T)>\}$
3n+1	E	$\sqrt{\frac{1}{2}}\{\|JKM\chi_J^{E,2}(I_TM_T)> + (-1)^{J+\gamma}\|J-KM\chi_J^{E,1}(I_TM_T)>\}$

Table 3.2. The total wavefunction in a XY_3-molecule excluding the nuclear spin of the X-nucleus.

The complete wavefunction can be found by multiplying the appropriate function of Table 3.2 with the spin function of the X-nuclear spin $|I_X M_X>$. This function is of A_1-symmetry under the C_{3v}-operators and does not affect the symmetry of the product function. If $\Psi^{\Gamma\xi}$ is one of the functions of Table 3.2 then the complete wavefunction is

$$|\Psi> = |\Psi^{\Gamma\xi}> \; |I_X M_X> \tag{3.25}$$

3.1.2 The hamiltonian

The general hyperfine and Zeeman hamiltonian $\mathcal{H}_{hyp}$ is discussed by many authors (ESH 52, GOR 55, FLY 64, FLY 70). An expression applicable, in principle to any $^1\Sigma$-molecule in the absence of external electric fields can be found e.g. in (VER 69). For the symmetric top molecule XY_3 in the ground electronic and vibrational state the hamiltonian including all relevant contributions can be written as

$$\begin{aligned}
\mathcal{H}_{hyp} = {} & \underline{\underline{V}}^X \cdot \underline{\underline{Q}}^X + \sum_{K=1}^{3} \underline{\underline{V}}^K \cdot \underline{\underline{Q}}^K + \underline{I}_X \cdot \underline{\underline{M}}^X \cdot \underline{J} + \sum_{K=1}^{3} \underline{I}_K \cdot \underline{\underline{M}}^K \cdot \underline{J} + \\
& + \sum_{K=1}^{3} \underline{I} \cdot \underline{\underline{D}}_{XK} \cdot \underline{I}_K + \sum_{K<L} \underline{I}_K \cdot \underline{\underline{D}}_{KL} \cdot \underline{I}_L + \\
& - \mu_N \, \underline{H} \cdot \underline{\underline{G}} \cdot \underline{J} - \tfrac{1}{2} \, \underline{H} \cdot \underline{\underline{\chi}} \cdot \underline{H} - g_X \mu_N (1 - \sigma^X_{av}) \, \underline{I}_X \cdot \underline{H} \\
& - g_Y \mu_N \sum_{K=1}^{3} (1 - \sigma^K_{av}) \, \underline{I}_K \cdot \underline{H} \\
& + g_X \mu_N \, \underline{I}_X \cdot (\underline{\underline{\sigma}}^X - 1 \, \sigma^X_{av}) \cdot \underline{H} + g_Y \mu_N \sum_{K=1}^{3} \underline{I}_K \cdot (\underline{\underline{\sigma}}^K - 1 \, \sigma^K_{av}) \cdot \underline{H}
\end{aligned} \tag{3.26}$$

In this expression $\underline{H}$ is the magnetic field, X stands for the X-nucleus and K=1,2 and 3 for the respective Y-nuclei. All tensors in the hamiltonian (indicated by $\underline{\underline{\ }}$) are second rank Cartesian tensors. $\underline{\underline{V}}^K$ is the gradient tensor of the electric field at the K-th nucleus, while $\underline{\underline{Q}}^K$ is the quadrupole tensor of this nucleus, $\underline{\underline{M}}^K$ is the spin-rotation tensor $\underline{\underline{D}}_{KL}$ the spin-spin interaction tensor, $\underline{\underline{G}}$ is the molecular magnetic moment tensor, $\underline{\underline{\chi}}$ is the molecular magnetic susceptibility tensor, g_K is the "g"-factor of the K-th nucleus, μ_N is the nuclear magneton, and $\underline{\underline{\sigma}}^K$ is the nuclear shielding tensor:

$$\sigma^K_{av} \equiv (\sigma^K_{aa}+\sigma^K_{bb}+\sigma^K_{cc})/3.$$

All tensors appearing in $\mathcal{H}_{hyp}$ depend upon the electronic and nuclear positions and momenta in the molecule. Expressions for the cartesian components of these tensors are given in Table 5.1.

The symmetry of the molecule has implications upon the tensors appearing in $\mathcal{H}_{hyp}$. The symmetry operations only affect the Y-nuclei. So all tensors in the hamiltonian that do not belong to these nuclei must be invariant under the C_{3v} operations. Let $\underline{\underline{T}}$ be a general tensor not belonging *) to one of the Y-nuclei. Then in the molecular frame of reference shown in Fig. 3.1 $\underline{\underline{T}}$ has the form

$$\underline{\underline{T}} = \begin{pmatrix} T_{aa} & 0 & 0 \\ 0 & T_{aa} & 0 \\ 0 & 0 & T_{cc} \end{pmatrix} \qquad (3.27)$$

*) not belonging means that $\underline{T}$ does not interact with the nuclear magnetic or quadrupole moment of the Y-nuclei, (e.g. $\underline{\underline{V}}^X$, $\underline{\underline{M}}^X$, $\underline{\underline{G}}$, $\underline{\underline{\chi}}$, and $\underline{\underline{\sigma}}^X$ respectively).

In the following $T_{\perp} = T_{aa}$ and $T_{\parallel} = T_{cc}$ ($\perp$ and $\parallel$ mean perpendicular and parallel to the symmetry axis respectively).

The tensors which interact with the Y-nuclei are related to each other. If $\underline{\underline{T}}^K$ is a tensor interacting with the K-th Y-nucleus then in the frame of Fig. 3.1

$$\underline{\underline{T}}^2 = R(\tfrac{2\pi}{3})\ \underline{\underline{T}}^1\ R(-\tfrac{2\pi}{3})$$
$$\underline{\underline{T}}^3 = R(-\tfrac{2\pi}{3})\ \underline{\underline{T}}^1\ R(\tfrac{2\pi}{3}) \qquad (3.28)$$

where $R(\alpha)$ is a rotation over α about the molecular symmetry axis. The tensor $\underline{\underline{T}}^1$ must be invariant under a reflection in the bc plane. Thus in the molecular reference system

$$\underline{\underline{T}}^1 = \begin{pmatrix} T^Y_{aa} & 0 & 0 \\ 0 & T^Y_{bb} & T^{Y*}_{bc} \\ 0 & T^Y_{bc} & T^Y_{cc} \end{pmatrix} \qquad (3.29a)$$

Then by applying the relations (3-28) we get for $\underline{\underline{T}}^2$ and $\underline{\underline{T}}^3$

$$\underline{\underline{T}}^{2,3} = \begin{pmatrix} (T^Y_{aa} + 3\,T^Y_{bb})/4 & \mp\sqrt{3}\,(T^Y_{aa} - T^Y_{bb})/4 & \mp\tfrac{1}{2}\sqrt{3}\,T^{Y*}_{bc} \\ \mp\sqrt{3}(T^Y_{aa} - T^Y_{bb})/4 & (3\,T^Y_{aa} + T^Y_{bb})/4 & -\tfrac{1}{2}\,T^{Y*}_{bc} \\ \mp\tfrac{1}{2}\sqrt{3}\,T^Y_{bc} & -\tfrac{1}{2}\,T^Y_{bc} & T^Y_{cc} \end{pmatrix} \qquad (3.29b)$$

The + sign holds for $\underline{\underline{T}}^3$ and the - sign for $\underline{\underline{T}}^2$.

In the absence of external fields, i.e. when $\underline{H}=0$, the hamiltonian $\mathcal{H}_{hyp}$ is invariant under $O(3)\times C_{3v}$, where $O(3)$ is the

group of orthogonal transformations in threedimensional space. The symbol × means a direct product. Because the full invariance group of $\mathcal{H}_{hyp}$ is a direct product, the hamiltonian can separately be reduced over C_{3v} and O(3). If $\underline{H} \neq 0$ then the invariance group becomes $SO(2) \times C_{3v}$.

First we shall discuss the reduction of $\mathcal{H}_{hyp}$ over C_{3v}. The tensors of the type of Eq. (3.27) transform as a scalar under the C_{3v} operations, and are therefore of A_1 symmetry. The tensors $\underline{\underline{T}}^K$ transform under S_3 as vectors, as can be seen by applying the C_{3c} operator to the matrices in Eq(3.29). Therefore we define

$$\underline{\underline{T}}^{A_1} = \frac{1}{3} (\underline{\underline{T}}^1 + \underline{\underline{T}}^2 + \underline{\underline{T}}^3) \tag{3.30a}$$

$$\underline{\underline{T}}^{E,1} = \frac{1}{6} (2\underline{\underline{T}}^1 - \underline{\underline{T}}^2 - \underline{\underline{T}}^3) \tag{3.30b}$$

$$\underline{\underline{T}}^{E,2} = \frac{1}{2} (\underline{\underline{T}}^2 - \underline{\underline{T}}^3)$$

The first tensor is an A_1-symmetric tensor S_3. The remaining tensors are of E-symmetry. In the molecular reference frame we obtain

$$\underline{\underline{T}}^{A_1} = \begin{pmatrix} \tfrac{1}{2}(T^Y_{aa} + T^Y_{bb}) & 0 & 0 \\ 0 & \tfrac{1}{2}(T^Y_{aa} + T^Y_{bb}) & 0 \\ 0 & 0 & T^Y_{cc} \end{pmatrix} \tag{3.31a}$$

$$\underline{\underline{T}}^{E,1} = \begin{pmatrix} (T^Y_{aa} - T^Y_{bb})/4 & 0 & 0 \\ 0 & -(T^Y_{aa} - T^Y_{bb})/4 & \tfrac{1}{2} T^{Y*}_{bc} \\ 0 & \tfrac{1}{2} T^Y_{bc} & 0 \end{pmatrix} \tag{3.31b}$$

$$\underline{\underline{T}}^{E,2} = \begin{pmatrix} 0 & -\sqrt{3}(T^{Y}_{aa}-T^{Y}_{bb})/4 & -\tfrac{1}{2}\sqrt{3}\ T^{Y*}_{bc} \\ -\sqrt{3}(T^{Y}_{aa} - T^{Y}_{bb})/4 & 0 & 0 \\ -\tfrac{1}{2}\sqrt{3}\ T^{Y}_{bc} & 0 & 0 \end{pmatrix} \quad (3.31c)$$

Let furthermore $\underline{I}^{A_1} = \underline{I}_T = \underline{I}_1 + \underline{I}_2 + \underline{I}_3$ (3.32a)

$$\underline{I}^{E,1} = 2\underline{I}_1 - \underline{I}_2 - \underline{I}_3 \quad (3.32b)$$

$$\underline{I}^{E,2} = \underline{I}_2 - \underline{I}_3 \quad (3.32c)$$

$$\underline{\underline{II}}^{A_1} = \underline{I}_1 \otimes \underline{I}_2 + \underline{I}_2 \otimes \underline{I}_3 + \underline{I}_3 \otimes \underline{I}_1 \quad (3.32c)$$

$$\underline{\underline{II}}^{E,1} = 2\ \underline{I}_2 \otimes \underline{I}_3 - \underline{I}_1 \otimes \underline{I}_2 - \underline{I}_3 \otimes \underline{I}_1 \quad (3.32e)$$

$$\underline{\underline{II}}^{E,2} = \underline{I}_3 \otimes \underline{I}_1 - \underline{I}_1 \otimes \underline{I}_2 \quad (3.32f)$$

The $\underline{\underline{II}}^{\Gamma\xi}$ - tensors are second rank cartesian tensors the tensor $\underline{I}_K \otimes \underline{I}_L$ is a tensorial product of the vectors $\underline{I}_K$ and $\underline{I}_L$.

Substituting in $\mathcal{H}_{hyp}$ we get

$$\mathcal{H}_{hyp} = \mathcal{H}^{A}_{hyp} + \mathcal{H}^{E}_{hyp} \quad (3.33a)$$

with

$$\mathcal{H}^{A}_{hyp} = \underline{V}_X \cdot \underline{\underline{Q}}_X + \underline{I}_X \cdot \underline{\underline{M}}_X \cdot \underline{J} + \underline{V}^{A_1}_Y \cdot \underline{\underline{Q}}^{A_1}_Y + \underline{I}_T \cdot \underline{\underline{M}}^{A_1}_Y \cdot \underline{J} + \underline{I}_X \cdot \underline{\underline{D}}^{A_1}_{XY} \cdot \underline{I}_T +$$

$$+ \underline{\underline{D}}^{A_1}_{YY} \cdot \underline{\underline{II}}^{A_1} - \mu_N \underline{H} \cdot \underline{\underline{G}} \cdot \underline{J} - \tfrac{1}{2}\ \underline{H} \cdot \underline{\underline{\chi}} \cdot \underline{H} - g_X \mu_N \underline{I}_X (1-\underline{\underline{\sigma}}_X) \cdot \underline{H} - g_Y \mu_N \underline{I}_T \cdot (1-\underline{\underline{\sigma}}^{A_1}_Y) \cdot \underline{H} \quad (3.33b)$$

$$\mathcal{H}^{E}_{hyp} = \underline{V}^{E,1}_Y \cdot \underline{\underline{Q}}^{E,1}_Y + \underline{V}^{E,2}_Y \cdot \underline{\underline{Q}}^{E,2}_Y + \underline{I}^{E,1} \cdot \underline{\underline{M}}^{E,1}_Y \cdot \underline{J} + \underline{I}^{E,2} \cdot \underline{\underline{M}}^{E,2}_Y \cdot \underline{J}$$

$$+ \underline{I}^{E,1} \cdot \underline{\underline{D}}^{E,1}_{XY} \cdot \underline{I}_X + \underline{I}^{E,2} \cdot \underline{\underline{D}}^{E,2}_{XY} \cdot \underline{I}_X + \underline{\underline{D}}^{E,1}_{YY} \cdot \underline{\underline{II}}^{E,1} + \underline{\underline{D}}^{E,2}_{YY} \cdot \underline{\underline{II}}^{E,2} +$$

$$+ g_Y \mu_N (\underline{I}^{E,1} \cdot \underline{\underline{\sigma}}^{E,1}_Y \cdot \underline{H} + \underline{I}^{E,2} \cdot \underline{\underline{\sigma}}^{E,2} \cdot \underline{H}) \quad (3.33c)$$

The terms in $\mathcal{H}^{A}_{hyp}$ are products of A-type tensors, while $\mathcal{H}^{E}_{hyp}$ contains E-type tensors.

So far we reduced $\mathcal{H}_{hyp}$ over S_3, yielding tensors which belong to the irreducible representations of this group. The next step is to reduce the hamiltonian over O(3). The irreducible tensors in O(3) are tensors that transform like the spherical harmonics. The way in which irreducible tensors can be constructed from Cartesian tensors can e.g. be found in (FAN 59). For a hermitian second rank Cartesian tensor $\underline{\underline{T}}$, we have

$$
\begin{aligned}
T^{(0)}_{0} &= -(T_{aa} + T_{bb} + T_{cc})/\sqrt{3} \\
T^{(2)}_{0} &= (2\,T_{cc} - T_{aa} - T_{bb})/\sqrt{6} \\
T^{(2)}_{\pm 1} &= [\mp(T_{ac} + T_{ca}) - i(T_{bc} + T_{cb})]/2 \\
T^{(2)}_{\pm 2} &= [(T_{aa} - T_{bb}) \pm i(T_{ab} + T_{ba})]/2
\end{aligned}
\qquad (3.34)
$$

For a tensor of the type of Eq(3.27) we have in the molecular frame of reference

$$
\begin{aligned}
\hat{T}^{(0)}_{0} &= -(2T_{\perp} + T_{\parallel})/\sqrt{3} \\
\tilde{T}^{(2)}_{0} &= \sqrt{\tfrac{2}{3}}\,(T_{\parallel} - T_{\perp}) \\
\tilde{T}^{(2)}_{q} &= 0 \text{ for } q \neq 0
\end{aligned}
\qquad (3.35)
$$

For the tensor $\underline{\underline{T}}^{A_1}$ of Eq(3.31a) the components $\tilde{T}^{A_1(0)}_{0}$ and $\tilde{T}^{A_1(2)}_{0}$ are identical to the corresponding components in Eq(3.34), for $q \neq 0$ we have

$$
\tilde{T}^{A_1(2)}_{q} = 0
$$

For the tensors $\underline{\underline{T}}^{E,1}$ and $\underline{\underline{T}}^{E,2}$ we get using Eqs(3.31b) and (3.31c)

$$\tilde{T}^{E,1(0)}_{0} = \tilde{T}^{E,1(2)}_{0} = \tilde{T}^{E,2(0)}_{0} = \tilde{T}^{E,2(2)}_{0} = 0$$

$$\tilde{T}^{E,1(2)}_{\pm 1} = -\frac{i}{4}\left(T^{Y}_{bc} + T^{Y*}_{bc}\right)$$

$$\tilde{T}^{E,1(2)}_{\pm 2} = \frac{1}{4}\left(T^{Y}_{aa} - T^{Y}_{bb}\right) \qquad (3.36)$$

$$\tilde{T}^{E,2(2)}_{\pm 1} = \pm\frac{\sqrt{3}}{4}\left(T^{Y}_{bc} + T^{Y*}_{bc}\right)$$

$$\tilde{T}^{E,2(2)}_{\pm 2} = \mp\frac{i\sqrt{3}}{4}\left(T^{Y}_{aa} - T^{Y}_{bb}\right)$$

All sperical tensors thus far have been defined in the molecular frame of reference. The wavefunction, however is defined in the space fixed frame. The spherical tensors transform like the spherical harmonic functions under a rotation. In the convention of Edmonds (EDM 57) the components of a tensor in the space fixed frame ($T^{(\nu)}_{q}$) are thereby related to the components of the tensor in the molecule fixed system ($\tilde{T}^{(\nu)}_{q}$) by

$$\tilde{T}^{(\nu)}_{q} = \sum_{q'} T^{(\nu)}_{q'} \mathfrak{D}^{(\nu)}_{q'q}(\psi\vartheta\varphi) \qquad (3.37a)$$

and the inverse transformation

$$T^{(\nu)}_{q'} = \sum_{q} \tilde{T}^{(\nu)}_{q} \mathfrak{D}^{(\nu)}_{qq'}(-\varphi-\vartheta-\psi)$$

$$= \sum_{q} (-1)^{q-q'} \tilde{T}^{(\nu)}_{q} \mathfrak{D}^{(\nu)}_{-q'-q}(\psi\vartheta\varphi) \qquad (3.37b)$$

In the hamiltonian of Eq(3.33) products appear of the type $\underline{A}.\underline{\underline{T}}.\underline{B}$, where $\underline{A}$ and $\underline{B}$ are cartesian vectors and $\underline{\underline{T}}$ is a second rank cartesian tensor. This cartesian product can be expressed as a product of spherical tensors (HUI 66)

$$\underline{A}.\underline{\underline{T}}.\underline{B} = \sum_{\nu=0}^{2} (-1)^{\nu}\sqrt{2\nu+1}\ \{A^{(1)}\{T^{(\nu)}B^{(1)}\}^{(1)}\}^{(0)} \qquad (3.38a)$$

For a hermitian cartesian tensor $\underline{\underline{T}}$ ν can only take the values zero and two. The right hand side of Eq(3.38) can be written out in the components of the irreducible tensors and vectors in the usual way (EDM 57) using spherical tensor techniques. The other type of interactions appearing in Eq(3.33) are of the form $\underline{\underline{T}}.\underline{\underline{U}}$, where $\underline{\underline{T}}$ and $\underline{\underline{U}}$ are traceless hermitian cartesian tensors. In that case

$$\underline{\underline{T}}.\underline{\underline{U}} = \sum_{q} (-1)^{q} T^{(2)}_{q} U^{(2)}_{-q} \qquad (3.38b)$$

as can be found in (JUD 63).

3.1.3 The matrix elements of $\mathcal{H}_{hyp}$

i. General considerations

The matrix elements of the symmetrized hamiltonian of Eq(3.33) can be calculated in the representation of Eq(3.25) using the spherical tensor formulae in Eq(3.35) through (3.38). The general matrix element is

$$\langle\Psi|\mathcal{H}_{hyp}|\Psi'\rangle = \langle\Psi^{\Gamma\xi}I_X M_X|\ \mathcal{H}_{hyp}|\Psi^{\Gamma'\xi'}I_X M'_X\rangle \qquad (3.39)$$

where Γ indicates the irreducible representation to which the spin function of the Y-nuclei belongs under S_3.

Before calculating the matrix elements we examine the implications of the symmetry of wavefunction and hamiltonian in order to avoid unnecessary calculations. As in the derivation of the total wavefunction we consider the matrix elements for the different irreducible representations of S_3 separately.

(a) Spin function of A_1 symmetry

With the aid of the functions in Table 3.2 we obtain for the matrix elements for K and K' positive

$$\langle\Psi^{A_1}|\mathcal{H}_{hyp}|\Psi'^{A_1}\rangle = \tfrac{1}{2}[\langle JKM\,\chi^{A_1}(I_T M_T) I_X M_X|\mathcal{H}_{hyp}|J'K'M'\chi^{A_1}(I_T'M_T') I_X M_X'\rangle$$

$$+(-1)^{J+J'+\gamma+\gamma'}\langle J-KM\chi^{A_1}(I_T M_T) I_X M_X|\mathcal{H}_{hyp}|J'-K'M'\chi^{A_1}(I_T'M_T') I_X M_X'\rangle +$$

$$+(-1)^{J+\gamma}\langle J-KM\chi^{A_1}(I_T M_T) I_X M_X|\mathcal{H}_{hyp}|J'K'M'\chi^{A_1}(I_T'M_T') I_X M_X'\rangle +$$

$$+(-1)^{J'+\gamma'}\langle JKM\chi^{A_1}(I_T M_T) I_X M_X|\mathcal{H}_{hyp}|J'-K'M'\chi^{A_1}(I_T'M_T') I_X M_X'\rangle] \tag{3.40}$$

Because the spin functions are of A_1-symmetry, the spin operator in $\mathcal{H}_{hyp}$ giving non-zero matrix elements must also be of A_1-symmetry, consequently the $\underline{I}^{E,1}$ and $\underline{I}^{E,2}$ operators in Eq(3.33) do not contribute to this matrix element. Let $R_c(\varphi_o)$ be a rotation over an angle φ_o about the c-axis. We know from Eq(3.8a) that $|JKM\rangle$ (:) $\mathfrak{D}^{(J)}_{MK}(\psi\vartheta\varphi)$, and we have

$$R_c(\varphi_o)\mathfrak{D}^{(J)}_{MK}(\psi\vartheta\varphi) = e^{iK\varphi_o}\mathfrak{D}^{(J)}_{MK}(\psi\vartheta\varphi) \tag{3.41}$$

The A_1 symmetric tensors given in Eq(3.27) and (3.31a) remain unchanged under $R_c(\varphi_o)$. Since the matrix element (3.40) must be of A_1-symmetry under this operation and both K and K' are positive, the last two terms must be zero and furthermore K=K'. Operating with the operator σ_a using Eq(3.16b) gives both for bosons and for fermions

$$\sigma_a \langle JKM\ \chi^{A_1}(I_T M_T) I_X M_X | \mathcal{H}_{hyp} | J'K'M' \chi^{A_1}(I_T' M_T') I_X M_X' \rangle$$

$$= (-1)^{J+\gamma}(-1)^{J'+\gamma'} \langle J-KM\ \chi^{A_1}(I_T M_T) I_X M_X | \mathcal{H}_{hyp} | J'-K'M' \chi^{A_1}(I_T' M_T') I_X M_X' \rangle$$

The matrix element on the left hand side must be of A_1 symmetry, and therefore remain unchanged under σ_a, thus the first two terms in Eq(3.40) must be equal. So we finally have

$$\langle \Psi^{A_1} | \mathcal{H}_{hyp} | \Psi^{A_1} \rangle =$$

$$\delta_{KK'} \langle JKM\ \chi^{A_1}(I_T M_T) I_X M_X | \mathcal{H}_{hyp}^{A} | J'KM' \chi^{A_1}(I_T' M_T') I_X M_X' \rangle \qquad (3.42)$$

$$K=3n,\ J+\gamma = J'+\gamma'$$

In the case K=0 the invariance of the A_1-symmetric tensors under a rotation about the c-axis requires (as for the case that $K \neq 0$) that K' must also be zero. The operator σ_a gives $J+\gamma = J'+\gamma'$, therefore the resulting matrix element is identical to that in Eq(3.42).

The matrix elements for spin functions of A_2-symmetry are identical to those for A_1-symmetric spin functions.

(b) Spin function of E-symmetry

In the case K=3n+1 the matrix element becomes

$$\langle \Psi^E | \mathcal{H}_{hyp} | \Psi^E \rangle = \tfrac{1}{2} [\langle JKM \chi^{E,2}(I_T M_T) I_X M_X | \mathcal{H}_{hyp} | J'K'M \chi^{E,2}(I_T' M_T') I_X M_X' \rangle$$

$$+(-1)^{J+\gamma+J'+\gamma'} \langle J-KM \chi^{E,1}(I_T M_T) I_X M_X | \mathcal{H}_{hyp} | J'-K'M' \chi^{E,1}(I_T' M_T') I_X M_X' \rangle$$

$$+(-1)^{J+\gamma} \langle J-KM \chi^{E,1}(I_T M_T) I_X M_X | \mathcal{H}_{hyp} | J'K'M' \chi^{E,2}(I_T' M_T') I_X M_X' \rangle$$

$$+(-1)^{J'+\gamma'} \langle JKM \chi^{E,2}(I_T M_T) I_X M_X | \mathcal{H}_{hyp} | J'-K'M \chi^{E,1}(I_T' M_T') I_X M_X' \rangle] \qquad (3.43)$$

The tensors in $\mathcal{H}_{hyp}$ of A_1-symmetry only contribute to the first terms in Eq(3.43) as can be seen from the same argument as under (a). The operator $R_c(\varphi_o)$ gives K=K', and the operator σ_a $J+\gamma=J'+\gamma'$.

The tensors in $\mathcal{H}_{hyp}$ of E-symmetry are not invariant under an arbitrary rotation about the c-axis, because from Eqs(3.36) it is seen that the non-zero components transform like $Y^{(2)}_{\pm 1}$ and $Y^{(2)}_{\pm 2}$. We have

$$R_c(\varphi_o)\ Y^{(2)}_q = e^{iq\varphi_o}\ Y^{(2)}_q\ ,\ q = 0, \pm 1, \pm 2 \qquad (3.44)$$

In order the matrix element to be of A_1-symmetry, Eq(3.44) requires that for the first two terms in Eq(3.43) K' must be equal to $K \pm q$ and for the third and fourth term $K' = -K \pm q$. For the first two terms, however, the matrix element of the spin operator is zero as we shall see in part ii of this section, so that the E-type tensors only contribute for the last two terms of Eq(3.43). If we require that K>0, only the matrix elements for K=K'=1 and q=2 are non zero ones. So we have

$$\langle \Psi^E | \mathcal{H}_{hyp} | \Psi^E \rangle = \langle JKM\chi^{E,2}(I_T M_T) I_X M_X | \mathcal{H}^A_{hyp} | J'K'M'\chi^{E,2}(I_T'M_T') I_X M_X' \rangle \delta_{KK'}$$

$$+(-1)^{J+\gamma}\delta_{K1}\langle J-KM\chi^{E,1}(I_T M_T) I_X M_X | \mathcal{H}^E_{hyp} | J'K'M'\chi^{E,2}(I_T'M_T') I_X M_X' \rangle \qquad (3.45)$$

For K and K' equal to 3n-1 the matrix element is similar to Eq(3.43). For the A_1-type tensors in $\mathcal{H}_{hyp}$ the result is identical to Eq(3.45), while for the E-type tensors the relation $K' = K \pm q$ has no solutions for this case.

(c) Matrix elements off-diagonal in Γ

Because of the absence of A_2-type spin operators in $\mathcal{H}_{hyp}$ we have

$$< \Psi^{A_1} | \mathcal{H}_{hyp} | \Psi^{A_2} > = 0 \qquad (3.46)$$

The only operators that can couple states with different Γ are the E-type tensors. The transformation of these tensors under a rotation about the symmetry axis given in Eq(3.44) yield the following "selection" rules

$$K' = K \pm 2 \text{ for the } T^{E,\xi}_{\pm 2}{}^{(2)} \text{ components} \qquad (3.47a)$$

$$K' = K \pm 1 \text{ for the } T^{E,\xi}_{\pm 1}{}^{(2)} \text{ components} \qquad (3.47b)$$

In addition the E-type spin operators can in principle couple from a spin state with a certain symmetry to a state with E-symmetry.

It is seen from Eq(3.47) and (3.36) that the $\Delta K = \pm 1$ coupling is established by the off-diagonal tensor component $T^{\bar{Y}}_{bc}$, while the $\Delta K = \pm 2$ originates from the difference $T^{Y}_{aa} - T^{Y}_{bb}$.

So far we discussed only the selection rules for γ and K. The rules for J and I_T follow from spherical tensor techniques. For all tensors in $\mathcal{H}_{hyp}$ we have $J' = J \pm 2$, $J \pm 1$ and J, for the first rank spin operators of E-type $I'_T = I_{T} \pm 1$, I_T; and for the second rank spin operators $I'_T = I_{T} \pm 2$, $I_{T} \pm 1$, and I_T.

ii. The angular momentum operators

The symmetrized angular momentum operators $\underline{I}_X$, $\underline{I}_T$, $\underline{I}^{E,1}$ and $\underline{I}^{E,2}$ appear in the expressions for the matrix elements. The

spin functions $|I_\chi M_\chi>$ are eigenfunctions of the I_χ^2 and $I_{\chi z}$ operators. The functions $|\chi^{\Gamma_E}(I_T M_T)>$ are eigenfunctions of the operators I_T^2 and I_{Tz}. Therefore these operators are diagonal in I_T. The E-type operators, however, can have non zero matrix elements off-diagonal in I_T. If we are only interested in $\Delta K=0$ matrix elements, which will be discussed from now on, then the E-type spin operators only act on E-type spin functions as is clear from Eq(3.45), and we have for the reduced matrix element

$$<\chi^{E,1}(I_T)\| \; I^{E,1}\| \chi^{E,2}(I_T')>= <\chi^{E,1}(I_T)\| 3I_1-I_T\| \chi^{E,2}(I_T')>$$

as can be seen by substituting Eq(3.32b). By applying spherical tensor techniques (EDM 57) this matrix element can be evaluated. We obtain (remembering that $\underline{I}_T$ is an A_1-type operator) using Eq(3.12)

$$<\chi^{E,1}(I_T)\| I^{E,1}\| \chi^{E,2}(I_T')> = 3<\chi^{E,1}(I_T)\| \; I_1\| \chi^{E,2}(I_T')> =$$

$$\sum_{I_{23}} C^{*E,1}_{I_{23}}(I_T) C^{E,2}_{I_{23}}(I_T') (-1)^{I_Y+I_{23}+I_T+1} \; 3. \begin{Bmatrix} I_T & 1 & I_T' \\ I_Y & I_{23} & I_Y \end{Bmatrix} [(2I_T'+1)(2I_T'+1) I_Y(I_Y+1)(2I_Y+1)]^{\frac{1}{2}}$$

(3.48)

The reduced matrix elements of the above type are given in Table 3.3 for I_Y up to 3/2.

The reduced matrix element of the $\underline{I}^{E,2}$ operator can be expressed in the matrix element of Eq(3.48). If the operator (132) is applied to the left hand side of (3.48), we get using Eq(3.13c)

$$(132)<\chi^{E,1}(I_T)\| I^{E,1}\| \chi^{E,2}(I_T')> =$$

$$e^{2\pi i/3}<\chi^{E,1}(I_T)\| \; 2I_3-I_1-I_2\| \chi^{E,2}(I_T')>$$

From Eqs(3.32b,c) this can be written as

I_Y		1/2	1		3/2			
	I_T	1/2	2	1	7/2	5/2	3/2	1/2
1/2	1/2	-2						
1	2		$-1/2$	$-\sqrt{3}/2$				
	1		$-\sqrt{3}/2$	$-1/2$				
3/2	7/2				$-\frac{2}{7}$	$-\frac{2}{7}\sqrt{6}$		
	5/2				$-\frac{2}{7}\sqrt{6}$	$-\frac{4}{35}$	$-\frac{1}{5}\sqrt{6}$	
	3/2					$-\frac{1}{5}\sqrt{6}$	$-\frac{8}{5}$	$-\sqrt{\frac{3}{5}}$
	1/2						$-\sqrt{\frac{3}{5}}$	2

Table 3.3. The matrix elements $\langle \chi^{E,1}(I_T) \| \; I^{E,1} \| \; \chi^{E,2}(I_T') \rangle / [\, I_T(I_T+2)(2I_T+1)]^{\frac{1}{2}}$ for Y nuclear spin ½, 1 and 3/2.

$$e^{2\pi i/3} \langle \chi^{E,1}(I_T) \| \; -\frac{1}{2} I^{E,1} - \frac{3}{2} I^{E,2} \| \chi^{E,2}(I_T') \rangle \tag{3.49}$$

The original matrix element (3.48) has to be invariant under the (132) operation, so (3.49) must be equal to (3.48). After some simple algebraic manipulations we obtain

$$\langle \chi^{E,1}(I_T) \| \; I^{E,2} \| \chi^{E,2}(I_T') \rangle = \frac{i}{\sqrt{3}} \langle \chi^{E,1}(I_T) \| \; I^{E,1} \| \chi^{E,1}(I_T') \rangle \tag{3.50}$$

The spin-spin interaction between the Y-nuclei involves the second rank operators $\underline{II}^{\Gamma\xi}$. The $\underline{II}^{A_1}$-operator defined in Eq (3.32d) can be written as

$$\underline{II}^{A_1} = \tfrac{1}{2} \, (\underline{I}_T \otimes \underline{I}_T - \underline{I}_1 \otimes \underline{I}_1 - \underline{I}_2 \otimes \underline{I}_2 - \underline{I}_3 \otimes \underline{I}_3) \tag{3.51}$$

It is seen from Eq(3.42) and (3.45) that it appears in matrix elements of the type

$$\langle\chi^{\Gamma\xi}(I_T)\|\{\underline{II}^{A_1}\}^{(2)}\|\chi^{\Gamma\xi}(I'_T)\rangle =$$

$$\tfrac{1}{2}\langle\chi^{\Gamma\xi}(I_T)\|\{\underline{I}_T\otimes\underline{I}_T - \underline{I}_1\otimes\underline{I}_1 - \underline{I}_2\otimes\underline{I}_2 - \underline{I}_3\otimes\underline{I}_3\}^{(2)}\|\chi^{\Gamma\xi}(I'_T)\rangle \tag{3.52}$$

By applying the symmetry operators (123) and (132) to this matrix element we see that the last three operators in $\underline{II}^{A_1}$ must give the same contribution. Consequently

$$\langle\chi^{\Gamma\xi}(I_T)\|\{\underline{II}^{A_1}\}^{(2)}\|\chi^{\Gamma\xi}(I'_T)\rangle = \tfrac{1}{2}\langle\chi^{\Gamma\xi}(I_T)\|\{\underline{I}_T\underline{I}_T\}^{(2)}\|\chi^{\Gamma\xi}(I'_T)\rangle -$$

$$-\tfrac{3}{2}\langle\chi^{\Gamma\xi}(I_T)\|\{I_1 I_1\}^{(2)}\|\chi^{\Gamma\xi}(I'_T)\rangle =$$

$$\sqrt{5}\left[(-1)^{2I_T}\delta_{I_T I'_T}\begin{Bmatrix}1 & 2 & 1\\ I_T & I_T & I_T\end{Bmatrix} I_T(I_T+1)(2I_T+1) - \frac{3}{2}\sum_{I_{23}} C^{*\Gamma\xi}_{I_{23}}(I_T)C^{\Gamma\xi}_{I_{23}}(I'_T)\right.$$

$$\left.(-1)^{2I_{23}-I_Y+I_T}\cdot\begin{Bmatrix}I_T & 2 & I'_T\\ I_Y & I_{23} & I_Y\end{Bmatrix}\begin{Bmatrix}1 & 2 & 1\\ I_Y & I_Y & I_Y\end{Bmatrix} I_Y(I_Y+1)(2I_Y+1)\right] \tag{3.53}$$

For the $\underline{II}^{E,1}$-operator we must calculate $\langle\chi^{E,1}(I_T)\|\{\underline{II}^{E,1}\}^{(2)}\|\chi^{E,2}(I'_T)\rangle$. From its definition (3.32e) we see

$$\underline{II}^{E,1} = 3\,\underline{I}_2\otimes\underline{I}_3 - \underline{II}^{A_1} \tag{3.54}$$

The A-type tensor gives no contribution to this matrix element, because then the matrix element is not invariant under (132). So we get

$$\langle \chi^{E,1}(I_T) \| \{II\}^{E,1(2)} \| \chi^{E,2}(I'_T) \rangle = 3 \langle \chi^{E,1}(I_T) \| \{I_2 I_3\}^{(2)} \| \chi^{E,2} \rangle$$

$$= \sum_{I_{23} I'_{23}} C^{*E,1}_{I_{23}}(I_T) C^{E,2}_{I'_{23}}(I'_T) (-1)^{I_{23}+I_Y+I'_T} 3\sqrt{5} \left[(2I_T+1)(2I'_T+1)\right]^{\frac{1}{2}} \cdot$$

$$\cdot I_Y(I_Y+1)(2I_Y+1) \left[(2I_{23}+1)(2I'_{23}+1)\right]^{\frac{1}{2}} \begin{Bmatrix} I_T & 2 & I'_T \\ I'_{23} & I_Y & I_{23} \end{Bmatrix} \begin{Bmatrix} I_Y & I_Y & 1 \\ I_Y & I_Y & 1 \\ I_{23} & I'_{23} & 2 \end{Bmatrix} \quad (3.55)$$

iii. Calculation of the matrix elements

In the calculation of the matrix elements we shall only take into account the terms diagonal in K. The general expressions for these elements are given in Eqs.(3.42) and (3.45).

(a) Quadrupole interaction X-nucleus

The operator for the X-quadrupole is $\underline{\underline{V}}_X \cdot \underline{\underline{Q}}_X$. It is a product of A-type tensors. The transformation to irreducible spherical tensors is given in Eq(3.38b). Because the tensors in this interaction are A-type we have from Eqs(3.42) and (3.45)

$$\langle \Psi^{\Gamma\xi} | \underline{\underline{V}}_X \cdot \underline{\underline{Q}}_X | \Psi'^{\Gamma\xi} \rangle =$$

$$= \delta_{KK'} \sum_q (-1)^q \langle JKM \chi^{\Gamma\xi}(I_T M_T) I_X M_X | V^{(2)}_{X,q} Q^{(2)}_{X,-q} | J'KM' \chi^{\Gamma\xi}(I'_T M'_T) I_X M'_X \rangle$$

$$= \delta_{KK'} \delta_{I_T I'_T} \delta_{M_T M'_T} \langle JK \| V^{(2)}_X \| J'K \rangle \langle I_X \| Q^{(2)}_X \| I_X \rangle \cdot$$

$$\cdot \sum_q (-1)^{q+J-M+I_X-M_X} \begin{pmatrix} J & 2 & J' \\ -M & q & M' \end{pmatrix} \begin{pmatrix} I_X & 2 & I_X \\ -M_X & -q & M'_X \end{pmatrix} \quad (3.56)$$

The first reduced matrix element can be evaluated with the aid of the Wigner-Eckart theorem; the tensor components are then transformed to the molecular frame using Eq(3.37b)

$$\langle J_K \| V^{(2)} \| J'_K \rangle = \frac{\langle JKM | V^{(2)}_{X0} | J'KM \rangle}{(-1)^{J-M} \begin{pmatrix} J & 2 & J' \\ -M & 0 & M \end{pmatrix}} = V^{(2)}_{X\,0} \frac{\langle JKM | \mathcal{D}^{(2)}_{00} | J'KM \rangle}{(-1)^{J-M} \begin{pmatrix} J & 2 & J' \\ -M & 0 & M \end{pmatrix}}$$

This matrix element is an integral over three $\mathcal{D}$-functions yielding

$$\langle J_K \| V^{(2)}_X \| J'_K \rangle = \sqrt{\frac{2}{3}} (V^X_{\|} - V^X_{\perp}) (-1)^{J-K} [(2J+1)(2J'+1)]^{\frac{1}{2}} \begin{pmatrix} J & 2 & J' \\ -K & 0 & K \end{pmatrix} \tag{3.57}$$

The trace of $\underline{\underline{V}}_X$ must be zero, and hence $V^X_{\perp} = -\frac{1}{2} V^X_{\|} = \frac{1}{2} q_X$.

The reduced matrix element in Eq(3.56) for the X-quadrupole moment is usually written as

$$\langle I_X \| Q^{(2)}_X \| I_X \rangle = \frac{\langle I_X I_X | Q^{(2)}_0 | I_X I_X \rangle}{\begin{pmatrix} I_X & 2 & I_X \\ -I_X & 0 & I_X \end{pmatrix}} = \frac{eQ_X}{2\sqrt{6}} \left[\frac{(2I_X+3)(2I_X+2)(2I_X+1)}{2I_X(2I_X-1)} \right]^{\frac{1}{2}} \tag{3.58}$$

Substituting Eqs(3.57) and (3.58) into Eq(3.56) we obtain

$$\langle \Psi^{\Gamma\xi} | \underline{\underline{V}}_X \cdot \underline{\underline{Q}}_X | \Psi'^{\Gamma\xi} \rangle =$$

$$= (-1)^{J-M+I_X-M_X+J-K+1} \delta_{I_T I'_T} \delta_{M_T M'_T} \delta_{KK'} \frac{eq_X Q_X}{4} \cdot$$

$$\cdot \begin{pmatrix} J & 2 & J' \\ -K & 0 & K \end{pmatrix} \left[\frac{(2J+1)(2J'+1)(2I_X+3)(2I_X+2)(2I_X+1)}{2I_X(2I_X-1)} \right]^{\frac{1}{2}}$$

$$\cdot \sum_q (-1)^q \begin{pmatrix} J & 2 & J' \\ -M & -q & M' \end{pmatrix} \begin{pmatrix} I_X & 2 & I_X \\ -M_X & q & M'_X \end{pmatrix} \tag{3.59}$$

and for the contribution diagonal in J

$$\langle \Psi^{\Gamma\xi} | \underline{V}_X \cdot \underline{Q}_X | \Psi'^{,\Gamma\xi} \rangle =$$

$$= (-1)^{J-M+I_X-M_X} \delta_{KK'} \delta_{I_T I_T'} \delta_{M_T M_T'} \frac{eq_X Q_X}{4} \left[1 - \frac{3K^2}{J(J+1)} \right] \cdot$$

$$\cdot \left[\frac{J(J+1)(2J+1)(2I_X+1)(2I_X+2)(2I_X+3)}{(2I_X-1)2I_X} \right]^{\frac{1}{2}} \cdot$$

$$\cdot \sum_q (-1)^q \begin{pmatrix} J & 2 & J \\ -M & -q & M' \end{pmatrix} \begin{pmatrix} I_X & 2 & I_X \\ -M_X & q & M_X' \end{pmatrix} \tag{3.60}$$

(b) Spin rotation X-nucleus

We shall calculate only the matrix element diagonal in J, because off diagonal matrix elements give energy corrections less than 1 Hz. Using Eq(3.38a) and the fact that the spin-rotation interaction of the X-nucleus belongs to $\mathcal{H}^A_{hyp}$ the matrix element for this interaction is

$$\langle \Psi^{\Gamma\xi} | \underline{I}_X \cdot \underline{\underline{M}}_X \cdot \underline{J} | \Psi'^{,\Gamma\xi} \rangle = \sum_{\nu,q} (-1)^{\nu+q+1} \sqrt{\frac{2\nu+1}{3}}$$

$$\langle JKM_X{}^{\Gamma\xi}(I_T M_T) I_X M_X | \{ M_X^{(\nu)} J \}^{(1)}_{-q} I_{X_q} | J'KM'\chi^{\Gamma\xi}(I_T' M_T') I_X M_X' \rangle =$$

$$\sum_{\nu,q} (-1)^{q+J-M+I_X-M_X} \delta_{I_T I_T'} \delta_{M_T M_T'} \begin{pmatrix} J & 1 & J \\ -M & -q & M' \end{pmatrix} \begin{pmatrix} I_X & 1 & I_X \\ -M_X & q & M_X' \end{pmatrix}$$

$$[J(J+1)(2J+1)I_X(I_X+1)(2I_X+1)]^{\frac{1}{2}} \sqrt{2\nu+1} \; (-1)^{\nu} \langle J \| M_X^{(\nu)} \| J \rangle \begin{Bmatrix} J & J & J \\ \nu & 1 & 1 \end{Bmatrix}$$

Substituting the 6j-symbol in the above expression for the possible ν-values zero and two, and transformating $M_X^{(\nu)}$ to the molecular frame the following result is obtained.

$$\langle\Psi^{\Gamma\xi}|\underline{I}_X.\underline{\underline{M}}_X.\underline{J}|\Psi'^{\Gamma\xi}\rangle =$$

$$=(-1)^{J-M+I_X-M_X}\,\delta_{KK'}\delta_{I_TI'_T}\,\delta_{M_TM'_T}\left[M_\perp^X+\frac{K^2}{J(J+1)}\,(M_\parallel^X-M_\perp^X)\right].$$

$$.\left[J(J+1)(2J+1)I_X(I_X+1)(2I_X+1)\right]^{\frac{1}{2}}\sum_q(-1)^q\begin{pmatrix}J&1&J\\-M&-q&M'\end{pmatrix}\begin{pmatrix}I_X&1&I_X\\-M_X&q&M'_X\end{pmatrix}$$

(3.61)

(c) Quadrupole interaction Y-nuclei

It is seen from Eq(3.33b) and (3.33c) that part of this interaction belongs to $\mathcal{H}^A_{hyp}$ and part to $\mathcal{H}^E_{hyp}$. For the part belonging to $\mathcal{H}^A_{hyp}$ we have

$$\langle\Psi^{\Gamma\xi}|\underline{\underline{V}}_Y^{A_1}.\underline{\underline{Q}}_Y^{A_1}|\Psi'^{\Gamma\xi}\rangle =$$

$$\sum_q(-1)^q\langle JKM\chi^{\Gamma\xi}(I_TM_T)I_XM_X|V_{Y\,-q}^{A_1(2)}\,Q_q^{A_1(2)}|J'KM'\chi^{\Gamma\xi}(I'_TM'_T)I_XM'_X\rangle =$$

$$\sum_q(-1)^{q+J-M+I_T-M_T}\,\delta_{M_XM'_X}\begin{pmatrix}J&2&J'\\-M&-q&M'\end{pmatrix}\begin{pmatrix}I_T&2&I'_T\\-M_T&q&M'_T\end{pmatrix}$$

$$\langle J\|V_Y^{A_1(2)}\|J'\rangle\langle\chi^{\Gamma\xi}(I_T)\|Q_Y^{A_1(2)}\|\chi^{\Gamma\xi}(I'_T)\rangle$$

The first reduced matrix element can be treated as in Eq(3.57), but now $q_Y=V^Y_{aa}+V^Y_{bb}-2V^Y_{cc}$. For the second reduced matrix element the expansion given in Eq(3.12) has to be used for further evaluation. If we define Q_Y analogously to Q_X in Eq(3.58) then

$$\langle \Psi^{\Gamma\xi} | \underline{\underline{V}}_Y^{A_1} \cdot \underline{\underline{Q}}_Y^{A_1} | \Psi'^{\Gamma\xi} \rangle =$$

$$(-1)^{J-M+I_T-M_T+J-K+1} \delta_{KK'} \delta_{M_X M'_X} \frac{3eq_Y Q_Y}{4} \cdot$$

$$\cdot \begin{pmatrix} J & 2 & J' \\ -K & 0 & K \end{pmatrix} \left[\frac{(2J+1)(2J'+1)(2I_T+1)(2I'_T+1)(2I_Y+3)(2I_Y+2)(2I_Y+1)}{2I_Y(2I_Y-1)} \right]^{\frac{1}{2}}$$

$$\cdot \sum_q (-1)^q \begin{pmatrix} J & 2 & J' \\ -M & -q & M' \end{pmatrix} \begin{pmatrix} I_T & 2 & I'_T \\ -M_T & q & M'_T \end{pmatrix} \cdot$$

$$\cdot \sum_{I_{23}} C^{*\Gamma\xi}_{I_{23}}(I_T)\, C^{\Gamma\xi}_{I_{23}}(I'_T)\, (-1)^{I_{23}+I_Y+I_T} \begin{Bmatrix} I_T & 2 & I'_T \\ I_Y & I_{23} & I_Y \end{Bmatrix} \qquad (3.62a)$$

The part of the quadrupole interaction belonging to $\mathcal{H}^E_{hyp}$ only contributes for K=1 terms as was shown in Sect. 3.1.3(i), Eq (3.45). The matrix element becomes

$$\langle \Psi^E | \underline{\underline{V}}_Y^{E,1} \cdot \underline{\underline{Q}}_Y^{E,1} + \underline{\underline{V}}_Y^{E,2} \underline{\underline{Q}}_Y^{E,2} | \Psi^E \rangle =$$

$$\sum_q (-1)^{q+J-M+I_T-M_T} \delta_{M_X M'_X} \begin{pmatrix} J & 2 & J' \\ -M & -q & M' \end{pmatrix} \begin{pmatrix} I_T & 2 & I'_T \\ -M_T & q & M'_T \end{pmatrix} \cdot (-1)^{J+\gamma} \delta_{K1}$$

$$[\langle J \| V_Y^{E,1(2)} \| J' \rangle \langle \chi^{E,1}(I_T) \| Q_Y^{E,1(2)} \| \chi^{E,2}(I'_T) \rangle +$$

$$+ \langle J \| V_Y^{E,2(2)} \| J' \rangle \langle \chi^{E,1}(I_T) \| Q_Y^{E,2(2)} \| \chi^{E,2}(I'_T) \rangle]$$

In Eq(3.50) we obtained a relation between the matrix elements of the $I^{E,1}$ and $I^{E,2}$ operator. Because the definition of the E-type quadrupole operators is basically the same as for the

E-type spin operators (as far as the transformation properties under S_3 are concerned) the relation (3.50) will also hold for $Q_Y^{E,1}$ and $Q_Y^{E,2}$, and we end up with

$$\langle \Psi^{E,1} | \underline{V}_Y^{E,1} \cdot \underline{\underline{Q}}_Y^{E,1} + \underline{V}_Y^{E,2} \cdot \underline{\underline{Q}}_Y^{E,2} | \Psi'^{E,2} \rangle$$

$$= (-1)^{J-M+I_T-M_T+J-1+J+\gamma} \delta_{K1} \delta_{M_X M'_X} \frac{3eQ_Y}{4\sqrt{6}} (V_{aa}^Y - V_{bb}^Y) \cdot$$

$$\cdot \begin{pmatrix} J & 2 & J' \\ 1 & -2 & 1 \end{pmatrix} \left[\frac{(2J+1)(2J'+1)(2I_T+1)(2I'_T+1)(2I_Y+3)(2I_Y+2)(2I_Y+1)}{2I_Y(2I_Y-1)} \right]^{\frac{1}{2}} \cdot$$

$$\cdot \sum_q (-1)^q \begin{pmatrix} J & 2 & J' \\ -M & -q & M' \end{pmatrix} \begin{pmatrix} I_T & 2 & I'_T \\ -M_T & q & M'_T \end{pmatrix} \cdot$$

$$\cdot \sum_{I_{23}} C_{I_{23}}^{E,1*}(I_T)\, C_{I_{23}}^{E,2}(I'_T)\, (-1)^{I_{23}+I_Y+I_T} \begin{Bmatrix} I_T & 2 & I'_T \\ I_Y & I_{23} & I_Y \end{Bmatrix} \qquad (3.62b)$$

(d) Spin-rotation Y-nuclei

As in the case of the spin-rotation of the X-nucleus only the contribution diagonal in J and K is considered. The transformation from the cartesian tensors to the spherical tensors is given in Eq(3.38a). For the $M_Y^{A_1}$-tensor we find

$$\langle \Psi^{\Gamma\xi} | \underline{I}_T \cdot \underline{\underline{M}}_Y^{A_1} \cdot \underline{J} | \Psi'^{\Gamma\xi} \rangle =$$

$$= \sum_{\nu,q} (-1)^{q+1} \sqrt{\frac{2\nu+1}{3}} \langle \Psi^{\Gamma\xi} | I_{T,q} \{ M_Y^{A_1}(\nu)\, J \}_{-q}^{(1)} | \Psi'^{\Gamma\xi} \rangle =$$

$$= (-1)^{J-M+I_T-M_T} \delta_{KK'} \delta_{M_X M'_X} \delta_{I_T I'_T} \left[\frac{M_{aa}^Y + M_{bb}^Y}{2} + \frac{K^2}{J(J+1)} \left(M_{cc}^Y - \frac{M_{aa}^Y + M_{bb}^Y}{2} \right) \right] \cdot$$

$$\cdot [J(J+1)(2J+1) I_T(I_T+1)(2I_T+1)]^{\frac{1}{2}} \sum_q (-1)^q \begin{pmatrix} J & 1 & J \\ -M & -q & M' \end{pmatrix} \begin{pmatrix} I_T & 1 & I_T \\ -M_T & q & M'_T \end{pmatrix} \qquad (3.63a)$$

Note that this term is diagonal in I_T. The E-type tensors are in general not diagonal in I_T and we get

$$\langle\Psi^{E,1}|\underline{J}.\underline{\underline{M}}_Y^{E,1}.\underline{I}^{E,1}|\Psi'^{E,2}\rangle + \langle\Psi^{E,1}|\underline{J}.\underline{\underline{M}}_Y^{E,2}.\underline{I}^{E,2}|\Psi^{E,2}\rangle =$$

$$\sum_q (-1)^{q+J-M+I_T-M_T}\delta_{K,1}\delta_{M_X M'_X}\begin{pmatrix} J & 1 & J \\ -M & -q & M' \end{pmatrix}\begin{pmatrix} I_T & 1 & I_T \\ -M_T & q & M'_T \end{pmatrix}$$

$$[J(J+1)(2J+1)]^{\frac{1}{2}}\sqrt{5}\begin{Bmatrix} J & J & J \\ 2 & 1 & 1 \end{Bmatrix}$$

$$[(-1)^{J+\gamma}\langle J\|M_Y^{E,1(2)}\|J\rangle\langle\chi^{E,1}(I_T)\|I^{E,1}\|\chi^{E,2}(I'_T)\rangle +$$

$$+ (-1)^{J+\gamma}\langle J\|M_Y^{E,2(2)}\|J\rangle\langle\chi^{E,1}(I_T)\|I^{E,2}\|\chi^{E,2}(I'_T)\rangle]$$

The relation (3.50) for the reduced matrix elements of the spin operators, and the transformation of $M_Y^{E,\xi(2)}$ to the molecular frame of reference yield for this matrix element

$$\langle\Psi^{E,1}|\underline{J}.\underline{\underline{M}}_Y^{E,1}.\underline{I}^{E,1} + \underline{J}.\underline{\underline{M}}_Y^{E,2}.\underline{I}^{E,2}|\Psi^{E,2}\rangle$$

$$= (-1)^{J-M+I_T-M_T+J+\gamma}\delta_{K1}\delta_{M_X M'_X}\left(\frac{M_{aa}^Y - M_{bb}^Y}{4}\right) \cdot$$

$$\cdot [J(J+1)(2J+1)]^{\frac{1}{2}}\langle\chi^{E,1}(I_T)\|I^{E,1}\|\chi^{E,2}(I'_T)\rangle$$

$$\sum_q (-1)^q \begin{pmatrix} J & 1 & J \\ -M & -q & M' \end{pmatrix}\begin{pmatrix} I_T & 1 & I'_T \\ -M_T & q & M'_T \end{pmatrix} \qquad (3.63b)$$

The reduced matrix element in Eq(3.63b) is given in Table (3.4). It is seen from this Table that for $I_Y=\frac{1}{2}$ the operator is diagonal in I_T if only one rotational level is considered. For higher values of I_Y also off-diagonal matrix elements in I_T appear.

(e) Spin-spin interaction X-Y

The direct spin-spin interaction can be calculated from the molecular geometry. The tensor components are given in Table 5.1. If ϑ_o is the angle between the XY-bond and the symmetry axis and r_{XY} the distance between the X-nucleus and the Y-nucleus, then, since the D_{XY}-tensors are traceless, we have for the A_1-tensor using Eq(3.38a)

$$\underline{I}_X \underline{\underline{D}}^{A_1}_{XY} \cdot \underline{I}_T = \sqrt{5}\,\{I_X \{D^{A_1}_{XY}{}^{(2)} I_T\}^{(1)}\}^{(0)} = \sqrt{5}\{\{I_X I_T\}^{(2)} D^{A_1}_{XY}{}^{(2)}\}^{(0)}$$

$$= \sum_{qq_1q_2} D^{A_1}_{XY}{}^{(2)}_{-q}\, I_{X\,q_1}\, I_{T\,q_2}\, \sqrt{5} \begin{pmatrix} 1 & 1 & 2 \\ q_1 & q_2 & -q \end{pmatrix}$$

The same expansion holds for the E-type tensors.

Now the matrix elements become

$$\langle \Psi^{\Gamma\xi} | \underline{I}_X \cdot (\underline{\underline{D}}^{A_1}_{XY} \cdot \underline{I}_T + \underline{\underline{D}}^{E,1}_{XY} \cdot \underline{I}^{E,1} + \underline{\underline{D}}^{E,2}_{XY} \cdot \underline{I}^{E,2}) | \Psi', \Gamma\xi \rangle$$

$$= \sum_{qq_1q_2} (-1)^{J-M+I_X-M_X+I_T-M_T} \begin{pmatrix} J & 2 & J \\ -M & -q & M' \end{pmatrix} \begin{pmatrix} I_X & 1 & I_X \\ -M_X & q_1 & M'_X \end{pmatrix} \begin{pmatrix} I_T & 1 & I'_T \\ -M_T & q_2 & M'_T \end{pmatrix}$$

$$\begin{pmatrix} 1 & 1 & 2 \\ q_1 & q_2 & -q \end{pmatrix} \sqrt{5}\ [I_T(I_T+1)(2I_T+1)]^{\frac{1}{2}} \cdot [I_X(I_X+1)(2I_X+1)]^{\frac{1}{2}}$$

$$\cdot \left[\langle J \| D^{A_1}_{XY}{}^{(2)} \| J \rangle\ \delta_{I_T I'_T} + \frac{\langle \chi^{E,1}(I_T) \| I^{E,1} \| \chi^{E,2}(I'_T) \rangle}{[I_T(I_T+1)(2I_T+1)]^{\frac{1}{2}}} \cdot (-1)^{J+\gamma} \delta_{K1} \right.$$

$$\left. \cdot \langle J \| D^{E,1(2)}_{XY} + \frac{i}{\sqrt{3}} D^{E,2(2)}_{XY} \| J \rangle \right]$$

The reduced matrix elements can be expressed in ϑ_o and r_{XY} using the Wigner-Eckart theorem, and transforming the tensor components to the molecular frame. The result is

$$\langle\Psi^{\Gamma\xi}|\underline{I}_X\cdot(\underline{\underline{D}}^{A_1}_{XY}\cdot\underline{I}_T + \underline{\underline{D}}^{E,1}_{XY}\cdot\underline{I}^{E,1} + \underline{\underline{D}}^{E,2}_{XY}\cdot\underline{I}^{E,2})|\Psi',\Gamma\xi\rangle =$$

$$= \frac{\mu_o\mu_N^2 g_X g_Y}{4\pi r_{XY}^3}\,(-1)^{J-M+I_X-M_X+I_T-M_T}\cdot$$

$$\cdot\left[(1-\frac{3K^2}{J(J+1)})(1-\frac{3}{2}\sin^2\vartheta_o)\delta_{KK'}\delta_{I_TI_T'} - \right.$$

$$\left. - (-1)^{J+\gamma}\delta_{K1}\,\frac{3}{4}\sin^2\vartheta_o\,\frac{\langle\chi^{E,1}(I_T)\|I^{E,1}\|\chi^{E,2}(I_T')\rangle}{[I_T(I_T+1)(2I_T+1)]^{\frac{1}{2}}}\right]\cdot$$

$$\cdot\left[I_T(I_T+1)(2I_T+1)I_X(I_X+1)(2I_X+1)\,\frac{30J(J+1)(2J+1)}{(2J-1)(2J+3)}\right]^{\frac{1}{2}}\cdot$$

$$\sum_{qq_1q_2}\begin{pmatrix}J & 2 & J\\ -M & -q & M'\end{pmatrix}\begin{pmatrix}I_X & 1 & I_X\\ -M_X & q_1 & M'_X\end{pmatrix}\begin{pmatrix}I_T & 1 & I_T'\\ -M_T & q_2 & M_T'\end{pmatrix}\begin{pmatrix}1 & 1 & 2\\ q_1 & q_2 & -q\end{pmatrix} \tag{3.64}$$

(f) Spin-spin interaction Y-Y

The direct spin-spin interaction between the Y-nuclei can be expressed in spherical tensor components using Eq(3.38b). Substituted in the matrix element gives

$$\langle\Psi^{\Gamma\xi}|\underline{\underline{D}}^{A_1}_{YY}\cdot\underline{\underline{II}}^{A_1} + \underline{\underline{D}}^{E,1}_{YY}\cdot\underline{\underline{II}}^{E,1} + \underline{\underline{D}}^{E,2}_{YY}\cdot\underline{\underline{II}}^{E,2}|\Psi',\Gamma\xi\rangle =$$

$$= \sum_q (-1)^q\langle\Psi^{\Gamma\xi}|D^{A_1(2)}_{YY-q}\,II^{A_1(2)}_q + D^{E,1(2)}_{YY-q}\,II^{E,1(2)}_q +$$

$$+ D^{E,2(2)}_{YY-q} \; II^{E,2(2)}_{q} |\Psi', \Gamma\xi>$$

$$= \frac{\mu_o \mu_N^2 q_Y^2}{4\pi r_{YY}^3} \sum_q (-1)^{q+J-M+I_T-M_T} \delta_{M_X M'_X} \begin{pmatrix} J & 2 & J \\ -M & -q & M' \end{pmatrix} \begin{pmatrix} I_T & 2 & I'_T \\ -M_T & q & M'_T \end{pmatrix}$$

$$\left[\frac{30J(J+1)(2J+1)}{(2J+1)(2J-1)}\right]^{\frac{1}{2}} \left[<\chi^{\Gamma\xi}(I_T) \| II^{A_1(2)} \| \chi^{\Gamma\xi}(I'_T)> \left(\frac{3K^2}{J(J+1)} - 1\right) \cdot \frac{1}{2} + \right.$$

$$\left. + (-1)^{J+\gamma} \delta_{K,1} <\chi^{E,1}(I_T) \| II^{E,1(2)} \| \chi^{E,2}(I'_T)> (-\frac{3}{4}) \right] \qquad (3.65)$$

For $I_Y = \frac{1}{2}$ the spin of the E-type levels is $I_T = \frac{1}{2}$, hence the second 3j-symbol in Eq(3.65) is zero, and the interaction vanishes for these states.

(g) Molecular magnetic moment and susceptibility

These interactions involve A_1-type tensors and hence can be treated in essentially the same way as the spin-rotation interaction of the X-nucleus. If in the space fixed frame the quantization axis is chosen along $\underline{H}$ then the matrix elements diagonal in J are

$$<\Psi^{\Gamma\xi}| -\mu_N \underline{H}.\underline{\underline{G}}.\underline{J} - \tfrac{1}{2} \underline{H}.\underline{\underline{\chi}}.\underline{H} |\Psi', \Gamma\xi> =$$

$$\delta_{MM'} \delta_{M_T M'_T} \delta_{I_T I'_T} \delta_{M_X M'_X} \left[-\mu_N M H (g_\perp + \frac{K^2}{J(J+1)} (g_\parallel - g_\perp)) - \frac{1}{6}(2\chi_\perp + \chi_\parallel) H^2 + \right.$$

$$\left. + \frac{3M^2 - J(J+1)}{(2J+3)(2J-1)} \left(1 - \frac{3K^2}{J(J+1)}\right) \frac{2}{3} (\chi_\parallel - \chi_\perp) H^2 \right] \qquad (3.66)$$

(h) Nuclear magnetic moment of the X-nucleus

It is seen in Eq(3.33b) that the operators in this interaction belong to $\mathcal{H}^{A}_{hyp}$. Let

$$\sigma^{X}_{av} = \frac{1}{3}\,(\sigma^{X}_{aa} + \sigma^{X}_{bb} + \sigma^{X}_{cc}) = \frac{2}{3}\,\sigma^{X}_{\perp} + \frac{1}{3}\,\sigma^{X}_{\parallel}$$

then the matrix elements of the scalar interaction $-\mu_N g_X \underline{I}_X \cdot \underline{H}\,(1-\sigma^{X}_{av})$ are

$$\langle \Psi^{\Gamma\xi} | -\mu_N g_X \underline{I}_X \cdot \underline{H}(1-\sigma^{X}_{av}) | \Psi', \Gamma\xi \rangle = -\delta_{MM'}\delta_{I_T I'_T}\delta_{M_T M'_T}\delta_{M_X M'_X}\mu_N g_X H(1-\sigma^{X}_{av})M_X \tag{3.67a}$$

The remaining interaction is the anisotropic nuclear shielding, which involves an irreducible tensor of rank two·

$$\mu_N g_X \underline{I}_X \cdot (\underline{\underline{\sigma}}^{X} - \sigma^{X}_{av}\underline{\underline{1}}) \cdot \underline{H} \equiv \mu_N g_X \underline{I}_X \cdot \underline{\underline{\sigma}}^{X}_{an} \cdot \underline{H}$$

This cartesian tensor product can be written as a product of irreducible tensors using Eq(3.38a), which in turn can be expressed in the spherical tensor components. In total

$$\underline{I}_X \cdot \underline{\underline{\sigma}}^{X}_{an} \cdot \underline{H} = \sqrt{5}\, H \sum_q \sigma^{X(2)}_{an,-q}\; I_{X_q} \begin{pmatrix} 2 & 1 & 1 \\ -q & q & 0 \end{pmatrix}$$

Herewith the matrix elements become

$$\langle \Psi^{\Gamma\xi} | \mu_N g_X \underline{I}_X \cdot \underline{\underline{\sigma}}^{X}_{an} \cdot \underline{H} | \Psi', \Gamma\xi \rangle$$

$$= \sum_q (-1)^{J-M+I_X-M_X} \delta_{I_T I'_T}\delta_{M_T M'_T} \begin{pmatrix} J & 2 & J \\ -M & -q & M' \end{pmatrix} \begin{pmatrix} I_X & 1 & I_X \\ -M_X & q & M'_X \end{pmatrix}$$

$$\begin{pmatrix} 2 & 1 & 1 \\ -q & q & 0 \end{pmatrix} \left[I_X(I_X+1)(2I_X+1) \right]^{\frac{1}{2}} \langle J \| \sigma^{X(2)}_{an} \| J \rangle \sqrt{5}\, g_X \mu_N H$$

The reduced matrix element can be evaluated with the aid of the Wigner Eckart theorem and then transformed to the molecular frame of reference. The result is

$$\langle \Psi^{\Gamma\xi} | \mu_N g_X \underline{I}_X \cdot \underline{\underline{\sigma}}^X_{an} \cdot \underline{H} | \Psi', \Gamma\xi \rangle =$$

$$= \mu_N g_X H \, (-1)^{J-M+I_X-M_X} \delta_{I_T I_T'} \delta_{M_T M_T'} \delta_{KK'} \frac{1}{3}(\sigma^X_{\parallel} - \sigma^X_{\perp}) \left(\frac{3K^2}{J(J+1)} - 1 \right) \cdot$$

$$\cdot \left[\frac{I_T(I_T+1)(2I_T+1) \cdot 30 J(J+1)(2J+1)}{(2J+3)(2J-1)} \right]^{\frac{1}{2}} \sum_q \begin{pmatrix} J & 2 & J \\ -M & -q & M' \end{pmatrix} \begin{pmatrix} I_T & 1 & I_T' \\ -M_T & q & M_T' \end{pmatrix} \begin{pmatrix} 2 & 1 & 1 \\ -q & q & 0 \end{pmatrix} \tag{3.67b}$$

(i) Magnetic moment of the Y-nuclei

As for the X-nucleus we define the average shielding as

$$\sigma^{A_1}_{av} = \frac{1}{3} (\sigma^{A_1}_{aa} + \sigma^{A_1}_{bb} + \sigma^{A_1}_{cc})$$

and

$$\underline{\underline{\sigma}}^{A_1}_{an} = \underline{\underline{\sigma}}^{A_1}_{Y} - \sigma^{A_1}_{av} \underline{\underline{1}}$$

The E-type tensors have zero trace and so they are already second rank irreducible tensors. Proceeding in the same way as for the X-nucleus we obtain

$$\langle \Psi^{\Gamma\xi} | -\mu_N g_Y \underline{I}_T \cdot \underline{H} (1 - \sigma^{A_1}_{av}) | \Psi', \Gamma\xi \rangle = -\delta_{MM'} \delta_{I_T I_T'} \delta_{M_T M_T'} \delta_{M_X M_X'} \mu_N g_Y H \cdot$$

$$\cdot (1 - \sigma^{A_1}_{av}) \, M_T \tag{3.68a}$$

$$\langle \Psi^{\Gamma\xi} | g_Y \mu_N (\underline{I}_T \cdot \underline{\underline{\sigma}}^{A_1}_{an} \cdot \underline{H} + \underline{I}^{E,1} \cdot \underline{\underline{\sigma}}^{E,1}_{Y} \cdot \underline{H} + \underline{I}^{E,2} \, \underline{\underline{\sigma}}^{E,2}_{Y} \cdot \underline{H}) | \Psi', \Gamma\xi \rangle =$$

$$= g_Y \mu_N H \, (-1)^{J-M+I_T-M_T} \delta_{M_X M_X'} \cdot$$

$$\cdot \left[\left(\frac{3K^2}{J(J+1)} - 1 \right) \delta_{I_T I_T'} \delta_{KK'} \left(\frac{\sigma^Y_{cc}}{3} - \frac{\sigma^Y_{aa} + \sigma^Y_{bb}}{6} \right) + \right.$$

$$\left. + \frac{(-1)^{J+\gamma}}{4} \delta_{K1} (\sigma^Y_{aa} - \sigma^Y_{bb}) \frac{\langle \chi^{E,1}(I_T) \| I^{E,1} \| \chi^{E,2}(I_T') \rangle}{[I_T(I_T+1)(2I_T+1)]^{\frac{1}{2}}} \right] \cdot$$

$$\left[\frac{I_X(I_X+1)(2I_X+1) \cdot 30 J(J+1)(2J+1)}{(2J+3)(2J-1)} \right]^{\frac{1}{2}} \sum_q \begin{pmatrix} J & 2 & J \\ -M & -q & M' \end{pmatrix} \begin{pmatrix} I_X & 1 & I_X \\ -M_X & q & M_X' \end{pmatrix} \begin{pmatrix} 2 & 1 & 1 \\ -q & q & 0 \end{pmatrix}$$

(3.68b)

iv. The coupling constants

In a rotational transition the tensor components T_{aa}, T_{bb} and T_{cc} cannot be measured directly. What can be determined are the so called coupling constants. They are certain linear combinations of the tensor components. From the derived formulae for the matrix elements it is obvious how the coupling constants could be defined. For a general tensor $\underline{\underline{T}}$ we therefore introduce a coupling constant t_{JK} which is given by *)

$$t_{JK} = \tfrac{1}{2}(T_{aa}+T_{bb}) + \frac{K^2}{J(J+1)} (T_{cc} - \tfrac{1}{2}(T_{aa}+T_{bb})) +$$

$$+ \frac{(-1)^{J+\gamma}}{4} \delta_{K1} (T_{aa} - T_{bb}) \frac{\langle \chi^{E,1}(I_T) \| I^{E,1} \| \chi^{E,2}(I_T) \rangle}{[I_T(I_T+1)(2I_T+1)]^{\frac{1}{2}}} \qquad (3.69)$$

For the A_1-type tensors of Eq(3.27) the last term in (3.69) vanishes because $T_{aa}=T_{bb}$ for these tensors. For the traceless tensors in $\mathcal{H}_{hyp}$ we have $T_{aa}+T_{bb}+T_{cc} = 0$.

There are two interactions in the hamiltonian of Eq(3.33) whose coupling constants cannot be described by this formula.

*) The coupling constant is defined diagonal in J,K and I_T.

These interactions are the Y-quadrupole interaction and the spin-spin interaction between the Y-nuclei. For the quadrupole it is obvious from Eqs(3.62a) and (3.62b) to define (diagonal in J,K and I_T)

$$q^Y_{JK} = \left[\frac{3K^2}{J(J+1)} - 1\right] \tfrac{1}{2}(V^Y_{cc} - \tfrac{1}{2}(V^Y_{aa} + V^Y_{bb})) +$$

$$+ \frac{\sum_{I_{23}} |C^{E,1}_{I_{23}}(I_T)|^2 (-1)^{2I_Y} \begin{Bmatrix} I_T & 2 & I_T \\ I_Y & I_{23} & I_Y \end{Bmatrix}}{\sum_{I_{23}} |C^{E,1}_{I_{23}}(I_T)|^2 (-1)^{I_{23}} \begin{Bmatrix} I_T & 2 & I_T \\ I_Y & I_{23} & I_Y \end{Bmatrix}} \frac{(-1)^{J+\gamma}}{4} \delta_{K,1}(V^Y_{aa} - V^Y_{bb}) \tag{3.70}$$

and for the YY-spin-spin interaction from Eq(3.65)

$$d^{YY}_{JK} = \frac{\mu_o \mu_N^2 g_Y^2}{4\pi r^3_{YY}} \left[\tfrac{1}{2}\left(\frac{3K^2}{J(J+1)} - 1\right) - (-1)^{J+\gamma}\delta_{K1}\frac{3}{4} \frac{\langle \chi^{E,1}(I_T) \| II^{E,1(2)} \| \chi^{E,2}(I_T)\rangle}{\langle \chi^{E,1}(I_T) \| II^{A_1(2)} \| \chi^{E,1}(I_T)\rangle}\right] \tag{3.71}$$

The coupling constants for $I_Y = \frac{1}{2}$ are given in Appendix II.

3.2 THE ASYMMETRIC ROTOR

An asymmetric rotor molecule is a molecule which has three different inertial moments in the principle axis system. Measurements have been performed on two asymmetric rotor molecules, D_2O and SO_2. The hamiltonian for the first molecule contains the same interactions as $\mathcal{H}_{hyp}$ in Eq(3.26). The matrix elements in the case of D_2O are calculated by Verhoeven (VER 69).

The hamiltonian of SO_2 is very simple because of the absence of nuclear spins. In the electronic and vibrational ground state of the molecule, and in external magnetic field $\underline{H}$ the

(Zeeman) hamiltonian $\mathcal{H}_Z$ is

$$\mathcal{H}_Z = -\mu_N \underline{H}.\underline{\underline{G}}.\underline{J} - \tfrac{1}{2}\, \underline{H}.\underline{\underline{\chi}}.\underline{H}$$

The magnetic coupling constants ($g_{J\tau}$ and $\chi_{J\tau}$) for an asymmetric top molecule in a rotational state J_τ are usually defined as

$$g_{J\tau} = \sum_\alpha \frac{g_{\alpha\alpha} \langle J_\alpha^2 \rangle}{J(J+1)} \qquad (3.72)$$

and

$$\chi_{J\tau} = \sum_\alpha \frac{\langle J_\alpha^2 \rangle}{J(J+1)} \left(\chi_{\alpha\alpha} - \chi_{av}\right) \qquad (3.73)$$

where the sum over α runs over the principle axes of the molecule and $\langle J_\alpha^2 \rangle$ is the expectation value of J_α^2 in the state J_τ .

The matrix elements can be written as

$$\langle J_\tau M | \mathcal{H}_Z | J_\tau M' \rangle = \delta_{MM'} \cdot \left[-M g_{J\tau} \mu_N H - \tfrac{1}{2} \chi_{av} H^2 + \frac{3M^2 - J(J+1)}{(2J+3)(2J-1)} \chi_{J\tau} H^2 \right] \qquad (3.74)$$

3.3 THE INTERNAL ROTOR

3.3.1 The hyperfine and Zeeman hamiltonian

The hyperfine hamiltonian for an internal rotor with one degree of freedom for the field free case and in the absence of nuclear vibrations has been developed by Heuvel (HEU 72). The main difference between a rigid rotor and an internal rotor is that in the latter case the velocity $\dot{\underline{r}}_K$ of a nucleus K depends not only upon the overall velocity of the nuclear frame but also upon the internal angular velocity $\dot{\alpha}$, where α is the angle between the two parts of the molecule rotating with respect to each other. For a molecule with only one degree of freedom an axis $\underline{\lambda}$ and for each nucleus a vector $\underline{\sigma}_K$ can be found such that $\underline{\sigma}_K . \underline{\lambda} = 0$ and

$$\dot{\underline{r}}_K = \underline{\omega} \times \underline{r}_K + \dot{\alpha}\, \underline{\lambda} \times \underline{\sigma}_K \qquad (3.75)$$

In this equation $\underline{\omega}$ is the overall angular velocity and $\underline{r}_K$ the position of the K-th nucleus with respect to the center of mass of the molecule. Let m_K be the mass of the K-th nucleus then the overall inertia tensor of the molecule is

$$I_{gg'} = \sum_K m_K (r_K^2 \delta_{gg'} - r_{Kg} r_{Kg'}) \tag{3.76}$$

This tensor is called $\underline{\underline{I}}^{rr}$ in (HEU 72). The quantities F, $\underline{\rho}$, and $\underline{\underline{A}}$ defined by Heuvel can be written as

$$\underline{\underline{A}} \equiv \tfrac{1}{2} (\underline{\underline{I}})^{-1} \tag{3.77a}$$

$$\underline{\rho} \equiv 2 \underline{\underline{A}} \cdot \sum_K m_K (\underline{\sigma}_K \times \underline{\lambda}) \times \underline{r}_K \tag{3.77b}$$

$$\frac{1}{F} \equiv \sum_K 2 m_K \sigma_K^2 - 2 \underline{\rho} . \underline{\underline{I}} . \underline{\rho} \tag{3.77c}$$

The equations (3.77b) and (3.77c) follow from the definitions of Heuvel by substituting therein the various inertia tensors. Furthermore it is customary to define an effective rotational tensor via

$$A^{eff}_{gg'} \equiv A_{gg'} + F \rho_g \rho_{g'} \tag{3.77d}$$

Then the rotational hamiltonian in Eq(8) of (HEU 72) is equal to

$$\mathcal{H}_{rot} = \underline{R} . \underline{\underline{A}}^{eff} . \underline{R} + F P^2 + 2F \underline{\rho} . \underline{R} P + V(\alpha) \tag{3.78}$$

where $\underline{R}$ is the nuclear contribution to the overall angular momentum and P the nuclear contribution to the internal angular momentum, $V(\alpha)$ is the hindering potential. The advantage of Eq(3.78) above Eq(8) of (HEU 72) is that the coupling between $\underline{R}$ and P is more obvious, but moreover the calculation of the hyperfine operators is easier.

For the overall angular velocity $\underline{\omega}$ and the internal angular velocity $\dot{\alpha}$ we obtain

$$\underline{\omega} = 2\ \underline{\underline{A}}^{eff}.\underline{R} + 2\ F\ \underline{\rho}\ P \tag{3.79b}$$

$$\dot{\alpha} = 2\ F\ \underline{\rho}.\underline{R} + 2\ F\ P \tag{3.79b}$$

The angular momentum $\underline{R}$ is the difference of the total angular momentum $\underline{J}$ and the electronic angular momentum $\underline{L}$. We get for $\mathcal{H}_{rot}$

$$\mathcal{H}_{rot} = \underline{J}.\underline{\underline{A}}^{eff}.\underline{J} + F\ P^2 + 2\ F\ \underline{\rho}.\underline{J}\ P - 2\underline{L}.\underline{\underline{A}}^{eff}.J - 2F\underline{\rho}.\underline{L}\ P + \\ + V(\alpha) + \underline{L}.\underline{\underline{A}}^{eff}.\underline{L} \tag{3.80}$$

For $^1\Sigma$-molecules $\langle\underline{L}\rangle = 0$ and we approximate

$$\underline{\omega} = 2\ \underline{A}^{eff}.\underline{J} + 2P\ F\ \underline{\rho} \tag{3.81a}$$

$$\dot{\alpha} = 2\ F\ \underline{\rho}.\underline{J} + 2P\ F \tag{3.81b}$$

The last term in $\mathcal{H}_{rot}$ shifts all rotational energy levels in a certain electronic state by the same amount and is therefore not observable in rotational transitions. The fourth and fifth term in Eq(3.80) are zero in first order in $^1\Sigma$-molecules. The second order contributions of these terms, however are not negligible. The hamiltonian can therefore be written as

$$\mathcal{H}_{rot} = \mathcal{H}_1 + \mathcal{H}_2 + V(\alpha) \tag{3.82a}$$

$$\mathcal{H}_1 = \underline{J}.\underline{\underline{A}}^{eff}.\underline{J} + 2F\ \underline{\rho}.\underline{J}\ P + F\ P^2 \tag{3.82b}$$

$$\mathcal{H}_2 = -2\underline{L}.\underline{\underline{A}}^{eff}.\underline{J} - 2F\ \underline{\rho}.\underline{L}\ P \tag{3.82c}$$

The spin-rotation and spin-spin interaction are discussed by Heuvel. Therefore we treat only the magnetic interactions. The

important magnetic interactions are discussed by many authors. For the present treatment we shall follow Verhoeven (VER 69). The relevant interactions are

$$h_1 = -\frac{e}{4}\sum_K Z_K \underline{H}.\underline{r}_K \times \dot{\underline{r}}_K + \frac{e}{4}\sum_i \underline{H}.\underline{r}_i \times \underline{v}_i \qquad (3.83a)$$

$$h_2 = \frac{e^2}{8m}\sum_i (\underline{H}\times\underline{r}_i).(\underline{H}\times\underline{r}_i) \qquad (3.83b)$$

$$h_3 = \frac{\mu_o}{4\pi}\frac{e^2}{2m}\sum_{i,K}(\underline{H}\times\underline{r}_i).\frac{g_K\mu_N\underline{I}_K\times\underline{r}_{iK}}{r_{iK}^3} \qquad (3.83c)$$

$$h_4 = \frac{e\mu_o\mu_N}{4\pi}\left[\sum_{i,K} g_K \frac{\underline{r}_{ik}\times(\underline{v}_i - \gamma_K\underline{r}_K).\underline{I}_K}{r_{iK}^3} - \right. \qquad (3.83d)$$

$$\left. - \sum_{L>K} Z_L\, g_K \frac{\underline{r}_{LK}\times(\dot{\underline{r}}_L - \gamma_K\dot{\underline{r}}_L)}{r_{LK}^3}\right]$$

In these equations $Z_K, g_K, \underline{I}_K, \underline{r}_K$ and $\dot{\underline{r}}_K$ are the number of protons, the nuclear g-factor, the nuclear spin, position in the CM system and velocity of the K-th nucleus respectively, $-e, m, \underline{r}_i$ and $\underline{v}_i$ the charge, mass, position in the CM-system and velocity of the i-th electron respectively, μ_N is the nuclear magneton, and $\underline{H}$ the magnetic field. The sum over K and L runs over all nuclei, the sum over i runs over all electrons.

The first term describes the interaction of the magnetic field $\underline{H}$ with the rotating charges of nuclei and electrons in the molecule. The second term represents the interaction of the magnetic field with the induced magnetic moment; this term has also a nuclear contribution, but this contribution is negligible. The term h_3 gives the interaction of the magnetic moment of the K-th nucleus with the molecular charge distribution disturbed by the external field. Again the nuclear part of

this interaction is neglected. The last term is simply the interaction of the nuclear magnetic moment with the magnetic field produced by the rotating charges in the molecule.

The terms in h_1, h_2, h_3, and h_4 can be worked out using the equations for $\dot{\underline{r}}_K$, $\underline{\rho}$ and $\dot{\alpha}$.

For the first term we get

$$h_1 = - \mu_N \underline{H}.\underline{\underline{G}}^{(n)}.\underline{J} - \mu_N \underline{H}.\underline{g}^{(n)} P + \mu_B \underline{H}.\underline{L} \qquad (3.84)$$

where $\underline{\underline{G}}^{(n)}$ is the nuclear contribution to the G-tensor due to the overall rotation of the molecule, and $\underline{g}^{(n)}$ the contribution to the g-vector due to the internal rotation. We have

$$G^{(n)}_{gg'} = \frac{e}{2\mu_N} \sum_K Z_K \left[\sum_{g''} (r_K^2 \delta_{gg''} - r_{Kg} r_{Kg''}) A^{eff}_{g''g'} + \right.$$
$$\left. + (\underline{r}_K.\underline{\lambda})\ \sigma_{Kg} F \rho_{g'} - (\underline{r}_K.\underline{\gamma}_K) \lambda_g F \rho_{g'} \right] \qquad (3.85)$$

$$\underline{g}^{(n)} = \frac{e}{2\mu_N} \sum_K Z_K F \left[r_K^2 \underline{\rho} - (\underline{r}_K.\underline{\rho}) \underline{r}_K + (\underline{r}_K.\underline{\lambda}) \underline{\sigma}_K - (\underline{r}_K.\underline{\sigma}_K) \underline{\lambda} \right] \qquad (3.86)$$

The third term in h_1 is zero in first order for $^1\Sigma$-molecules, however the second order contribution of this term to the hyperfine energy is important.

The interaction h_2 of Eq(3.83b) is of purely electronic origin. If $|o\rangle$ denotes the electronic $^1\Sigma$-state then the first order contribution of h_2 to the energy is

$$\langle o|h_2|o\rangle = -\tfrac{1}{2}\ \underline{H}.\underline{\underline{\chi}}^{(d)}.\underline{H} \qquad (3.87)$$

where the cartesian components of the diamagnetic susceptibility tensor $\underline{\underline{\chi}}^{(d)}$ are given by

$$\chi^{(d)}_{gg'} = \frac{e^2}{4m} \langle 0| \sum_i r_{ig} r_{ig'} - r_i^2 \delta_{gg'} |0\rangle \qquad (3.88)$$

The higher order contributions of h_2 may be neglected.

The first order contribution due to h_3 can be written as

$$\langle o|h_3|o\rangle = \sum_K g_K \mu_N \underline{I}_K \cdot \underline{\underline{\sigma}}_K^{(d)} \cdot \underline{H} \qquad (3.89)$$

Herein $\underline{\underline{\sigma}}_K^{(d)}$ is the diamagnetic shielding tensor of the K-th nucleus. Its cartesian components are given by

$$\sigma_{gg'}^{(d)} = \frac{\mu_o e^2}{8\pi m} \langle o| \sum_i \frac{(\underline{r}_i \cdot \underline{r}_{iK})\delta_{gg'} - r_{ig} r_{iKg'}}{r_{iK}^3} |o\rangle \qquad (3.90)$$

Higher order terms are negligible.

The terms in Eq(3.83d) can be rewritten as

$$h_4 = \frac{\mu_o e \mu_N}{4\pi} \sum_{i,K} g_K \frac{(\underline{r}_{iK} \times \underline{v}_i) \cdot \underline{I}_K}{r_{iK}^3} + \sum_K \underline{I}_K \cdot (\underline{M}_K^{(n)} \cdot \underline{J} + \underline{m}_K^{(n)P+M_K^{(e1)}} \cdot \underline{J} + \underline{m}_K^{(e1)P}) \qquad (3.91)$$

The first term in Eq(3.91) is zero in first order in the electronic $^1\Sigma$-state as shown by Gunther Mohr et al (GUN 54), the other terms in this equation have been treated by Heuvel. We find

$$M_{Kgg'}^{(n)} = \frac{-e\mu_o \mu_N g_K}{4\pi} \sum_{L \neq K} \frac{Z_L}{r_{LK}^3} \left[\sum_{g''} \{ (\underline{r}_{LK} \cdot \underline{r}_L - \gamma_K \underline{r}_{LK} \cdot \underline{r}_K) \delta_{gg''} - (r_{Lg} - \gamma_K r_{Kg}) r_{LKg''} \} A_{g''g'}^{eff} + \{ (\underline{r}_{LK} \cdot \underline{\lambda})(\sigma_{Lg} - \gamma_K \sigma_{Kg}) - \underline{r}_{LK} \cdot (\underline{\sigma}_L - \gamma_K \underline{\sigma}_K) \lambda_g \} R_{g'} \right] \qquad (3.91)$$

$$\underline{m}_K^{(n)} = - \frac{e\mu_o \mu_N g_K F}{4\pi} \sum_{L \neq K} \frac{Z_L}{r_{LK}^3} \left[(\underline{r}_{LK} \cdot \underline{r}_L)\underline{\rho} - \gamma_K (\underline{r}_{LK} \cdot \underline{r}_K)\underline{\rho} - (\underline{r}_{LK} \cdot \underline{\rho})(\underline{r}_L - \gamma_K \underline{r}_K) + (\underline{r}_{LK} \cdot \underline{\lambda})(\underline{\sigma}_L - \gamma_K \underline{\sigma}_K) - \{ (\underline{r}_{LK} \cdot \underline{\sigma}_L) + \gamma_K (\underline{r}_{LK} \cdot \underline{\sigma}_K) \} \cdot \underline{\lambda} \right] \qquad (3.92)$$

$$M^{(e1)}_{Kgg'} = -\frac{e\mu_o\mu_N g_\lambda \gamma_K}{4\pi} \sum_i \langle o| \sum_{g''} \{(\underline{r}_{iK}\cdot\underline{r}_K)\delta_{gg''} - r_{iKg} r_{iKg''}\} A^{eff}_{g''g'} +$$

$$+ F\{(\underline{r}_{iK}\cdot\underline{\lambda})\sigma_{kG} - (\underline{r}_{LK}\cdot\underline{\sigma}_K)\lambda_g\}\rho_{g'} r^{-3}_{iK}|o\rangle \qquad (3.93)$$

$$\underline{m}^{(e1)}_K = -\frac{e\mu_o\mu_N g_K \gamma_K F}{4\pi} \sum_i \langle o| r^{-3}_{iK} (\underline{r}_{iK}\cdot\underline{r}_K)\underline{\rho} - (\underline{r}_{iK}\cdot\underline{\rho})\underline{r}_K +$$

$$+ (\underline{r}_{LK}\cdot\underline{\lambda})\underline{\sigma}_K - (\underline{r}_{LK}\cdot\underline{\sigma}_K)\underline{\lambda}|o\rangle \qquad (3.94)$$

So far we discussed only the operators that give first order electronic contributions. The terms in the total hamiltonian giving important second order contributions can be taken from Eq(3.82c), (3.84) and (3.91). They are $\mathcal{H}_2$ and

$$h^{(2)}_1 = \mu_B \underline{L}\cdot\underline{H} \qquad (3.95)$$

$$h^{(2)}_4 = \frac{e\mu_o\mu_N}{4\pi} \sum_{i,K} g_K \frac{(\underline{r}_{iK}\times\underline{v}_i)\cdot\underline{I}_K}{r^3_{iK}} \qquad (3.96)$$

The second order contributions are of the form

$$\sum_n \left[\langle o|h_p|n\rangle\langle n|h_q|o\rangle + (1-\delta_{pq})\langle o|h_q|n\rangle\langle n|h_p|o\rangle\right] (E_o - E_n)^{-1} \qquad (3.97)$$

where h_p and h_q are two of the operators of Eq.(3.82c), (3.95) or (3.96). The summation runs over all excited electronic states $|n\rangle$ with energy E_n. The second term in the Eq(3.97) is the complex conjugate, abbreviated as c.c., of the first term. The term for $h_p = h_q = \mathcal{H}_2$ gives no contribution to the hyperfine structure and therefore will not be considered. The remaining second order effects are

$$\mathcal{H}^{(2)} = -\mu_N(\underline{H}.\underline{\underline{G}}^{(e)}.\underline{J} + \underline{H}.\underline{g}^{(e)}P) - \tfrac{1}{2}\,\underline{H}.\underline{\underline{\chi}}^{(p)}.\underline{H} + \sum_K g_K\mu_N\underline{H}.\underline{\underline{\sigma}}_K^{(p)}.\underline{I}_K$$

$$+ \sum_K \{\underline{I}_K.\underline{\underline{M}}_K^{(e2)}.\underline{J} + \underline{I}_K.\underline{m}_K^{(e2)}P + \sum_{L>K} \underline{I}_K.\underline{\underline{D}}_{KL}^{(e)}.\underline{I}_L\} \qquad (3.98)$$

The various tensors and vectors are defined as

$$G_{gg'}^{(e)} = \frac{2\mu_B}{\mu_N}\sum_n [\langle o|L_g|n\rangle\langle n|\sum_{g''} L_{g''}A_{g''g'}^{eff}|o\rangle + c.c\,]/(E_o-E_n) \qquad (3.99)$$

This tensor is the electronic contribution to the overall molecular G-tensor. It is due to the second order effect of the first term in $\mathcal{H}_2$ and $h_1^{(2)}$. The second term in $\mathcal{H}_2$ combined with $h_1^{(2)}$ gives the electronic contribution to the g-vector due to the internal rotation:

$$\underline{g}^{(e)} = \frac{2\mu_B}{\mu_N}\sum_n [\langle o|\underline{L}|n\rangle\langle n|F\underline{\rho}.\underline{L}|o\rangle + c.c.\,]/(E_o-E_n) \qquad (3.100)$$

The paramagnetic susceptibility $\underline{\underline{\chi}}^{(p)}$ originates in the second order effect of $h_1^{(2)}$. The cartesian components are given by

$$\chi_{gg'}^{(p)} = -2\mu_B^2 \sum_n \langle o|L_g|n\rangle\langle n|L_{g'}|o\rangle/(E_o-E_n) \qquad (3.101)$$

The paramagnetic nuclear shielding of the K-th nucleus is due to the effect of $h_1^{(2)}$ and $h_4^{(2)}$. Here the cartesian components are

$$\sigma_{Kgg'}^{(p)} = \frac{e\mu_o\mu_B}{4\pi}\sum_n [\langle o|L_g|n\rangle\langle n|\sum_i r_{iK}^{-3}(\underline{r}_{iK}\times\underline{v}_i)_{g'}|o\rangle + c.c.]/(E_o-E_n) \qquad (3.102)$$

The second order electronic contribution to the overall spin-rotation tensor of the K-th nucleus $\underline{\underline{M}}_K^{(e2)}$ comes from the first

term of $\mathcal{H}_2$ combined with $h_4^{(2)}$. The cartesian components for this tensor are

$$M^{(e2)}_{Kgg'} = \frac{-e\mu_o\mu_N g_K}{2\pi} \sum_n \langle o| \sum_{g''} L_{g''} A^{eff}_{g''g'} |n\rangle\langle n| \sum_i r_{iK}^{-3} (\underline{r}_{iK} \times \underline{v}_i)_g |o\rangle + c.c.]/(E_o - E_n) \tag{3.103}$$

The second term in $\mathcal{H}_2$ combined with $h_4^{(2)}$ gives the second order contribution to the spin-internal rotation vector

$$\underline{m}^{(e2)}_K = \frac{-e\mu_o\mu_N g_K}{2} \sum_n [\langle o|F\underline{\rho}.\underline{L}|n\rangle\langle n|\sum_i r_{iK}^{-3}(\underline{r}_{iK}\times\underline{v}_i)|o\rangle + c.c.]/(E_o - E_n) \tag{3.104}$$

The last term in Eq(3.98) is the so called electron coupled spin-spin interaction, due to the second order effect of $h_4^{(2)}$. For this tensor we have

$$D^{(e)}_{KLgg'} = \frac{e^2\mu_o^2\mu_N^2 g_K g_L}{16\pi^2} \sum_n [\langle o| \sum_i r_{iK}^{-3}(\underline{r}_{iK}\times\underline{v}_i)_g |n\rangle\langle n| \sum_i r_{iL}^{-3}(\underline{r}_{iL}\times\underline{v}_i)_{g'} |o\rangle + c.c.]/(E_o - E_n) \tag{3.105}$$

This term is usually neglegible, except for large nuclei. A more important contribution to the spin-spin interaction is via the contact interaction. This interaction, however, will not be discussed here.

The interactions in Eqs(3.83) do not completely describe the Zeeman and hyperfine structure of the molecule. If no nuclear quadrupoles are present, then the additional terms to the Zeeman and hyperfine interactions are the direct spin-spin interaction between the nuclear magnetic moments, and the interactions of the nuclear magnetic moments with the external field. These interactions can be written as

$$h_6 = \sum_{K>L} \underline{I}_K . \underline{\underline{D}}^{(n)}_{KL} . \underline{I}_L \tag{3.106}$$

$$h_7 = \sum_K -\mu_N g_K \underline{I}_K . \underline{H} \tag{3.107}$$

The spin-spin interaction tensor $\underline{\underline{D}}_{KL}^{(n)}$ is given in Table 5.1. The total hyperfine and Zeeman hamiltonian due to h_1 through h_7 can be written as

$$\mathcal{H}_{hyp} = \sum_K \underline{I}_K \cdot (\underline{\underline{M}}_K \cdot \underline{J} + \underline{m}_K P) + \sum_{K>L} \underline{I}_K \cdot \underline{\underline{D}}_{KL} \cdot \underline{I}_L -$$

$$- \mu_N \underline{H} \cdot (\underline{\underline{G}} \cdot \underline{J} + \underline{g} P) - \tfrac{1}{2} \underline{H} \cdot \underline{\chi} \cdot \underline{H} - \sum_K g_K \mu_N \underline{I}_K \cdot (1 - \underline{\underline{\sigma}}_K) \cdot \underline{H} \tag{3.108}$$

In this equation the vectors and tensors are defined as

$$\underline{\underline{M}}_K \equiv \underline{\underline{M}}_K^{(n)} + \underline{\underline{M}}_K^{(e1)} + \underline{\underline{M}}_K^{(e2)} \tag{3.109a}$$

$$\underline{m}_K \equiv \underline{m}_K^{(n)} + \underline{m}_K^{(e1)} + \underline{m}_K^{(e2)} \tag{3.109b}$$

$$\underline{\underline{D}}_{KL} \equiv \underline{\underline{D}}_{KL}^{(n)} + \underline{\underline{D}}_{KL}^{(e)} \tag{3.109c}$$

$$\underline{\underline{G}} \equiv \underline{\underline{G}}^{(n)} + \underline{\underline{G}}^{(e)} \tag{3.109d}$$

$$\underline{g} \equiv \underline{g}^{(n)} + \underline{g}^{(e)} \tag{3.109e}$$

$$\underline{\chi} \equiv \underline{\chi}^{(d)} + \underline{\chi}^{(p)} \tag{3.109f}$$

$$\underline{\underline{\sigma}}_K \equiv \underline{\underline{\sigma}}_K^{(d)} + \underline{\underline{\sigma}}_K^{(p)} \tag{3.109g}$$

The hamiltonian $\mathcal{H}_{hyp}$ differs from the hamiltonian for a rigid rotor, as can be seen by comparison of Eq(3.26) and (3.108). Apart from the fact that the tensors in Eq(3.108) are functions of α, there are two additional terms in the hamiltonian caused by the internal rotation, e.g. the vectors in Eq(3.109b) and (3.109e).

The examined internal rotors are hydrogen peroxyde and

methyl alcohol. The H_2O_2-molecule has a twofold potential barrier shown in Fig. 3.3, and CH_3OH a threefold barrier. Both molecules, however, can be described (in first order) by symmetric top wave functions (HUN 64, HEU 72) such that the matrix elements are basically the same as for the symmetric rotor.

The methyl alcohol molecule is discussed in detail by Heuvel in zero field. Expressions for the matrix elements and the coupling constants can be found in (HEU 72). In this chapter we shall restrict ourselves to hydrogen peroxyde.

3.3.2 Hydrogen peroxyde

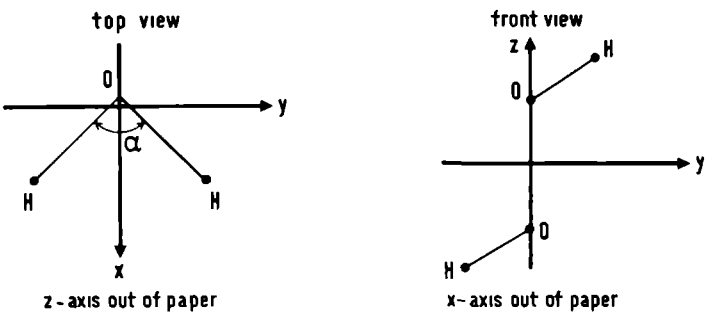

FIG.3.2 The geometry of the hydrogen peroxyde molecule.

The geometry of the molecule is shown in Fig. (3.2). The molecule fixed c-axis is chosen along the O-O bond. The a-axis is defined as the bissectrix of the projection of the OH bars on a plane perpendicular to the c-axis through the center of mass of the molecule.

The b-axis is chosen so that the system abc becomes right-handed.

The internal rotation in H_2O_2 is due to the relative motion of the OH-bars with respect to each other. This rotation is hindered by two interactions: the repulsion of the dipole moments of the OH bars and the interaction with the two non-bonding pairs of p-electrons associated with the oxygen atoms. The potential energy $V(\alpha)$ is given in Fig.3.3 as a function of α, the angle between the projection of the OH-bars in the

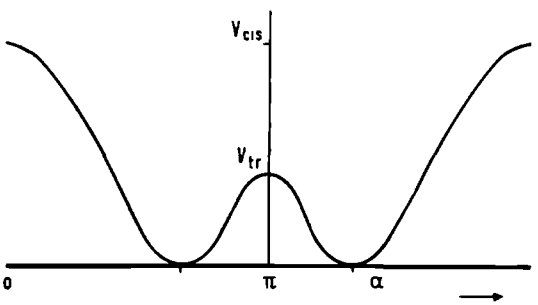

FIG. 3.3 The internal rotor potential in H_2O_2 as a function of the internal rotor angle α.

bc-plane. The situation when $\alpha=\pi$ is called the trans-position, while for $\alpha=0$ the molecule is in the cis-position. The corresponding barrier heights in the potential are V_{trans} and V_{cis}. They have been determined by Hunt *et al* (HUN 64), while the angle α_e, where the potential reaches its minimum, was obtained by Oelfke and Gordy (OEL 69)

$$V_{trans} = 386 \text{ cm}^{-1}$$

$$V_{cis} = 2460 \text{ cm}^{-1}$$

$$\alpha_e = 118^{\circ}4' \text{ *)}$$

*) This value is the average value of α_e in the states $\tau=1,2$ and $\tau=3,4$

In the abc-frame there is a coupling in the rotational hamiltonian between the internal rotation and the overall rotation (HUN 64). This coupling can be removed by applying a small rotation about the a-axis. Then the hamiltonian becomes (HUN 64)

$$\mathcal{H} = \mathcal{H}_{rot} + \mathcal{H}_{int} \tag{3.110a}$$

$$\mathcal{H}_{rot} = A(\alpha)J^2 + C(\alpha)J_c^2 + B(\alpha)(J_a^2+J_b^2) + D(\alpha)(J_bJ_c-J_cJ_b) \tag{3.110b}$$

$$\mathcal{H}_{int} = f(\alpha)P^2 + V(\alpha) \tag{3.110c}$$

The rotational constants A,B,C, and D all are functions of α. The constants B and D are very sensitive to α. Fortunately the dominant terms in the expression for $\mathcal{H}_{rot}$ are $A(\alpha)$ and $C(\alpha)$, which are in first order independent of α. Consequently the zeroth order basis functions of $\mathcal{H}_{rot}$ are the functions $|JKM\rangle$ discussed in Sect. 3.1.1. The basis functions for the overall plus internal rotation are then the $|JKM\rangle M(\alpha)$, where $M(\alpha)$ is a solution of the equation

$$\mathcal{H}_{int}M(\alpha) = E_{int}M(\alpha) \tag{3.111}$$

The hamiltonian $\mathcal{H}_{int}$ is invariant under a reflection in the trans plane σ(trans) and under a reflection in the cis-plane σ(cis). These reflections can be expressed in α:

$$\sigma(trans): \alpha \rightarrow 2\pi - \alpha \tag{3.112a}$$

$$\sigma(cis) : \alpha \rightarrow -\alpha \tag{3.112b}$$

In addition the molecule is invariant if one of the two OH-bars is rotated over 2π, while the other one is fixed. If ψ,ϑ,φ are the Euler angles of the molecule then the operation that describes this is given by (ELL 75)

$$C_{2c}: \varphi \rightarrow \varphi + (n_1+n_2)\pi \qquad (3.112c)$$
$$\alpha \rightarrow \alpha + (n_1-n_2)2\pi$$

Here one of the OH bars is rotated over $n_1 2\pi$, while the other one is rotated over $n_2 2\pi$. Because the molecule is invariant under this transformation, the total wavefunction has to be invariant too. The transformation of the $|JKM\rangle$ under C_{2c} (see Sect. 3.1.1) then requires for the internal rotor function $M(\alpha)$

$$M(\alpha) = e^{-iK\alpha/2} N(\alpha)$$

where N is a function of α with period 2π. The operations α(trans) and α(cis) leave $\mathcal{H}_{int}$ invariant and therefore complex numbers c_t and c_c can be found with $|c_t|=|c_c|= 1$ and

$$\sigma(\text{trans})\ M(\alpha) = c_t\ M(\alpha)$$
$$\sigma(\text{cis})\ M(\alpha) = c_c\ M(\alpha),$$

Furthermore

$$\sigma(\text{trans})^2 = \sigma(\text{cis})^2 = 1 : \alpha \rightarrow \alpha$$

$$\sigma(\text{trans})\sigma(\text{cis}) : \alpha \rightarrow \alpha - 2\pi$$

So

$$c_t = \pm 1$$
$$c_c = \pm 1$$
$$c_t\ c_c = (-1)^K$$

The wavefunctions for the internal rotation can now be classified according to their symmetry under these operations. The quantum number τ which describes this symmetry is given in Table 3.4. The states with a certain τ are ordered by the principal quantum number n (n=0 for the ground state and can further take integral values 1,2, . . . ordered in ascending energy). All measurements were performed in the n=0 state.

In addition to the symmetry operations described above, the molecule is invariant under a rotation about the a-axis over π. This interaction interchanges the two protons in the molecule, and the Pauli principle then implies that the wavefunction is antisymmetric under this operation. The antisymmetric spin function corresponds with total proton spin zero, while the symmetric spinfunction has total spin one. The total hydrogen spin in a particular state is given in Table 3.4.

J	Overall rot. state	int. rot. state	total spin hydr.nucl.
even	Ψ_{JK+}	$\tau = 1,2$	0
	Ψ_{JK-}	$\tau = 1,2$	1
	Ψ_{JK+}	$\tau = 3,4$	1
	Ψ_{JK-}	$\tau = 3,4$	0
odd	Ψ_{JK+}	$\tau = 1,2$	1
	Ψ_{JK-}	$\tau = 1,2$	0
	Ψ_{JK+}	$\tau = 3,4$	0
	Ψ_{JK-}	$\tau = 3,4$	1

Table 3.4. The H_2O_2 wavefunction and its spin symmetry.

More details about the wavefunction can be found in (HUN 64, ELL 75).

We mentioned in the beginning of this section that the coupling between $\underline{J}$ and P in H_2O_2 can be removed by a small rotation about the a-axis. This rotation is called a contact transformation. In the present notation this contact transfor-

mation implies that the term

$$\sum_K m_K (\underline{\sigma}_K \times \underline{\lambda}) \times \underline{r}_K = \underline{\underline{I}} \cdot \underline{\rho} \qquad (3.113)$$

given in Eq(3.77b) becomes zero in the new reference frame, as is shown in Appendix III.This causes severe implications upon the hyperfine hamiltonian of Eq(3.108). If we substitute zero for the term in Eq(3.113) in the tensors derived in Sect. 3.3.1 we have from Eq(3.100)

$$\underline{g}^{(e)} = 0$$

and from Eq(3.86)

$$\underline{g}^{(n)} = \frac{eF}{2\mu_N} \sum_K Z_K (\underline{\sigma}_K \times \underline{\lambda}) \times \underline{r}_K$$

Under the inversion operator the vector $\underline{g}^{(n)}$ transforms into $-\underline{g}^{(n)}$. Hence the first order contribution due to this term is zero, and the term $\underline{H}.\underline{g}$ P in Eq(3.108) vanishes in first order.

The matrix elements of $\mathcal{H}_{hyp}$ and the coupling constants are given in (ELL 75).

C H A P T E R 4

MEASUREMENTS

This chapter, like the previous one, is divided into three sections according to the class of molecules. Section 4.1 deals with the symmetric rotor molecules: ammonia $^{14}NH_3$, fluoroform CF_3H, and methyl chloride CH_3Cl. In Sect. 4.2 the asymmetric rotors D_2O and SO_2 are discussed. The last section contains the results for the internal rotors hydrogen peroxyde and methyl alcohol.

The hyperfine and Zeeman matrices for a rotational state under study were calculated using the expressions for the matrix elements of the various hyperfine and Zeeman operators derived in Chap.3. To prevent errors the Zeeman matrix was calculated numerically by a digital IBM 370/155 computer.

The transition frequencies $\nu_c(i)$ were calculated by diagonalizing the Zeeman hamiltonian for both levels involved in a transition. These frequencies were compared with the observed frequencies $\nu_o(i)$ and their uncertanties $\Delta\nu_o(i)$ in the function

$$\chi^2 = \sum_i \frac{(\nu_c(i) - \nu_o(i))^2}{(\Delta\nu_o)^2} \qquad (4.1)$$

where i runs over all observed frequencies.

The absolute minimum of χ^2 is found by means of a least squares fit of the coupling constants. This procedure is described by Bluyssen (BLU 68). The error in the coupling constant is the amount by which the coupling constant has to be increased or decreased, in order that χ^2 increases with one. For those constants that depend upon the magnetic field the ultimate error

depends upon the homogeneity of the field. For the super conducting magnet the ultimate error is one part in 1000 for linear effects and two parts in 1000 for quadratic, for the Bruker magnet the errors are ten times smaller.

molecule	transition	zero field	low field	high field
	$J_K \quad J'_{K'}$			
NH_3	$2_{2u} \quad 2_{2l}$	no	no	$\Delta M=\pm 1,0$
	$2_{1u} \quad 2_{1l}$	no	no	$\Delta M=0$
CF_3H	$1_o \quad 0_o$	yes	$\Delta M=\pm 1$	$\Delta M=0$
	$2_1 \quad 1_1$	yes	no	$\Delta M=0$
CH_3Cl	$1_o \quad 0_o$	yes	$\Delta M=\pm 1$	$\Delta M=0$
D_2O	$3_{-2} \quad 2_2$	no	no	$\Delta M=0$
SO_2	$2_{-2} \quad 1_0$	yes	$\Delta M=\pm 1$	no
	$4_{-4} \quad 3_{-2}$	yes	$\Delta M=\pm 1$	no
H_2O_2	$1_{1-2} \quad 0_{04}$	yes	$\Delta M=\pm 1$	no
	$2_{1-2} \quad 1_{04}$	yes	$\Delta M=\pm 1$	no
CH_3OH	$2_2 \quad 2_1$	yes	$\Delta M=\pm 1$	no
	$3_2 \quad 3_1$			
	$4_2 \quad 4_1$			

Table 4-1 Survey of the observed transitions.

Table 4.1 gives a survey of the performed experiments.

4.1 SYMMETRIC TOP MOLECULES

4.1.1 Ammonia $^{14}NH_3$

Zero field beam maser measurements on a large number of inversion transitions have been performed by Kukolich (KUK 67, 70), employing a Ramsey configuration of the stimulating field. This configuration allows a very accurate determination of the hyperfine transitions. An extension of the theory to include centrifugal distortion effects upon the nitrogen quadrupole interaction enabled Hougen (HOU 72) to refit these spectra, thereby removing the previous discrepancies between the calculated and the observed spectrum.

Zeeman experiments on the $\Delta M=\pm 1$ transitions at low magnetic fields were done by Kukolich (KUK 70a), and by Verhoeven (VER 70). Measurements at 100 kG on the $J_K=3_{2u} \rightarrow 3_{2l}$ inversion transition*) using a Bitter type magnet were also performed by Kukolich (KUK 73).

The original experiments at low fields by Kukolich and by Verhoeven yielded a discrepancy for the molecular susceptibility. A reinvestigation by Kukolich removed this discrepancy. The anisotropic susceptibility, however, is rather small in ammonia, and the measured value at low fields is subject to a large uncertainty (see Table 4.3). Therefore measurements were performed at a field of 69.76(7)kG. Another reason to measure in high field was to obtain the nuclear shielding of ^{14}N and H. The measurements were performed on the $J_K=2_{2u} \rightarrow 2_{2l}$ inversion

*) Here "u" stands for the upper inversion level, and "l" for the lower.

transition at 23722 MHz.

Transition						
M_J	M'_J	M_N	M_4	Calculated frequency	Measured frequency	St.dv.
2	1	0	-1/2	28 674.645	n.o.	
2	1	0	1/2	28 656.439	28 660.4	2.0
-1	-2	-1	1/2	28 525.502	28 526.9	4.0
-1	-2	1	1/2	28 509.387	28 513.3	4.0
-1	-2	-1	-1/2	28 498.807	28 496.6	4.0
-1	-2	1	-1/2	28 477.979	28 483.6	4.0
1	0	0	-1/2	28 093.161	n.o.	
1	0	0	1/2	28 073.924	28 076.6	2.0
0	-1	-1	1/2	28 044.239	28 041.1	3.0
0	-1	1	1/2	28 030.103	28 027.3	5.0
0	-1	-1	-1/2	28 026.023	28 022.8	5.0
0	-1	1	-1/2	28 011.022	28 008.9	3.0
1	0	1	-1/2	27 667.469	27 664.2	3.0
1	0	-1	-1/2	27 655.776	27 654.1	5.0
1	0	1	1/2	27 648.221	27 643.8	5.0
1	0	-1	1/2	27 638.049	27 633.9	3.0
0	-1	0	1/2	27 584.254	27 581.8	3.0
0	-1	0	-1/2	27 565.751	27 567.9	3.0
2	1	1	-1/2	27 308.846	27 309.7	5.0
2	1	-1	-1/2	27 292.154	27 292.5	5.0
2	1	1	1/2	27 278.493	27 275.3	5.0
2	1	-1	1/2	27 262.452	27 258.1	5.0
-1	-2	0	1/2	27 258.220	n.o.	
-1	-2	0	-1/2	27 244.114	n.o.	

Table 4.2. The $\Delta M = -1$ lines for the $J_K = 2_{2+} \rightarrow 2_{2-}$ transition in $^{14}NH_3$ at a magnetic field of 69.76 kG.
All frequencies are in kHz relative to ν_0 = 23722633.336 (4)kHz.
n.o. means not observed. For this fit χ^2 = 17.6

The observed and calculated frequencies for the Zeeman lines are given in Table 4.2. Only the high frequency part of the spectrum ($\Delta M=-1$ transitions) could be measured, because the Zeeman effect at 70 kG is considerably larger than the tuning range of the cavity. The standard deviations for the line positions are large because of the line broadening due to the inhomogeneity of the field. Another reason for the inaccuracy is the large overlap of the Zeeman lines.

The spectrum has been fitted using the zero field coupling constants calculated by Hougen (HOU 72) and the magnetic moment observed by Verhoeven (VER 70). The coupling constants obtained in the fit of this spectrum are given in Table 4.3.

coupling constant	observed value	units	transition
χ_{JK}	0.08361(55)	kHz/kG^2	$^2_{2u} \rightarrow ^2_{2l}$ $\Delta M=\pm 1$
$\mu_N \sigma^N_{JK}$	-0.026(24)	kHz/kG	
$\mu_N \Delta g_{JK}$	-0.1317(31)	kHz/kG	$^2_{1u} \rightarrow ^2_{1l}$ $\Delta M=0$
$\mu_N \Delta\sigma^H_{JK}$	-0.065(22)	kHz/kG	
$\mu_N \Delta g_{JK}$	-0.037(5)	kHz/kG	$^2_{2u} \rightarrow ^2_{2l}$ $\Delta M=0$

Table 4.3 Coupling constants for the studied ammonia transitions

To obtain the inversion effect upon the molecular G-tensor $\Delta M=0$ transitions were performed. It was hoped that the dependence of this tensor would be apparent at 70 kG.

The initial measurements were performed upon the $J_K = 2_{2u} \rightarrow 2_{2l}$ transition. The observed spectrum at 70 kG consisted of two partly resolved lines at a distance of 10.15 kHz. An analysis of this spectrum showed that these peaks were due to the $|M|=2$ lines. The effect was indeed due to the G-tensor. The coupling constant is given in Table 4.3.

A comparison with the experiment of Kukolich at 100 kG, mentioned above, suggested that a larger effect could be expected for a level with low K(ELL 75a). Therefore measurements were performed on the 2_1 inversion transition. The spectrum of this transition is much more complicated because of the presence of the δ_{K1} terms in the coupling constants (see Chap. 3 for the origin of these terms), which cause a considerable hyperfine splitting. The advantage of these terms is, however, that also the δ_{K1}-part of the hydrogen nuclear shielding could in principle be observed.

The observed and calculated spectrum is given in Table 4.4. The coupling constants obtained from the fit are given in Table 4.3. We see that the effect of the hydrogen nuclear shielding is indeed observable. The measurements were performed at different fields in order to obtain a possible effect of the dependence of the molecular susceptibility upon the inversion state. No such effect was seen.

4.1.2 Fluoroform CHF_3

For this symmetric rotor molecule two rotational transitions were studied: (a) the $J_K = 1_o \rightarrow 0_o$ transition at a frequency of

Transition					
M_J	M_N	M_H	calc. frequency	observed frequency	St.dv.
-2	1	1/2	54.028	53.3	1.0
-2	0	1/2	49.124	49.3	1.0
-2	-1	1/2	42.898	n.o	
-1	-1	1/2	25.560	24.2	1.5
-1	0	1/2	23.564	22.1	1.5
-1	1	1/2	20.079	20.2	1.5
2	-1	-1/2	15.472	12.8	2.0
1	1	-1/2	9.294	8.9	2.0
2	0	-1/2	8.871	4.8	4.0
1	0	-1/2	5.463	3.9	4.0
2	1	-1/2	3.493	1.9	4.0
1	-1	-1/2	3.112	0.0	4.0
-1	1	-1/2	-1.687	-4.9	4.0
-1	0	-1/2	-5.169	-7.0	4.0
-2	-1	-1/2	-6.115	-7.4	3.0
-1	-1	-1/2	-7.130	-9.0	4.0
-2	0	-1/2	-12.293	-11.4	3.0
-2	1	-1/2	-17.273	-15.4	3.0
1	-1	1/2	-21.483	-21.8	3.0
1	0	1/2	-23.898	-23.8	2.0
1	1	1/2	-27.707	-25.8	2.0
2	1	1/2	-40.318	-40.7	1.5
2	0	1/2	-45.612	-44.7	1.5
2	-1	1/2	-52.272	-52.7	1.0

Table 4.4 The $\Delta M=0$ lines of the $2_{1u} \rightarrow 2_{1l}$ transition at a field of 69.86 kG. All frequencies in kHz relative to 23098819.011 kHz. The χ^2 for this fit is 9.3.

20.7 GHz and (b) the $J_K=2_1 \rightarrow 1_1$ at 41.4 GHz. We shall discuss them separately.

(a) The $J_K = 1_0 \rightarrow 0_0$ transition

The original zero field measurements using an effusive source yielded values of the coupling constants which were in sharp disagreement with the coupling constants observed by Kukolich et al (KUK 71, REY 72). In both observations hyperfine lines essential for a complete determination of the coupling constants were not observed. The repeated measurements employing a nozzle source showed a much better signal to noise ratio. This spectrum and the resulting coupling constants agreed with the remeasured values of Kukolich (KUK 72b, REY 74). The coupling constants obtained are given in Table 4.6.

Weak field measurements at 8.0093 kG on the $\Delta M=\pm 1$ transitions proved the usefullness of the state scrambler. The high frequency side could easily be measured by direct recording at an integration time of 10 s without the use of a scrambler. The low frequency part, however was not observed, even after long averaging (about 100x) with a CAT. Moreover the total intensity of the high frequency part is comparable to the total zero field intensity indicating that the focussed molecules relax to the upper M-level as explained in Chapter 2.

Using a state scrambler the lower levels could partly be populated. A noise generator was used as a source of the RF power inducing $\Delta M=\pm 1$ transitions. A population of the desired level would require a $\Delta M=2$ transition. So the population has to occur in two steps, thereby requiring a rather large amount of RF power. The large RF power caused a considerable increase of noise at the detector. Nonetheless the low levels could be

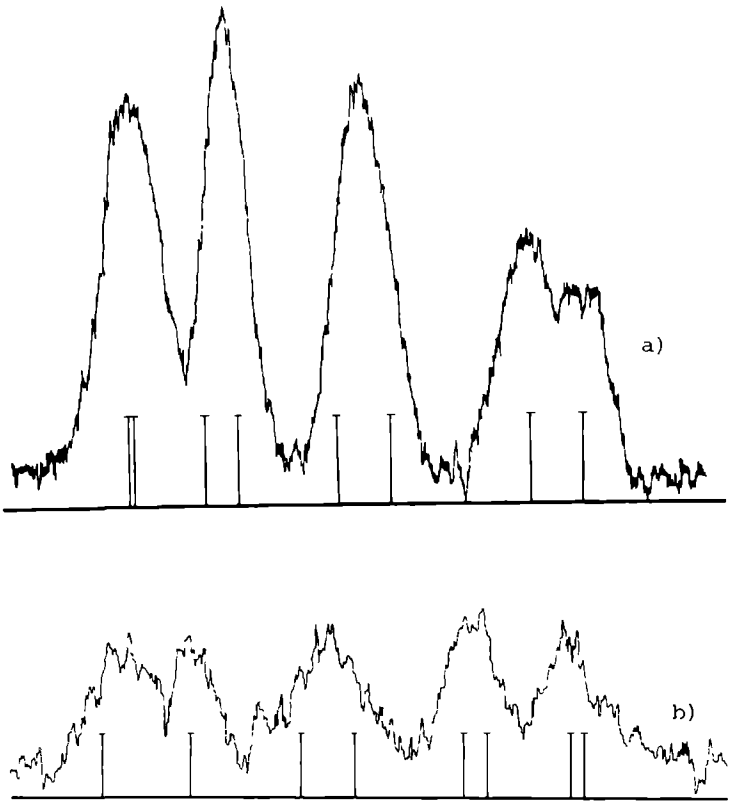

FIG. 4.1 The $J_K = 1_0 \rightarrow 0_0$ transition of CF_3H at a field of 8.0093 kG a) High freq.part measured directly at 10 s RC time b) Low freq. part measured after 32 sweeps with a CAT.

populated. Fig. 4.1a shows the S/N ratio for the upper frequency part observed without the scrambler and by direct recording at 10 s RC-time. In Fig. 4.1b the lower frequency part is depicted; this spectrum was observed after 32 sweeps with a CAT using the scrambler. Each sweep was recorded at 1s. The observed and calculated frequencies for these measurements are given in Table 4.5. These measurements yield values for the coupling constants of the G-tensor (g_{JK}) and the anisotropic susceptibility coupling constant (χ_{JK}) given in Table 4.6. It is seen that the error in χ_{JK} as obtained in low field is rather large.

To observe the fluorine and hydrogen nuclear shielding coupling constants, σ^F_{JK} and σ^H_{JK} respectively, measurements were performed in high magnetic field. The observed frequencies at a field of 68.81 kG are given in Table 4.5. Only $\Delta M=0$ transitions were observed which yielded all the necessary information about the Zeeman effect of this transition. It is seen from Table 4.6 that both shielding constants are obtained from the high field spectrum, although the error in σ^H is rather large. Another effect that can be obtained more accurately in high field is the susceptibility. The value of χ_{JK} in high field is 100x more accurate than the value obtained in low field.

To determine the molecular quadrupole moment, discussed in Chap.5, another transition with $K\neq0$ is needed. Our attention was focussed on the $2_1 \rightarrow 1_1$ transition, because this is the transition with $K\neq0$ at the lowest frequency.

(b) The $J_K = 2_1 \rightarrow 1_1$ transition

The zero field frequency of this transition is at 41.4 GHz. Because of the geometry of the superconducting magnet only cylindrical cavities can be used. The mostly used TM_{010} cavity

Transition							
M_J	M'_J	M_F	M_H	Calc. freq.	Obs.freq.	St.dv.	Magn.field
-1	0	-3/2	-1/2	237.134	237.0	1.0	
-1	0	-3/2	1/2	236.672	237.0	1.0	
-1	0	-1/2	-1/2	230.623	229.7	1.0	
-1	0	-1/2	1/2	228.747	229.7	1.0	
-1	0	1/2	-1/2	221.434	219.3	2.0	
-1	0	1/2	1/2	217.220	219.3	2.0	
-1	0	3/2	-1/2	209.110	207.8	2.0	
-1	0	3/2	1/2	202.559	203.2	2.0	8.0093 kG
1	0	3/2	1/2	-205.683	-206.6	3.0	
1	0	3/2	-1/2	-206.143	-206.6	3.0	
1	0	1/2	-1/2	-212.188	-213.2	3.0	
1	0	1/2	1/2	-214.063	-213.2	3.0	
1	0	-1/2	-1/2	-221.369	-223.4	3.0	
1	0	-1/2	1/2	-225.579	-223.4	3.0	
1	0	-3/2	-1/2	-233.689	-233.4	3.0	
1	0	-3/2	1/2	-240.236	-239.2	3.0	
0	0	-3/2	1/2	-257.749	-257.7	0.3	
0	0	-3/2	-1/2	-265.275	-265.3	0.3	
0	0	-1/2	-1/2	-272.091	-273.8	1.5	
0	0	3/2	-1/2	-274.946	-273.8	1.5	68.81 kG
0	0	1/2	-1/2	-275.464	-277.2	1.5	
0	0	-1/2	1/2	-278.342	-277.2	1.5	
0	0	1/2	1/2	-280.160	-280.5	1.5	
0	0	3/2	1/2	-281.955	-280.5	1.5	

Table 4.5. Results for the low field $\Delta M = \pm 1$ transitions and the high field $\Delta M = 0$ transitions of the $J_K = 1_0 \rightarrow 0_0$ transition of fluoroform, yielding χ^2 of 6.09 and 4.84 respectively. All frequencies are in kHz relative to ν_0 = 20697695.4(2)kHz.

Transition	coupling constant	value	units	remarks
	c^F_{JK}	10.37(13)	kHz	
	c^H_{JK}	-3.0(6)	kHz	
	$\mu_N g_{JK}$	27.644(71)	kHz/kG	
$1_o \rightarrow 0_o$	χ_{JK}	-0.120(44)	kHz/kG^2	from low field
	χ_{JK}	-0.14428(23)	kHz/kG^2	from high field
	$\mu_N \sigma^F_{JK}$	-0.1041(54)	kHz/kG	
	$\mu_N \sigma^H_{JK}$	0.0094(73)	kHz/kG	
	$\mu_N \lvert g_{21}-g_{11} \rvert$	0.746(15)	kHz/kG	
$2_1 \rightarrow 1_1$	ν_o	41395180.5(4)	kHz	
	$\Delta\nu$	23.09(88)	kHz	

Table 4.6 Coupling constants for fluoroform

has a diameter of 5.4 mm at this frequency, which is rather small. A larger diameter has the TE_{011} but such a cavity was expected to give problems with the coupling, because already at 23.72 we had a lot of trouble. The problems at this frequency were overcome, but at a frequency of 41 GHz the mechanical requirements are much more stringent.

Another solution at high frequencies is to use a resonator

consisting of two parallel circular disks. For a reasonable Q-factor the diameter of such a resonator should be about 14 wavelengths e.g. 10.5 cm. The bore in the superconducting magnet is only 6.5 cm, so it is impossible to mount it in this magnet. This resonator is only suitable in a polar magnet such as the Bruker magnet. However, in a polar magnet the magnetic field is perpendicular to the molecular beam, thereby introducing a motional Stark effect. Symmetric top molecules, which are in a rotational state with $K \neq 0$ have a very strong (first order) Stark effect. The velocity spread in the beam, which is about 5% - 10% for a nozzle beam, will influence the linewidth. At 8 kG, which is about the maximum field of the Bruker magnet and a typical velocity of 500 m/s for the molecules in the beam, the linewidth is from 50-100 kHz! In the superconducting magnet the maximum angle between the molecular velocity and the magnetic field in the cavity is 4/160 radians. The energy contribution of the Stark effect is proportional to the cube of this maximum angle and therefore negligible within the accuracy of the experiment at fields below about 30 kG. So our choice was a cylindrical TM_{010} cavity in the superconducting magnet, the best solution under the given circumstances.

The linear Stark effect has also implications for the state selection. Because only levels with positive Stark effect can be selected only the levels with M= -2 and -1 of the upper ($J_K = 2_1$) state are focussed, while those in the M=2 and 1 level are defocussed. The focussation of the M=-2 level is much better than the focussation of the M= -1 level, because the Stark effect of the latter is only one half of the Stark effect of the other. Thus at low state selector fields mainly the J,M = 2, -2 level is focussed. For the lower state (J=1, K=1)

the M= -1 level is focussed. The Stark energy of this level is about 1.5 x higher than the Stark energy of the J,M = 2,-2 level of the upper state. Consequently at low fields the M=-1 level of the lower state is focussed best, thereby yielding an anti-maser (absorption) signal rather than a maser (emission) signal.

The anti-maser signal was detected with an optimum S/N ratio of about 10 at 15 kV on the rods of the hexapole. When the voltage increased the signal decreased and at 20 kV it disappeared completely. Further increase of the voltage resulted in a maser signal. The explanation for this effect is that, as mentioned above, the (J,M) = (1,-1) level, which has the strongest Stark effect is focussed at low fields resulting in an optimum focussing at 15 kV. A further increase of the voltage on the selector gives no improvement, because the molecules that approach the selector rods experience such a strong force towards the axis, that they shoot through it thereby leaving the focuser at large angles with respect to the axis and so they do not enter the cavity. The levels with weaker Stark effect, however, have not reached optimum focussation at 15 kV, so that an increase of the voltage results in better focussation for these levels. It is pointed out above that the levels with weak Stark effect belong to the J=2 state. Because this state is the upper state this explains, why the maser signal is detected at higher state selector fields.

No attempt was made to resolve the zero field spectrum, because of the lack of any structure. In a magnetic field the spectrum consists of two (broad) lines, which are partly resolved. The distance between the two "lines" is independent of the magnetic field. It is called $\Delta\nu$ in Table 4.6 and is dis-

cussed in Chap.5.

From the shift of the lines in a magnetic field the magnetic moment could be determined. Measurements were performed at three different fields as listed in Table 4.7. The observed

calc. freq. (kHz)	obs. freq. (kHz)	Magn. field (kG)
41395202.58	41395203.4(15)	13.568
41395180.09	41395180.0(15)	
41395214.94	41395214.5(15)	27.397
41395193.04	41395194.3(15)	
41395262.51	41395263.5(40)	69.689
41395242.44	41395237.1(40)	

Table 4.7 Observed and calculated frequencies for the $2_1 \rightarrow 1_1$ transition in fluoroform

frequencies correspond to the tops of the two lines mentioned above. The errors in the high field line positions are large, because the S/N ratio is much less than at lower fields. This is due to discharge effects of the rest gas molecules in the vicinity of the state selector. The ions formed by the discharge (very weak and in the absence of magnetic fields completely negligible) are trapped in the high magnetic field and result in a current between the rods. This current drops the field of the selector and hence deteriorates the focussation.

The spectrum has been fitted by three constants: the distance between the two lines $\Delta\nu$; the difference between the g_{JK} of upper and lower state*); and the frequency of transition,

*) Only $g_{21}-g_{11}$ can be obtained in $\Delta M=0$ transitions.

if no hyperfine structure were present. The susceptibility anisotropy was taken from the $1_o \rightarrow 0_o$ transition. The shielding δ_{K1}-term was not fitted in this spectrum, because the observed lines were rather broad. The observed constants are discussed in Chap.5.

4.1.3 Methyl chloride $CH_3{}^{35}Cl$

We studied the $J_K = 1_o \rightarrow 0_o$ rotational transition in $CH_3{}^{35}Cl$ occurring at a frequency of 26.6 GHz. Because of the large quadrupole coupling constant of the ^{35}Cl-nucleus (74.7 MHz), the hyperfine splitting of this transition is so large that two TM_{010} cavities were needed in order to observe all hyperfine components (The thermal tuning range of such a cavity is not more than about 20 MHz).

As pointed in Chap.2 the zero field measurements were troubled by the poor Stark effect. In the coupling scheme $\underline{F}_1 = \underline{J} + \underline{I}_{Cl}$ where $\underline{I}_{Cl}$ stands for the chlorine nuclear spin (I_{Cl}=3/2), it is seen from Fig. 2.3 that the F_1=1/2 level is completely focussed, the F_1 = 3/2 is completely defocussed and the F_1 = 5/2 level is partly focussed ($M_{F1} = \pm 3/2$) and partly defocussed ($M_{F1} = \pm\ 1/2, \pm\ 3/2$).

To determine the chlorine quadrupole coupling constant and the spin-rotation constant transitions of all F_1 levels are needed for the fit. Therefore a transition of the type $\Delta J=0$ F_1=1/2 $\rightarrow$ F_1'=3/2 had to be induced in the scrambler. As this transition is forbidden in zero electric field, a large RF power is required to induce it. Unfortunately the frequency of this transition is about 34 MHz and lies within the bandwidth of the intermediate amplifier. The RF power produces a "signal" at the detector which exceeds the normal signal at the inter-

mediate frequency. So scrambling is not suitable in this case. The obvious way is to use a different intermediate frequency, but unfortunately the equipment needed was not available. The solution was found by measuring the transition in an electric beam resonance machine. In this machine the $\Delta J=0$ transition $(J,F_1)=(1,1/2) \rightarrow (1,3/2)$, which is a transition from a focussed level to a defocussed level, was observed in an electric field of 500 V/cm. Because the dipole moment is accurately known (MEE 75) the Stark effect can be calculated easily (ELL 75), and the zero field frequency of the $(1,1/2) \rightarrow (1,3/2)$ transition can be obtained. Now the distance between these levels is known. The frequency of the $(J,F_1) = (1,1/2) \rightarrow (0,3/2)$ is observed in the maser, and from the known distance between the $F_1=1/2$ and $F_1=3/2$ levels for $J=1$ the transition frequency of the $(J,F_1) = (1,3/2) \rightarrow (0,3/2)$ can be calculated. The zero magnetic field frequencies are given in Table 4.8. The quantum number F is defined as $\underline{F} = \underline{F}_1 + \underline{I}_H$, where $\underline{I}_H$ is the spin of the protons.

Because rather accurate values of g_{JK} and χ_{JK} were already known (VAN 70), we originally decided to measure only the high field Zeeman effect to obtain the chlorine and hydrogen nuclear shielding constants. Due to the poor Stark effect also in these measurements a large number of transitions was missing. It turned out to be impossible to determine the desired constants from this spectrum, because the missing lines contained essential information. Also working at two different fields, which in the case of fluoroform was sufficient to determine the coupling constants unambiguously, failed for this molecule.

In the high field measurements we studied only $\Delta M=0$ transitions, and to determine all coupling constants also $\Delta M=\pm 1$ transitions are needed. Because $\Delta M=\pm 1$ transitions at low field

Transition F	F'	F_1	F'_1	Calculated frequency	Observed frequency	Magn. field
2	1	1/2	3/2	26604368.286	26604368.4(5)	
1	0	1/2	3/2	26604367.182	26604367.4(5)	
1	0	5/2	3/2	26589430.701	n. o.	
2	1	5/2	3/2	26589424.992	26589425.3(15)	0.0
4	3	5/2	3/2	26589421.249	26589422.1(15)	
3	2	5/2	3/2	26589415.111	n. o.	
3	2	3/2	3/2	26570739.308	n. o.	
2	1	3/2	3/2	26570736.198	26570735.9(10)[a]	
1	0	3/2	3/2	26570728.323	26570729.1(10)[a]	
M_J	M'_J	M_{Cl}	M_H			
0	0	-3/2	3/2	26596244.376	26596244.2(5)	
0	0	-3/2	-3/2	26596244.140	26596244.2(5)	
0	0	-3/2	1/2	26596233.179	26596233.2(5)	
0	0	-3/2	-1/2	26596233.101	26596233.2(5)	
0	0	-1/2	3/2	26591816.282	n. o.	
0	0	-1/2	-3/2	26591815.767	n. o.	
0	0	-1/2	1/2	26591805.531	n. o.	
0	0	-1/2	-1/2	26591805.358	n. o.	69.70
0	0	1/2	-3/2	26582271.915	26582271.1(10)	
0	0	1/2	3/2	26582271.092	26582271.1(10)	
0	0	1/2	-1/2	26582260.933	26582261.1(10)	
0	0	1/2	1/2	26582260.658	26582261.1(10)	
0	0	3/2	-3/2	26577140.907	n. o.	
0	0	3/2	3/2	26577137.549	n. o.	
0	0	3/2	-1/2	26577128.833	n. o.	
0	0	3/2	1/2	26577127.714	n. o.	

Table 4.8 The $J_K = 1_0 \rightarrow 0_0$ transition in CH_3Cl in zero and magnetic field. All frequencies are in kHz. The magnetic field is in kG.
[a] These frequencies are obtained from EBR measurements, by taking the limit for the electric field to zero.
The χ^2 for this fit is 7.515.

Transition				Calculated	Observed	Magn.
F_1	M_{F_1}	M'_{F_1}	M_H	frequency	frequency	field
1/2	-1/2	1/2	-3/2	26606965.225	26606984.8(7)	
			-1/2	26606984.864	26606984.8(7)	
			1/2	26606984.818	26606984.8(7)	
			3/2	26606984.743	26606984.8(7)	
1/2	1/2	-1/2	3/2	26602212.599	26602212.0(7)	
			1/2	26602212.388	26602212.0(7)	
			-1/2	26602212.209	26602212.0(7)	
			-3/2	26602211.217	26602212.0(7)	
5/2	-3/2	-1/2	-3/2	26590995.534	26590994.6(20)	
			3/2	26590995.356	26590994.6(20)	
			-1/2	26590992.420	26590994.6(20)	
			1/2	26590992.362	26590994.6(20)	8.66645
5/2	-1/2	1/2	-3/2	26589525.750	n. o.	
			3/2	26589525.559	n. o.	
			-1/2	26589519.851	n. o.	
			1/2	26589519.278	n. o.	
5/2	1/2	-1/2	3/2	26589307.550	26589307.5(5)	
			-3/2	26589307.375	26589307.5(5)	
			1/2	26589301.638	26589301.4(5)	
			-1/2	26589301.107	26589301.4(5)	
5/2	3/2	1/2	3/2	26588212.427	n. o.	
			-3/2	26588212.281	n. o.	
			1/2	26588212.178	n. o.	
			-1/2	26588211.749	n. o.	

Table 4.8 (continued).

give a good accuracy for the coupling constants that have a strong Zeeman effect, we studied these transitions in the Bruker magnet at a field of 8.6 kG. Many Zeeman traces were not observed, but together with the zero and high field results a unique solution of the coupling constants could be obtained. The observed frequencies and the calculated frequencies are given in Table 4.8. For the calculation of the frequencies the second order contribution due to the chlorine quadrupole interaction had to be taken into account. This contribution shifts the J=0 levels by -4.38 kHz, and the $(J,F_1) = (1,1/2)$, $(1,3/2)$ and $(1,5/2)$ levels by 0.00, -0.95 and -2.52 kHz respectively.

The measurements yielded the coupling constants given in Table 4.9 The chlorine quadrupole coupling is so strong that in

coupling constant	value	units
eqQ	74743.3(14)	kHz
c_{JK}^{Cl}	1.83(19)	kHz
c_{JK}^{H}	-0.19(16)	kHz
$\mu_N g_{JK}$	-12.708(69)	kHz/kG
χ_{JK}	0.6992(3)	kHz/kG^2
$\mu_N(1-\sigma_{av}^{Cl})g_{Cl}$	417.264(42)	kHz/kG
$\mu_N\sigma_{JK}^{Cl}$	-0.200(18)	kHz/kG
$\mu_N\sigma_{JK}^{H}$	0.0031(39)	kHz/kG
ν_o	26585682.24(33)	kHz

Table 4.9 Coupling constants for CH_3Cl

the field of the Bruker magnet the coupling between J and I_{Cl} is not broken. The advantage is that the (shielded) chlorine nuclear magnetic moment $\mu_N g_{Cl}(1-\sigma_{av}^{Cl})$ can be obtained, and that the sign of the molecular G-tensor coupling constant g_{JK} can be determined. The coupling constants associated with the protons, e.g. the proton spin-rotation interaction c_{JK}^{H} and shielding anisotropy σ_{JK}^{H} are rather small as can be seen from this Table. The splitting between the F-levels in the zero field case stems mainly from the proton-proton spin-spin interaction, which has a strength of 10.15 kHz for the $J_K = 1_0$ level.

4.2 ASYMMETRIC TOP MOLECULES

4.2.1 Water D_2O

The transition studied was the $J_\tau = 3_{-2} \rightarrow 2_2$ transition occurring at a frequency of 10.9 GHz. Zero field measurements had been performed by Bluyssen (BLU 68) and low-field Zeeman measurements at 12 kG were studied by Verhoeven (VER 69). Measurements at a field of 70 kG were done on this transition, because it was hoped that the shielding at the deuteron could be observed. Its effect was too small in the low field measurements.

The measured and calculated spectrum is given in Table 4.10. The coupling constants obtained from this spectrum are given in Table 4.11. Even at a field of 68.76 kG the shielding of the deuteron is too small to be observed as can be seen from Table 4.11. More details about the experiment can be found in (ELL 73).

Transition				Calculated	Observed	Stand.
M_J	M_D	I_D	I'_D	frequency	frequency	Dev.
-1	0	0	2	-185.514	-185.5	0.5
-2	0	2	0	-173.040	-173.4	3.0
-2	0	2	2	-172.998	-173.4	3.0
-2	2	2	2	-172.817	-173.4	3.0
-2	-2	2	2	-171.368	-173.4	3.0
0	0	0	2	-157.222	-157.1	0.5
-2	1	2	2	-135.937	-135.6	3.0
-2	-1	2	2	-135.225	-135.6	3.0
-1	1	2	2	-134.009	-135.6	3.0
-1	-1	2	2	-133.647	-135.6	3.0
-2	0	0	0	-98.253	-96.5	3.0
-2	0	0	2	-98.211	-96.5	3.0
-1	2	2	2	-83.451	-82.8	3.0
-1	-2	2	2	-82.746	-82.8	3.0
-1	0	2	0	-82.141	-82.8	3.0
0	1	2	2	-75.903	-76.1	3.0
0	-1	2	2	-75.873	-76.1	3.0
1	0	0	2	-13.460	-13.5	0.1
0	2	2	2	3.858	5.1	3.0
0	-2	2	2	3.860	5.1	3.0
0	0	2	0	5.439	5.1	3.0
1	-1	2	2	37.966	38.7	3.0
1	1	2	2	38.316	38.7	3.0
1	-2	2	2	88.417	89.0	3.0
1	2	2	2	89.152	89.0	3.0
1	0	2	0	89.733	89.0	3.0
2	0	2	0	170.743	171.9	3.0
2	0	2	2	170.786	171.9	3.0
2	0	0	2	170.965	171.9	3.0
2	2	2	2	172.397	171.9	3.0
2	-1	2	2	207.779	208.0	3.0
2	1	2	2	208.509	208.0	3.0
2	0	0	0	245.592	245.6	1.0
2	0	0	2	245.643	245.6	1.0

Table 4.10 The $J_\tau = 3_{-2} \rightarrow 2_2$ transition in D_2O at a field of 68.76 kG. All frequencies are in kHz relative to ν_o. The χ^2 for this fit is 3.02.

coupling constant	value	units
$\chi_{3,-2}$	-0.0152(8)	kHz/kG^2
$\chi_{2,2}$	0.0201(4)	kHz/kG^2
$\sigma^D_{3,-2}$	<0.035	kHz/kG
$\sigma^D_{2,2}$	<0.025	kHz/kG

Table 4.11 Coupling constants observed for D_2O.

4.2.2 Sulphur dioxide SO_2

Sulphur dioxide is a bent asymmetric rotor molecule. Because of the absence of nuclear spins in the most abundant $^{32}S^{16}O_2$-isotope the zero field spectrum consists of one single line.

We studied the $J_\tau=2_{-2} \rightarrow 1_0$ transition at 12.3 GHz and the $J_\tau = 4_{-4} \rightarrow 3_{-2}$ transition at 29.3 GHz. The latter transition caused some difficulties discussed in Chap.2 due to the poor Stark effect. By the crossing of a populated level with a depleted level a repopulation was achieved. In Table 4.12 the observed and calculated frequencies for both transitions are given. The coupling constants $g_{J\tau}$ and $\chi_{J\tau}$ could for both transition well be resolved as can be seen in Table 4.13.

4.3 INTERNAL ROTOR MOLECULES

4.3.1 Hydrogen peroxide H_2O_2

Commercial hydrogen peroxide is available as an aequous solution that contains 30% of H_2O_2 by weight. The fraction of H_2O_2

Transition				Int.	Observed	Calculated	Magn.
J_τ	J'_τ,	M_J	M'_J	(Rel.)	frequency	frequency	field
		0	1	1	3186.4(4)	3186.6	
		2	1	6	1292.8(4)	1293.0	
		-1	0	3	932.2(10)	933.4	
2_{-2}	1_0	1	0	3	-940.6(4)	940.4	12.009 kG
		-2	-1	6	-1303.7(4)	-1303.5	
		0	-1	1	-3158.1(4)	-3157.6	
		+2	3	2	n.o.	1363.8	
		1	2	6	1138.1(4)	1137.9	
		0	1	12	909.2(4)	909.0	
		-1	0	20	677.3(4)	677.3	
		-2	-1	30	442.5(4)	442.7	
		-3	-2	42	205.2(4)	205.1	
		4	3	56	n.o.	27.6	
4_{-4}	3_{-2}	-4	-3	56	-35.1	-35.3	8.776 kG
		3	2	42	n.o.	-201.5	
		2	1	30	-432.9(10)	-433.5	
		1	0	20	-668.2(4)	-668.3	
		0	-1	12	-906.0(4)	-906.1	
		-1	-2	6	-1146.9(4)	-1146.7	
		-2	-3	2	-1390.3(4)	-1390.3	

Table 4.12 Observed and calculated frequencies for the $J_\tau = 2_{-2} \rightarrow 1_0$ and the $J_\tau = 4_{-4} \rightarrow 3_{-2}$ transitions in SO_2
All frequencies are in kHz relative to ν_o

Rot. level J_τ	$g_{J\tau}$	$\chi_{J\tau}$	$\nu_o(J_\tau \rightarrow J'_\tau)$
1_0	-0.34646(13)	-0.60(2)	12.2565835(6)
2_{-2}	-0.10235(5)	-0.96(2)	
3_{-2}	-0.13734(3)	-1.77(6)	29.3213304(4)
4_{-4}	-0.10182(3)	-1.07(6)	

Table 4.13 Coupling constants for SO_2. $g_{J\tau}$ is in units of nuclear magnetons, $\chi_{J\tau}$ in 10^{-6} erg./(G^2mole) and ν_o in GH_z.

molecules in the vapour is then less than 5%. So the solution had to be enriched. This purification was achieved by pumping the solution for at least 24 hours resulting in a 50% molecular fraction of H_2O_2 in the vapor (ELL 75).

In the present experiment we studied the transitions with low J-values that occur at a reasonable frequency for our beam maser. The only two transitions that can be considered are the $J_{K\tau} = 1_{1-2} \rightarrow 0_{04}$ and the $2_{1-2} \rightarrow 1_{04}$ transition.

The first transition occurs at 14.8 GHz. It is seen from Table 3.5 that the levels involved in this transition have a zero total nuclear spin. So the zero field spectrum consists of a single line. This line splits in a magnetic field into two ($\Delta M=+1$ and $\Delta M=-1$) components which were readily observed. The measured and calculated frequencies at a field of 8.652 kG are given in Table 4.14. The coupling constants that determine the spectrum e.g. $g_{JK\tau}$ and $\chi_{JK\tau}$ are listed in Table 4.16. In the calculation of the coupling constants the motional Stark effect

transition M	M'	calculated frequency	measured frequency
1	0	1854.123	1854.1(3)
-1	0	-1864.656	-1864.7(3)

Table 4.14 Observed and calculated frequencies for the $1_{1-2} \rightarrow 0_{04}$ transition in H_2O_2 at a field of 8.653 kG. The frequencies are in kHz relative to ν_o.

has been included (ELL 75).

The $2_{1-2} \rightarrow 1_{04}$ transitions occurs at 37.5 GHz. For this transition the proton spins couple to unity and the zero field spectrum is split due to the hyperfine interactions. This spectrum was observed by Heuvel (unpublished), but because of insufficient resolution the coupling constants could not be determined. However in a magnetic field these hyperfine constants as well as the Zeeman constants could be determined, because the different JM → J'M' lines give independent information about the hyperfine structure. The observed and calculated frequencies at a field of 8.6912 kG are given in Table 4.15. It is seen that the spin rotation constants that determine the hyperfine structure are well resolved ($c^H_{JK\tau}$ in Table 4.16), as well as the Zeeman constants $g_{JK\tau}$ and $\chi_{JK\tau}$. They are discussed in the next chapter.

4.3.2 Methyl alcohol CH_3OH

Because of the astrophysical interest (BAR 75) we studied the zero field and Zeeman transitions of some states in CH_3OH. The

Transition M	M'	M_I	Calc. freq.	Obs. freq.	St. dv	Magn. field
		1	-1037.61	n.o.		
2	1	0	-1026.40	n.o.		
		-1	-1018.86	n.o.		
		0	-428.14	-427.9	1.0	
0	1	-1	-427.90	-427.9	1.0	
		1	-427.86	-427.9	1.0	
		1	-312.53	-313.4	2.0	
1	0	0	-309.93	-309.5	2.0	
		-1	-303.13	-301.6	2.0	
		-1	266.28	265.9	2.0	8.6912 kG
-1	0	0	268.87	269.0	2.0	
		1	275.67	275.5	2.0	
		0	472.96	473.1	1.0	
0	-1	1	473.21	473.1	1.0	
		-1	473.26	473.1	1.0	
		-1	1021.11	1021.1	1.0	
-2	-1	0	1032.53	1032.9	1.0	
		1	1039.87	1039.5	1.0	
			-9.99	-10.2	0.5	
			5.68	8.4		
			7.21	8.4		
			10.19	8.4		0 kG
			12.62	8.4		
			14.15	8.4		

Table 4.15 The $J_{K\tau} = 2_{1-,2} \rightarrow 1_{04}$ transition of H_2O_2. All frequencies in kHz relative to ν_o = 37518298.2(4) kHz

Transition J_K	$J'_{K',\tau'}$	Coupling constant	Value	Units
		g_2^{11-}	214.86(2)	kHz/kG
$^1{}_{1-2}$	$^0{}_{04}$	χ_2^{11-}	-0.351(14)	kHz/kG^2
		ν_o	14829117.6(2)	kHz
		c_2^{21-}	-4.6(3)	kHz
		c_4^{10}	-0.0(4)	kHz
		g_2^{21-}	33.30(6)	kHz/kG
$^2{}_{1-2}$	$^1{}_{04}$	g_4^{10}	-51.84(5)	kHz/kG
		χ_2^{21-}	0.483(28)	kHz/kG^2
		χ_4^{10}	0.805(21)	kHz/kG^2
		ν_o	37518298.2(4)	kHz

Table 4.16 Coupling constants for $H_2\,O_2$

observed transitions are of E_1-type, $\Delta J=0$, $K=2 \rightarrow 1$ transitions for J=2, 3 and 4. These transitions are all in the neighbourhood of 24.93 GHz.

The zero field lines are all rather broad (ELL 74). For J=2, 3 and 4 the linewidth was 30.9, 23 and 19 kHz respectively. None of the observed spectra showed any structure.

In a magnetic field all transitions behave in a similar manner; each line splits into several components (Fig.4.2).

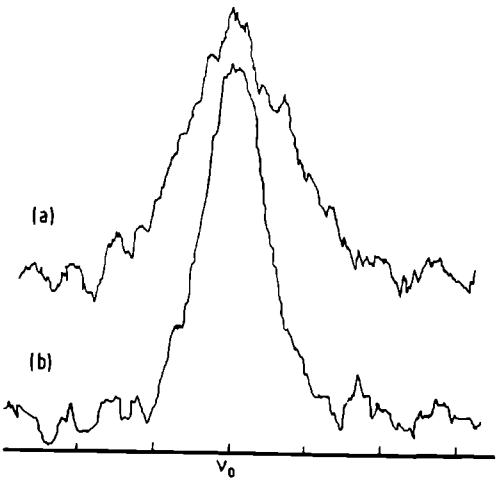

FIG. 4.2 The $J_K=2_2 \rightarrow 2_1$ line in CH_3OH (a) zero field, (b) field of 1kG; distance between the markers is 10kHz.

The zero field center line remains observable up to a field of 2-3 kG. This line is, however, much narrower than the zero field line; for J=2 the linewidth of the central line at a field of 2 kG is 9.3 kHz. It is clearly seen in Fig. 4.2 that the zero field line is considerably broader than the line in the magnetic field. The side lines in a magnetic field are very broad and their width increases with increasing field. A calculation pointed out that the broadening is due to the motional Stark effect. As in the case of fluoroform, discussed in Sect. 4.1.2, the E-type levels in methyl alcohol have linear Stark effect and motion with a velocity $\underline{v}$ in a magnetic field $\underline{H}$ the experienced electric field $\underline{v}\times\underline{H}$ causes a Stark effect of

$$E_{st} = - \frac{\mu_{\|} \underline{v}\times\underline{H}\ MK}{J\ (J+1)} \qquad (4.2)$$

where $\mu_{\|}$ is the component of the electric dipole moment along

the symmetry axis of the methyl group. Because this term is linear in the molecular velocity the velocity spread in the beam produces the line broadening. All experiments were performed in the Bruker magnet so $\underline{v} \perp \underline{H}$ and the resulting line broadening at 1kG and 600 m/s is 25 kHz. More details about the experiment can be found in (ELL 74). A discussion of the results is given in Chap.5.

C H A P T E R 5

RESULTS AND DISCUSSION

5.1 THE HYPERFINE TENSORS

The tensors appearing in the hamiltonian of Eq(3.26) are functions of the nuclear and electronic positions and velocities. They are given in Table 5.1 as derived by Verhoeven (VER 69) for an asymmetric rotor. The tensor components for a symmetric rotor can be obtained from those of Table 5.1 by equalizing two of the rotational constants (e.g. A=B).

The nuclear contribution to the various tensor components can in all cases be calculated from the known geometry in the ground vibrational state. The spin-spin tensors in Table 5.1 can therefore completely be calculated.

The electronic part of the spin-rotation tensor $\underline{\underline{M}}_e^K$ is proportional to the paramagnetic shielding $\underline{\underline{\sigma}}_p^K$

$$\underline{\underline{M}}_e^K = - \frac{2\mu_N g_K \hbar}{\mu_B} \underline{\underline{A}} \, \underline{\underline{\sigma}}_p^K \qquad (5.1)$$

In this equation μ_N is the nuclear magneton, g_K the g-factor of the K-th nucleus, $\hbar$ is Planck's constant, μ_B the Bohr magneton and $\underline{\underline{A}}$ the rotational tensor. When $\underline{\underline{\sigma}}^K$ is known the diamagnetic shielding is readily obtained by subtracting the paramagnetic part. The diamagnetic shielding $\underline{\underline{\sigma}}_d^K$ is a quantity that can be calculated from ab-initio calculations.

The electronic contribution to the molecular G-tensor is proportional to the second order contribution of the electronic angular momentum $\underline{L}$.

Nuclear magnetic shielding $\underline{\underline{\sigma}}^K = \underline{\underline{\sigma}}_d^K + \underline{\underline{\sigma}}_p^K$

$$\sigma_{d,aa}^K = e\frac{\mu_o}{4\pi}\frac{\mu_B}{\hbar} \langle 0| \sum_i (b_{iK}^2 + c_{iK}^2)/ r_{iK}^3 | 0\rangle$$

$$\sigma_{p,aa}^K = e\frac{\mu_o}{4\pi m}\frac{\mu_B}{\hbar} \sum_{n\neq 0} (\langle 0| \sum_i Q_{iK,a}/r_{iK}^3 |n\rangle\langle n| \sum_i Q_{ik,a}|0\rangle + \text{c. c.})/(E_0 - E_n)$$

Molecular quadrupole moment $\underline{\underline{\Theta}}$

$$\Theta_{aa} = \frac{e}{2}[\sum_K Z_K (2a_K^2 - b_K^2 - c_K^2) - \langle 0| \sum_i 2a_i^2 - b_i^2 - c_i^2 |0\rangle$$

Table 5.1 Hyperfine and magnetic interactions in symmetric or asymmetric molecules. The definition of the various symbols appearing in this Table is

$\underline{r}_i = (a_i, b_i, c_i)$ position of the i-th electron in cm. system
$\underline{r}_K = (a_K, b_K, c_K)$ position of the K-th nucleus in cm. system
$\underline{p}_i, \underline{p}_K$ lin. momentum of i-th electron and K-th nucleus respectively
$\underline{r}_{iK} = \underline{r}_i - \underline{r}_K$; $r_{iK} = |\underline{r}_{iK}|$
$\underline{r}_{KL} = \underline{r}_K - \underline{r}_L$; $r_{KL} = |\underline{r}_{KL}|$
$\underline{Q}_{iK} = \underline{r}_{iK} \times (\underline{p}_i - \underline{p}_K)$
m is the electron mass
e is the charge of the proton
μ_B is the Bohr magneton
μ_N is the nuclear magneton
E_n is the energy of the n-th electronic state
E_o is the energy of the ground electronic state
A_{aa} is the rotational constant about the a-axis
g_K is the g-factor of the K-th nucleus
Z_K is the number of protons in the K-th nucleus
$\frac{\mu_o}{4\pi}$ equals 10^{-7} H/m (SI units)

Nuclear quadrupole interaction

$$eQq^{K}_{aa} = eQ.\ \frac{\partial^2 V^K}{\partial a \partial a}$$

Spin rotation interaction $\underline{\underline{M}}^K = \underline{\underline{M}}^K_n + \underline{\underline{M}}^K_e$, with

$$M^K_{n,aa} = -2e\ \frac{\mu_o}{4\pi}\ \mu_N g_K A_{aa} \sum_{L \neq K} Z_L\ (b^2_{KL} + c^2_{KL})/r^3_{KL}$$

$$M^K_{e,aa} = -2e\ \frac{\mu_o}{4\pi m}\ \mu_N g_K A_{aa} \sum_{n \neq 0} (<0|\sum_i Q_{iK,a}/r^3_{iK}|n><n|\sum_i Q_{iK,a}|0> + c.c.)/(E_o - E_n)$$

Spin spin interaction

$$D_{KL,aa} = \mu^2_N\ \frac{\mu_o}{4\pi}\ g_K g_L\ (b^2_{KL} + c^2_{KL} - 2a^2_{KL})/r^5_{KL}$$

Molecular magnetic moment $\underline{\underline{G}} = \underline{\underline{G}}_n + \underline{\underline{G}}_e$

$$g_{n,aa} = 2\ \frac{\mu_B}{\mu_N}\ A_{aa} \sum_K m Z_K (b^2_K + c^2_K)$$

$$g_{e,aa} = 2\ \frac{\mu_B}{\mu_N} A_{aa} \sum_{n \neq 0} (<0|L_a|n><n|L_a|0> + c.c.)/(E_0 - E_n)$$

Magnetic susceptibility $\underline{\underline{\chi}} = \underline{\underline{\chi}}_d + \underline{\underline{\chi}}_p$

$$\chi_{d,aa} = \frac{-\mu^2_B}{\hbar^2} m <0|\sum_i (b^2_i + c^2_i)|0>$$

$$\chi_{p,aa} = \frac{-\mu^2_B}{\hbar^2} \sum_{n \neq 0} (<0|L_a|n><n|L_a|0> + c.c.)/(E_0 - E_n)$$

Table 5.1. Continued

$$g_{e,aa} = \frac{2\mu_B}{\mu_N} \sum_n \frac{|\langle o|L_a|n\rangle|^2}{E_o - E_n} A_{aa} \qquad (5.2)$$

In this equation n runs over all excited electronic states $|n\rangle$, with energy E_n; $|o\rangle$ is the electronic ground state with energy E_o.

In several series of molecules the electronic contribution to the molecular $\underline{\underline{G}}$-tensor is almost constant, although the total $\underline{\underline{G}}$-tensor differs notably. This effect has been observed in the series CH_3I, CH_3Br and CH_3Cl, where the electronic contribution is calculated as -0.6265, -0.6242 and -0.6330 respectively (VAN 70). It has also been observed by Ozier et al for the series CF_4, SiF_4 and GeF_4 where the observed electronic contribution is -0.50848, -0.50917 and -0.50382 respectively (OZI 76). In both series we have therefore that the second order contribution of the electronic angular momentum is in first order proportional to the moment of inertia. This relationship is as yet not well understood. Rigorous theoretical calculations on one electron properties involving excited electronic states have not been performed until now, so that no ab-initio calculations exist.

The components of the molecular quadrupole tensor are given in Table 5.1. From the definition we obtain a relation

$$\Theta_{aa} = -\frac{h\,e}{8\pi M_p}\left(\frac{2g_{aa}}{A_{aa}} - \frac{g_{bb}}{A_{bb}} - \frac{g_{cc}}{A_{cc}}\right) - \frac{2mc^2}{e}(2\chi_{aa} - \chi_{bb} - \chi_{cc}) \qquad (5.3)$$

where the rotational constant A_{aa}, A_{bb} and A_{cc} are expressed in Hz and M_p is the proton mass. It is seen in Table 5.1 that the components of Θ involve only the ground electronic wavefunction and can therefore be calculated by ab-initio methods. The importance of the molecular quadrupole moment is pointed out

in Chap.1 (see also ABR 57).

Finally from the diamagnetic susceptibility tensor it is easy to obtain the expectation value of the second moment of the electronic charge distribution

$$- e \langle o | \Sigma a_i^2 | o \rangle = + \frac{2mc^2}{e} (\chi_{d,bb} + \chi_{d,cc} - \chi_{d,aa}) \qquad (5.4)$$

In this equation the sum extends over all electrons.

For simple molecules ab-initio calculations yield the electronic ground state wavefunction. It is well-known that the total electronic energy in the molecule is not very sensitive to the electronic wavefunction. The one electron operators such as the diamagnetic shielding and the molecular quadrupole moment perform a much better test upon the reliability of the electronic wavefunction.

In the calculations of the tensor components given in Table 5.1 the values for the fundamental constants were taken from the tables of Cohen and Taylor (COH 73).

5.2 AMMONIA

In the ammonia molecule the nitrogen atom can tunnel through the potential barrier formed by the hydrogen atoms. The hindering potential as a function of the distance of the nitrogen nucleus to the plane through the hydrogens is shown in Fig. 5.1. This

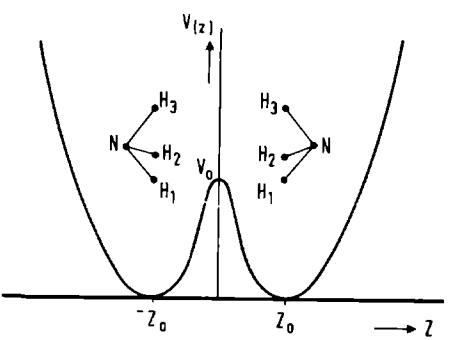

FIG. 5.1 The inversion potential in ammonia as a function of the distance of the N-nucleus to the plane of the hydrogens.

potential V is invariant under a reflection in the plane of the hydrogens. When during the inversion process the nitrogen nucleus approaches the plane of the hydrogen nuclei, the relative distance between the hydrogen atoms changes, such that the N-H distance remains almost the same. Consequently it is mainly the bond angle that changes in this process and hence it is a better parameter to describe the inversion than the distance of the N-atom to the plane of the H-atoms. The equilibrium angle (i.e. where V reaches a minimum) is obtained by Benedict et al (BEN 57). They obtained $\angle HNH = 106^{o}10'$. The barrier at $\angle HNH = 120^{o}$ is 2077 cm^{-1}.

If we call u_L and u_R the nuclear part of the molecular wavefunction in the configuration with the nitrogen nucleus in the -c and +c direction respectively then the two states are indistinguishable. Because of the symmetry of V under a reflection in the plane through the hydrogens, the proper nuclear wavefunctions are (TOW 55)

$$u_u = \frac{1}{\sqrt{2}} (u_L + u_R)$$
$$u_l = \frac{1}{\sqrt{2}} (u_L - u_R) \qquad (5.5)$$

In the state u_u there is a finite probability to find the nitrogen atom in the plane of the hydrogen atoms, whereas this probability is zero for the u_l state. Consequently the energy of the molecule in the u_u state is larger than the energy in the u_l state. The states u_u and u_l are called inversion states. A quantum number v can be associated with these functions. For the u_u state v=0 and for the u_l state v=1.

It is obvious that all molecular quantities depend upon v. For an arbitrary molecular interaction X we define

$$
\begin{aligned}
X^u &= \langle v=0 | X | v=0 \rangle \\
X^l &= \langle v=1 | X | v=1 \rangle \\
\Delta X &= X^u - X^l \\
\bar{X} &= \tfrac{1}{2}(X^u + X^l)
\end{aligned}
\qquad (5.6)
$$

A measure for the inversion dependence of X is the ratio $\Delta X/\bar{X}$.

Until the present investigation only the nitrogen quadrupole coupling and the rotational constant B showed an observable dependence upon v. For the nitrogen quadrupole coupling constant eqQ_N the inversion effect was observed by Kukolich (KUK 67). A refit upon these spectra by Hougen (HOU 72) yielded the ratio $\Delta(eqQ_N)/eqQ_N = 10.1(3)\times10^{-4}$. For the rotational constant Poynter and Kakar (POY 75) obtained a value of $\Delta B/B$ $-5.05(63)\times10^{-4}$ from microwave absorption measurements on a large number of ammonia transitions.

In Sect. 4.1.1 the inversion dependence of the molecular G-tensor has been reported. The sign for $g^u_{21}-g^l_{21}$ in Table 5.2 is obtained relative to the sign of the δ_{K1}-terms, which appear

coupling constant	observed value	calculated value	units	ref.
$g^u_{2_2} - g^l_{2_2}$	-0.48(9)	-0.51	10^{-4}nm	ELL 75
$g^u_{3_2} - g^l_{3_2}$	-1.38(8)	-1.33	10^{-4}nm	KUK 73
$g^u_{2_1} - g^l_{2_1}$	-1.73(4)	-1.74	10^{-4}nm	th. work

Table 5.2. Result for the inversion dependence of the g_{J_K} coupling constant.

for the proton spin-rotation interaction and the proton-nitrogen nuclear spin-spin interaction. Because the sign of these terms is known from zero field measurements, Table 5.2 gives the proper sign for $g^u_{21}-g^l_{21}$. Since the negative sign for $g^u_{32}-g^l_{32}$ was assumed by Kukolich (KUK 73), the sign of Δg_{22} had to be chosen negative, because a positive sign could not be fitted. A least squares fit upon the coupling constants given in Table 5.2 yields

$$\begin{aligned} \Delta g_\perp &= -2.15(6)\times 10^{-4} \\ \Delta g_\parallel &= +0.31(15)\times 10^{-4} \end{aligned} \qquad (5.7)$$

The relative effect for $g_\perp$ and $g_\parallel$ can be calculated using $\bar{g}_\perp = 0.5627(21)$ and $\bar{g}_\parallel = 0.5027(38)$ as observed by Verhoeven (VER 70). We obtain

$$\begin{aligned} \Delta g_\perp/\bar{g}_\perp &= -3.80(10)\times 10^{-4} \\ \Delta g_\parallel/\bar{g}_\parallel &= +0.61(30)\times 10^{-4} \end{aligned} \qquad (5.8)$$

From a classical point of view we expect that the molecular moment due to the rotating charges in the molecule about the symmetry axis would be less sensitive to the inversion than the component perpendicular to the axis. So the observed effect agrees with this intuitive expectation. The nuclear contribution to $\Delta g_\parallel$ and $\Delta g_\perp$ can be calculated from the geometry. From its definition in Table 5.1 the component of the nuclear contribution to the molecular G-tensor parallel to the symmetry axis of an XY_3 symmetric top molecule is given by

$$g_{n\parallel} = M_p Z_Y / M_Y \qquad (5.9)$$

where M_Y is the mass of the Y-nucleus, $Z_Y e$ its charge. So $g_{n\parallel}$ is independent of the molecular geometry and in the case of NH_3 $\Delta g_{n\parallel}=0$. If we assume that the ratio $\Delta B/\bar{B}$ observed by

Poynter and Kakar is due to the nuclear inversion dependence, then Δg_n can be calculated, and we obtain

$$\Delta g_{n\perp} = -1.05(12)\times10^{-4}$$

So from Eq(5.7) we have

$$\begin{aligned} \Delta g_{e\perp} &= -1.10(13)\times10^{-4} \\ \Delta g_{e\parallel} &= +0.31(15)\times10^{-4} \end{aligned} \qquad (5.10)$$

For the molecular magnetic susceptibility no dependece upon the inversion state was observed, because even at fields of 70 kG the effect was too small. The value of $\chi_\parallel - \chi_\perp$ is given in Table 5.3. The average magnetic susceptibility χ_{av} was observed by Barter et al (BAR 60) as $-16.3(8)\times10^{-6}$ ergG^{-2}mole^{-1}

molecular constant	ref. KUK 70,71	this work	ref. LAW 72	units
$g_\perp$	0.568(2)	0.5657(21)[a]		nm
$g_\parallel$	0.500(2)	0.5027(38)[a]		nm
$\chi_\parallel - \chi_\perp$	1.3(3)[b]	1.127(7)		10^{-6}erg.G^{-2}mole^{-1}
$\chi_{p\parallel} - \chi_{p\perp}$		2.720(44)		10^{-6}erg.G^{-2}mole^{-1}
$\chi_{d\parallel} - \chi_{d\perp}$		-1.593(44)	-1.624	10^{-6}erg.G^{-2}mole^{-1}
$\Theta_\parallel$	-3.3(4)[b]	-3.248(52)		10^{-26}esu.cm^2
$\sigma^N_\parallel - \sigma^N_\perp$		-250(230)		ppm
$\sigma^H_{aa} - \sigma^H_{bb}$		-31 (10)		ppm
$\sigma^H_{p,aa} - \sigma^H_{p,bb}$		77.00		ppm
$\sigma^H_{d,aa} - \sigma^H_{d,bb}$		-108 (10)	-63.145	ppm

Table 5.3. Molecular constants for NH_3. All values are averaged over the inversion states.

[a] Measured by Verhoeven (VER 70)

[b] After a reassignment (KUK 72)

The paramagnetic susceptibility is proportional to the electronic contribution to the G-tensor:

$$\chi_{p,aa} = - \frac{e^2 h \, g_{e,aa}}{16\pi m \, M_p \, A_{aa}} \qquad (5.11)$$

The diamagnetic contribution to $\underline{\underline{\chi}}$ is simply the difference between the total susceptibility and the paramagnetic part. Because of the large error in the observed average susceptibility (the error in χ_{av} is about as large as the observed value of $\chi_{\parallel} - \chi_{\perp}$) only $\chi_{p\parallel} - \chi_{p\perp}$ and $\chi_{d\parallel} - \chi_{d\perp}$ are given in Table 5.3.

The molecular quadrupole moment $\Theta_{\parallel}$ can be calculated from the values for $g_{\parallel}$ and $g_{\perp}$ and $\chi_{\parallel} - \chi_{\perp}$ using the relation Eq(5.3). The result is given in Table 5.3. We see that the value agrees with the value of Kukolich (KUK 72).

The shielding anisotropy of the protons was obtained from the $2_{1u} \rightarrow 2_{1l}$ transition. Unfortunately only $\sigma^H_{aa} - \sigma^H_{bb}$ could be observed. The paramagnetic shielding is calculated using the values for the components of the spin-rotation tensor obtained by Hougen (HOU 72) and the relation between $\underline{\underline{\sigma}}_p$ and $\underline{\underline{M}}_e$ given in Eq(5.1). The value for $\sigma^H_{p,aa} - \sigma^H_{p,bb}$ obtained in this way yields $\sigma^H_{d,aa} - \sigma^H_{d,bb}$. The average proton shielding in NH_3 $\sigma^H_{av} = 30.68$ ppm was obtained by Wofsy et al (WOF 71) from experimental values by Arrighini et al (ARR 70). Since the value of σ^H_{cc} is not known the components of $\underline{\underline{\sigma}}^H$ cannot be determined, so in Table 5.3 only the difference $\sigma^H_{aa} - \sigma^H_{bb}$ is given.

In view of the large error in the nitrogen shielding no attempt was made to calculate the paramagnetic and diamagnetic contribution to it.

An extensive calculation of the one electron properties of ammonia has been performed by Laws et al (LAW 72). Wherever

theoretical results are known they are given in Table 5.3. It is seen from this Table that there is a good agreement between the present experimental value of $\chi_{d\parallel} - \chi_{d\perp}$ and the theoretical one. The deviation between theory and experiment is less than 2%. For the diamagnetic proton shielding the difference between experiment and theory is, however more than 30%.

5.3 FLUOROFORM

The coupling constants given in Table 4.6 can be combined to determine the components of the various tensors in the fluoroform molecule. The nuclear contribution to these tensors is calculated using the geometry parameters obtained by Ghosh et al (GHO 52). The molecular magnetic moment and susceptibility are discussed in Sect. 5.3.1, while the spin-rotation interaction and the shielding follow in Sect. 5.3.2.

5.3.1 Molecular magnetic moment and susceptibility

In the measurements on the $J_K = 2_1 \rightarrow 1_1$, $\Delta M=0$ transitions only the absolute value of $g_{21}-g_{11}$ was observed. In this section we shall discuss the sign.

As pointed out in Sect. 4.1.2 (b) the J_K states with $K\neq 0$ possess linear Stark effect. In an external electric field E_o the Stark energy is given by

$$E_{st} = - \frac{\mu_E E_o MK}{J(J+1)} \qquad (5.12)$$

where μ_E is the electric dipole moment. In the employed state selector only states with positive Stark effect, so with negative M, are selected. In the $2_1 \rightarrow 1_1$ transition the (J,M)=(1,-1)

level has the best Stark effect, and is best focussed at low selector fields (see Sect. 4.1.2 (b)). This level, which possesses the highest energy in the electric field, will in the presence of a (large) magnetic field pass to the level with the highest magnetic energy. Majorana transitions are unlikely, because the level splitting due to the Zeeman effect is large. The level with the highest Zeeman energy in the 1_1-state is the (J,M)=(1,1), since the molecular magnetic moment is negative (FLY 70). The transition with the highest intensity is therefore the (J,M) = (1,1) → (2,1), and hence the observed shift is proportional to $-(g_{21}-g_{11})$. The observed shift is positive so $g_{11}>g_{21}$.

The components of the G-tensor are given in Table 5.4. The susceptibility anisotropy as observed from the $1_o \rightarrow 0_o$ transition in high field measurements is also given in this Table. From the molecular geometry the nuclear contribution to $g_\perp$ and $g_\parallel$ can be calculated using the formulae in Table 5.1. Subtracting this nuclear contribution gives $g_{e\perp}$ and $g_{e\parallel}$. From these constants $\chi_{p\perp}$ and $\chi_{p\parallel}$ can be obtained using Eq(5.11). The observed value for $\chi_\parallel - \chi_\perp$ gives then $\chi_{d\parallel} - \chi_{d\perp}$ by subtracting $\chi_{p\parallel} - \chi_{p\perp}$. The molecular quadrupole moment was calculated from the g-values and the anisotropic susceptibility using Eq(5.3). It is seen from Table 5.4 that the present value of $\Theta_\parallel$ agrees with the value of Flygare and Benson (FLY 70). These authors did not observe $g_\parallel$, but instead assumed that $g_\parallel$ in fluoroform is equal to the g-factor of the spherical top molecule CF_4, where g= -0.031. We see that the observed value of $g_\parallel$ in fluoroform is indeed of the same order of magnitude.

Recent studies by Ozier et al (OZI 76) on g-factors in spherical top molecules pointed out that the electronic part of

molecular constant	this work	previous results	units
$(M^F_{aa}+M^F_{bb})/2$	10.37(13)	10.3(6)[a]	kHz
$M^H_\perp$	-3.0(6)	-2.0(15)[a]	kHz
$g_\perp$	-0.036266(93)	-0.0359(8)[b]	nm
$g_\parallel$	-0.033330(93)		nm
$\chi_\parallel - \chi_\perp$	-1.727(35)	-1.2(6)[b]	10^{-6}cm^3/mole
$(\sigma^F_{aa}+\sigma^F_{bb}+\sigma^F_{cc})/3$		274.2[c]	ppm
$\sigma^F_{cc}-(\sigma^F_{bb}+\sigma^F_{cc})/2$	78.0(39)		ppm
$\sigma^H_\parallel - \sigma^H_\perp$	-66(46)		ppm
$g_{e\perp}$	-0.53697(50)		nm
$g_{e\parallel}$	-0.510761(93)		nm
$\chi_{d\parallel} - \chi_{d\perp}$	-83.99		10^{-6}cm^3/mole
$\Theta_\parallel$	4.867(24)	3.6(20)	10^{-26}esu.cm^2
$(\sigma^F_{aa}+\sigma^F_{bb})/2$	248.2		ppm
σ^F_{cc}	326.2		ppm
$(\sigma^F_{p,aa}+\sigma^F_{p,bb})/2$	-274.6		ppm
$\sigma^F_{p,cc}$	-331.1		ppm
$(\sigma^F_{d,aa}+\sigma^F_{d,bb})/2$	552.8		ppm
$\sigma^F_{d,cc}$	659.3		ppm

Table 5-4 Molecular constants for CF_3H. [a] Ref.(KUK 72), [b] ref.(FLY 70), [c] ref.(HIN 68)

the g-factor in the molecules CF_4, SiF_4 and GeF_4 are the same to within 1%. The value of g_e observed by Ozier *et al* for CF_4 is (OZI 76)

$$g_e = -0.50848(5)$$

This is very close to the value for $g_{e\|}$ in CF_3H in Table 5.4. Since we know that the component of the inertia tensor along the symmetry axis in fluoroform is almost equal to the inertial constant in CF_4 we may conclude from Eq(5.2) that

$$\left(\sum_n \frac{|\langle o|L_c|n\rangle|^2}{E_o - E_n} \right)_{CF_4} \simeq \left(\sum_n \frac{|\langle o|L_c|n\rangle|^2}{E_o - E_n} \right)_{CF_3H} \qquad (5.13)$$

Although this near equality is interesting of itself, its implications are not immediately evident, since excited molecular states are involved.

5.3.2 *Spin-rotation constants and nuclear shielding*

For the $2_1 \rightarrow 1_1$ rotational transition a hyperfine splitting $\Delta\nu$ was observed (see Table 4.6). This splitting turned out to be independent of the applied field.

The hyperfine interactions in fluoroform are the fluorine-proton spin-spin interaction, the fluorine spin-rotation interaction, and the proton spin-rotation interaction. For K=1 there is no fluorine spin-spin interaction since the total spin of the fluorine equals 1/2. The spin-spin interaction can be calculated using the known molecular geometry (GHO 52), and gives only a small contribution to the hyperfine energy. In most methyl compounds the spin-rotation interaction of the proton is small (except for methane). So the largest contribution to the hyperfine structure originates from the fluorine spin-ro-

tation interaction.

Since in the measurements the $\Delta M=0$ transitions were observed, for the spin-rotation interaction only $|c^F_{21}-c^F_{11}|$ can be obtained. From the selection rule $\gamma \rightarrow 1-\gamma$ for electric dipole transitions it is clear that the δ_{K1}-term in the difference drops out and we have

$$|c^F_{21}-c^F_{11}| = \frac{1}{3}\left|M^F_{cc} - \frac{M^F_{aa}+M^F_{bb}}{2}\right| \qquad (5.14)$$

The value of $M^F_{aa}+M^F_{bb}$ was observed from the zero field measurements on the $1_o \rightarrow 0_o$ transition. If we assume that the splitting $\Delta\nu$ is due to the spin-rotation interaction of the fluorine nucleus, then we have from Eq(5.14)

$$M^F_{cc} = +\ 79.6 \text{ kHz (for } c^F_{21}>c^F_{11}) \qquad (5.15a)$$

$$M^F_{cc} = -\ 58.8 \text{ kHz (for } c^F_{21}<c^F_{11}) \qquad (5.15b)$$

In the first case the trace of the $\underline{\underline{M}}^F$-tensor is positive ($\frac{1}{3}$ Tr($\underline{\underline{M}}^F$)=+33.4) and negative in the second case (-12.7). From the measurements on CF_4 (TIG 70) and CFH_3 (WOF 71) a negative sign should be preferable*). Both values for M^F_{cc}, however, are quite high. This is even better illustrated by the paramagnetic shielding that can be obtained from this tensor (Eq(5.1)). The nuclear contribution to M^F_{cc} is -5.66 kHz. Then we find for the shielding

$$\sigma^F_{p,cc} = -2647 \text{ ppm (for } c^F_{21}> c^F_{11}) \qquad (5.16a)$$

$$\sigma^F_{p,cc} = +1648 \text{ ppm (for } c^F_{21}<c^F_{11}) \qquad (5.16b)$$

*) Note that in (WOF 71) the spin-rotation tensor $\underline{\underline{C}}^F = -\underline{\underline{M}}^F$

The largest paramagnetic fluorine shielding observed until now is -690.1 ppm in F_2 (WOF 71). For this reason we are inclined to reject both values in Eq(5.15a) and (5.15b), and hence also the M^F_{cc} values in Eqs(5.15a) and (5.15b).

Now the question arises, what causes the splitting $\Delta\nu$? It has been mentioned above that $\Delta\nu$ is independent of the applied magnetic field, but it is too high to be caused by a hyperfine interaction, because even the largest, $\underline{\underline{M}}^F$, yield unacceptable results. The only solution is that $\Delta\nu$ is caused by a machine effect. Indeed, it is known that when a microwave cavity is not resonating in the usual TM_{010}-mode, but instead in a TM_{01q}-mode a splitting of the spectral lines occurs. If v is the velocity of the molecules and L the length of the cavity then lines appear at ν_o+qv/L and at ν_o-qv/L, where ν_o is the transition frequency. The distance between the components is therefore $2qv/L$. For fluoroform in a seeded beam and a cavity length of 16 cm, we have to assume q=4 to explain the measured splitting.

It is very well possible that a wrong mode is generated in the cavity because in the frequency region between 38-43 GHz many cavity resonances were observed. Most of them could not be identified as a TM or a TE mode. The mode we worked with was chosen, because of its relatively high Q-value, and because it was not very sensitive to a disturbance at the endcaps. Both properties are characteristic for the TM_{01q} modes with low q. Therefore we assume that indeed the TM_{014} mode is generated in the cavity.

Because of the presence of the ν_{K1}-terms in the coupling constants the spectrum consists out of eight lines. We pointed out above that the observed "lines" are most probably twice the same "line". Under this assumption each of the observed lines

should contain eight components. The observed lines, although rather broad, show little structure and no conclusions about the coupling constants can be drawn from the observed spectrum.

From the line broadening due to spin-rotation interaction in nuclear magnetic resonance molecular beam spectra Follet (FOL 70) obtained a relation between $M^F_{aa}+M^F_{bb}$ and M^F_{cc}. From the present value for $M^F_{aa}+M^F_{bb}$ we obtain

$$M^F_{cc} = 5.0(10) \text{ kHz}$$

The nuclear contribution to the spin-rotation tensor can be calculated from the molecular geometry. From the electronic contribution to $\underline{\underline{M}}^F$ the paramagnetic fluorine shielding $\underline{\underline{\sigma}}^F_p$ can be calculated using Eq(5.1). In the $1_o \rightarrow 0_o$ transition the value of $\sigma^F_{cc} - \frac{1}{2}(\sigma^F_{aa}+\sigma^F_{bb})$ was obtained, and together with the value for σ^F_{av} obtained by Hinderman and Cornwell (HIN 68) the values of σ^F_{cc} and $\frac{1}{2}(\sigma^F_{aa}+\sigma^F_{bb})$ can be calculated. The diamagnetic contribution is then obtained by subtracting the paramagnetic part. For the shielding tensors no error is given in Table 5.4, since the error in σ^F_{av} is not known. The error in the diamagnetic shielding component $\sigma^F_{d,cc}$ is however quite large (about 20%), because the error in M^F_{cc} is rather large.

Wofsy et al (WOF 71) have compared the diamagnetic fluorine shieldings in some fluorine containing molecules. The values of $\sigma^F_{d,av}$ in all these molecules is about 470 ppm. The present value, as obtained in Table 5.4 is

$$\sigma^F_{d,av} = 568.0 \text{ ppm}$$

This value is rather high, but it should be remembered that the error in $\sigma^F_{d,cc}$ is high too, although in order to get an overlap with the other average diamagnetic shieldings an error of 100 ppm has to be assumed.

We believe that a more accurate value of M_{cc}^{F} will lead to more reliable results. A more accurate value of M_{cc}^{F} can, however, only be obtained in states with relatively high K-values and consequently high J-values. The transitions with higher J appear at frequencies above 60 GHz, and beam maser measurements would require another type of resonator. More details about measuring at high frequencies are given in Sect. 5.9.

5.4 METHYL CHLORIDE

Measurements on the $J_K=1_o \rightarrow 0_o$ transition of $CH_3{}^{35}Cl$ were mainly performed to obtain the chlorine nuclear shielding, and, if possible, the hydrogen nuclear shielding.

Because of the large chlorine quadrupole moment there is a strong coupling between $\underline{J}$ and $\underline{I}_{Cl}$. At a field of 8 kG the quantum number associated with $\underline{F}_1=\underline{J}+\underline{I}_{Cl}$ is still a good quantum number. Although the strong coupling complicates the spectrum considerably, it has the advantage that the average chlorine nuclear shielding can be obtained. In addition the sign of the g_{JK} coupling constant can be unambiguously determined.

From the coupling constants for methyl chloride given in Chap. 4 the tensor components of Table 5.5 are obtained. The nuclear contributions to the tensor components are calculated using the geometry parameters obtained by Costain (COS 58).

As pointed out above it is seen from Table 5.5 that indeed both the average chlorine shielding and the anisotropic chlorine shielding is observed. The average value of $\underline{\underline{\sigma}}^{Cl}$ is calculated from $g_{Cl}(1-\sigma_{av}^{Cl})$ using $g_{Cl}= 0.547867(33)$. The result is

$$\sigma_{av}^{Cl} = 836(79) \text{ ppm}$$

This value agrees with the value obtained by Dubrulle *et al*

molecular constant	this work	previous results	units
eqQ^{Cl}	74743.4(15)	74749.6(13)[a]	kHz
$M_{\perp}^{Cl}$	1.83(20)	2.70(14)[a]	kHz
$g_{\perp}$	-0.016672(91)	-0.01653(28)[b]	nm
$\chi_{\parallel}-\chi_{\perp}$	-8.371(17)	-7.95(40)[b]	$10^{-6}cm^3$/mole
$g_{Cl}(1-\sigma_{av}^{Cl})$	0.547409(55)		nm
$\sigma_{\parallel}^{Cl}-\sigma_{\perp}^{Cl}$	1441(130)		ppm
$\sigma_{\parallel}^{H}-\sigma_{\perp}^{H}$	<2.2		ppm
g_{el}	-0.632023(91)		nm
$\sigma_{\parallel}^{Cl}$	1796(117)		ppm
$\sigma_{\perp}^{Cl}$	356(90)		ppm
σ_{dl}^{Cl}	1655(53)		ppm
$(M_{aa}^{H}+M_{bb}^{H})/2$	-0.19(16)		kHz

Table 5-5 molecular constants for $CH_3{}^{35}Cl$

[a] ref.(DUB 77)

[b] ref.(VAN 70)

(DUB 77) from the measured chemical shift by Saito (SAI 65). They obtain for σ_{av}^{Cl} a value of 890 ppm.

The nuclear contribution to $M_{\perp}^{Cl}$ can be obtained from the geometry, and $M_{e\perp}^{Cl}$ is then obtained by subtracting the nuclear part from the experimental results for $M_{\perp}^{Cl}$. From $M_{e\perp}^{Cl}$ the paramagnetic contribution to $\sigma_{\perp}^{Cl}$ can be derived using Eq(5.1). The diamagnetic shielding is then obtained by taking the difference $\sigma_{\perp}^{Cl}-\sigma_{p\perp}^{Cl}$.

For the hydrogen spin-rotation interaction as well as the hydrogen anisotropic shielding only an upper limit could be obtained. The low value for the spin-rotation constant was expected from results of Wofsy et al (WOF 71) on methyl fluoride.

Recently Dubrulle et al (DUB 77) reported high resolution beam absorption measurements on methyl chloride. The authors obtained values for eqQ^{Cl}, $c_{\perp}^{Cl}$ and $c_{\parallel}^{Cl}$. Their zero field frequency ν_o was obtained using for the rotational constant the value 13292876.30(7) kHz and for the centrifugal distortion constant d_J=18.089(1) kHz given in Table 2 of the quoted reference.

The most apparent discrepancy between the present results and the result of Dubrulle et al is the difference in the value of eqQ^{Cl}, as can be seen in Table 5.5. It has been mentioned in Sect. 2.2.2 that only two F_1-levels are focussed. For determination of the F_1=3/2 lines we had to calculate the Stark effect as explained in Sect. 4.1.3. In the calculation only second order Stark effect has been included, and it might be possible that also the fourth order effect contributes appreciably. Therefore we decided to refit the spectrum leaving out the F_1=3/2 levels and instead use ν_o obtained in (DUB 77). The new fit yielded

$$eqQ^{Cl} = 74752.8(36) \text{ kHz}$$
$$c_{\perp}^{Cl} = 1.6(4) \text{ kHz}$$

So we see that, although the value for eqQ^{Cl}_{Cl} is now in agreement with the result of Dubrulle et al the value for c_1^{Cl} deviates even more from the c_1^{Cl} value of (DUB 77). Because a simultaneous fit in zero and non-zero magnetic field was performed also new values for the other coupling constants were obtained. It appeared that the new value of g does not agree with the value of (VAN 70). For the average shielding we obtain

$$\sigma^{Cl}_{av} = 1078 \text{ ppm}$$

a value that does not agree with the value observed by Saito. Another reason to reject this fit is that the obtained χ^2 is much higher than the previous fit. This is basically due to one zero field line, which deviates more than 3 kHz from the observed position.

In conclusion the new fit must be rejected for two reasons first of all is the χ^2 worse than in the old fit, and secondly the values for the new coupling constants deviate from previous results of other investigations wherever available.

In addition we made an estimate of the fourth order Stark effect necessary to determine the position of the F_1=3/2 line. It appeared that its contribution is less than 500 Hz and hence negligible within the accuracy of the instrument. So we feel that the constants in Table 5.5 are reliable.

The difference between the present investigation and the observations by Dubrulle et al originates probably in the fact that in the measurements of (DUB 77) the proton spin-rotation interaction is not included in the fit. Although the component of this tensor perpendicular to the symmetry axis of the molecule is rather small, the component parallel to the symmetry axis can be quite large. In the comparable molecule CFH_3 Wofsy et al obtained (WOF 71)

$$(M^H_{aa}+M^H_{bb})/2 = 0.8(15) \text{ kHz}$$

$$M^H_{cc} = 14.66(7) \text{ kHz}$$

If we assume that the geometry of the methyl group is not disturbed by replacing F by Cl, then in fact $M^H_{n,cc}$ does not change at all as can be seen from Table 5.1, and we believe that $M^H_{e,cc}$ will not change very much too, because the latter term is most sensitive to the electrons close to the nucleus. Consequently in CH_3Cl the value of M^H_{cc} is expected to be approximately the same as the value given above. In (DUB 77) the authors observed a value for M^{Cl}_{cc} of 7.0(16), which is clearly smaller than the expected value for M^H_{cc}. Another interaction that has to be taken into account, for K=3 states, is the proton-proton spin-spin interaction; for the observed states it is about 3 kHz. We suggest that the spectrum of (DUB 77) has to be refitted, taking into account the interactions described above. We think that a new fit will yield definitely different values for the chlorine spin-rotation constants. Dubrulle et al use a method developed by Gierke and Flygare (GIE 72) for calculating σ_d in a semi empirical way. Using the measured spin rotation constants, they obtain

$$\sigma^{Cl}_{\parallel} - \sigma^{Cl}_{\perp} = +276.2 \text{ ppm}$$

a value which is about 1/6 of the experimental value given in Table 5.5.

Microwave absorption measurements by Vanderhart and Flygare (VAN 70) in a magnetic field of about 25 kG yielded values for g and $\chi_{\parallel} - \chi_{\perp}$. Their values are reproduced in Table 5.5. It is seen that both constants are in agreement with the present results. Because of higher resolution, however, the present results are more accurate.

Theoretical calculations by Bendazolli et al (BEN 73) using SCF-MO wavefunctions yield for the chlorine quadrupole coupling a value

$$eqQ^{Cl} = 78820 \text{ kHz}$$

This value differs by 6% from the present experimental value. Although they calculated the electric dipole moment, which involves $\langle o|\sum_i r_i|o\rangle$, they did not calculste other one electron properties, such as the diamagnetic shielding, or the molecular quadrupole moment.

In the present investigation we were not able to derive $\Theta_{\parallel}$ for methyl chloride, because $g_{\parallel}$ could not be determined. This tensor component can only be obtained in a transition with $K \neq 0$. So it requires states with $J \geqslant 1$. Out of the $\Delta J = \pm 1$ transitions with $K \neq 0$ the one at the lowest frequency is the $J_K = 2_1 \rightarrow 1_1$ transition at about 53 GHz. This frequency is beyond the range of our apparatus, because the diameter of the cavity becomes too small to obtain a reasonable S/N ratio. A discussion of the possibilities is given in Sect. 5.9.

Vanderhart and Flygare assume for $g_{\parallel}$ a value of 0.305(20). This is based on the fact that for CH_3Br and CH_3I the observed value of $g_{\parallel}$ is approximately the same. The error in this assumed value for $g_{\parallel}$ is so large that a determination of $\Theta_{\parallel}$ does not yield a more accurate result than their value.

The diamagnetic part of $\sigma_{\parallel}^{Cl}$ can be obtained if $\sigma_{p\parallel}^{Cl}$ is known. To calculate $\sigma_{p\parallel}^{Cl}$ we need $M_{\parallel}^{Cl}$. Although this tensor component is observed we do not believe that the value in (DUB 77) is reliable for reasons expained above.

Dubrulle et al have calculated average nuclear shieldings for ^{35}Cl from measurements on chemical shifts by NMR spectroscopy. The chemical shift is defined as the difference in nu-

clear shielding of the nucleus in different (chemical) environments. They used the approximate relation for σ_d given by Gierke and Flygare, and the spin-rotation constants to determine σ_p. By adding these quantities they obtain the absolute shielding in CH_3Cl, and from the chemical shifts other chlorine shieldings are obtained. Since we believe that their values for the spin-rotation constants are wrong, also the paramagnetic contributions in Table 4 of (DUB 77) to the chlorine shieldings should be revised. From the calculated value of $\sigma_{d,av}$ in (DUB 77), which is 1186 ppm, we can obtain $\sigma_{d\parallel}$ in using the value of $\sigma_{d\perp}$ in Table 5.5. In this way we obtain

$$\sigma_{d\parallel} = 248 \text{ ppm}$$

5.5 *WATER D_2O*

The measurements on D_2O yielded more accurate values for the susceptibility anisotropy as well as an upper limit for the deuteron shielding. The values of the susceptibility constants $\chi_{aa} - \chi_{av}$, $\chi_{bb} - \chi_{av}$ are obtained using Eq(3.73). It is seen from Table 5.6 that the present values agree with the less accurate values of Verhoeven (VER 69). For the deuteron shielding tensor components $\sigma^D_{aa} - \sigma^D_{av}$ and $\sigma^D_{bb} - \sigma^D_{av}$ only an upper limit could be obtained.

One electron properties of the water molecules have been calculated recently by Dunning et al (DUN 72). They calculated for the diamagnetic susceptibility tensor

$$\chi_{d,aa} = -15.9\times10^{-6} \text{ cm}^3/\text{mole} \quad *)$$
$$\chi_{d,bb} = -13.9\times10^{-6} \text{ cm}^3/\text{mole}$$
$$\chi_{d,cc} = -14.8\times10^{-6} \text{ cm}^3/\text{mole}$$

*) 1 $\text{cm}^3/\text{mole} = 1 \text{ erg } G^{-2}/\text{mole}$

molecular constant	ref (VER 69)	this work	units
$\chi_{aa}-\chi_{av}$	0.154(12)	0.1648(24)	$10^{-6}cm^3/mole$
$\chi_{bb}-\chi_{av}$	-0.066(16)	-0.0834(24)	$10^{-6}cm^3/mole$
$\sigma^D_{aa}-\sigma^D_{av}$		<132	ppm
$\sigma^D_{bb}-\sigma^D_{av}$		<257	ppm
$\chi_{d,aa}-\chi_{d,av}$		0.938(3)	$10^{-6}cm^3/mole$
$\chi_{d,bb}-\chi_{d,av}$		0.131(3)	$10^{-6}cm^3/mole$

Table 5-6 Molecular constants for D_2O from high field measurements

From the observed susceptibilities for D_2O the corresponding susceptibilities for H_2O can be obtained using (VER 69)

$$\chi_{d,gg}(H_2O) = \chi_{d,gg}(D_2O) + \mu_B^2 m\{2d\langle o|\Sigma_i b_i^H|o\rangle + \\ + n_{el}d^2\}[\delta_{ga} + \delta_{gc}] \qquad (5.17)$$

where (0,d,0) is the position of the CM of H_2O with respect to the CM of D_2O, and n_{el} the number of electrons in the molecule. The first term in the brackets can be obtained from the molecular dipole moment of 1.85D (in the -b direction). Making this substitution to the diamagnetic contributions in Table 5.6 yields

$$2\chi_{d,aa} - \chi_{d,bb} - \chi_{d,cc} = 2.868(10)\times10^{-6}cm^3/mole^{-1}$$
$$2\chi_{d,bb} - \chi_{d,aa} - \chi_{d,cc} = 0.282(10)\times10^{-6}cm^3/mole^{-1}$$

These values agree with the theoretical values. Although the authors calculated the average shielding, they did not report

the anisotropic shielding, so a comparison cannot be made.

5.6 SULPHUR DIOXIDE

The Zeeman effect was measured by Pochan et al (POC 69) and by Bhattacharyya and Dailey (BHA 69) in a Zeeman absorption spectrometer. There were rather large discrepancies in the components of the susceptibility tensor in SO_2 obtained by Pochan et al and by Bhattacharyya and Dailey and the results of ab-initio calculations by Rothenberg and Schaefer (ROT 70). The discrepancies originated most probably in the overlap of the Zeeman components and Stark interference as a result of insufficient resolution of the spectrometers employed.

In a molecular beam maser the resolution is about 50 times higher than in absorption spectrometers. In addition no Stark modulation is employed. In spite of a considerably lower field (8 kG in the present investigation versus 25 kG in (POC 69)) we were able to observe both the molecular G-tensor and the susceptibility anisotropy as accurately as in the measurements of Pochan et al. The present results confirm Pochan's results (Table 5.7).

It is seen that the molecular quadrupole moment, which can be calculated from the components of the $\underline{\underline{G}}$- and $\underline{\underline{\chi}}$-tensor using Eq(5.3) differs somewhat from the value calculated by Rothenberg and Schaefer. Although the sign for Θ_{aa}, Θ_{bb} and Θ_{cc} agrees, the magnitude differs by 30-60%.

Only low field measurements on SO_2 have been performed. High field measurements on the common isotope $^{32}S^{16}O_2$ would not lead to essentially new information, since it has no nuclear spins.

molecular constant	ref POC 69	ref BHA 69	this work	ref ROT 70	units
g_{aa}	-0.6037(5)		-0.6043(3)		nm
g_{bb}	-0.1161(2)		-0.11634(12)		nm
g_{cc}	-0.0882(4)		-0.08865(10)		nm
$\chi_{aa}-\chi_{av}$	2.13(18)	3.8(12)	1.86(4)		10^{-6}cm^3/mole
$\chi_{bb}-\chi_{av}$	1.02(11)	-1.4(5)	1.20(3)		10^{-6}cm^3/mole
$\chi_{cc}-\chi_{av}$	-3.35(25)	-2.4(6)	-3.06(5)		10^{-6}cm^3/mole
Θ_{aa}	-5.3(4)	-6.6(76)	-4.91(10)	-6.88	10^{-26}esu.cm^2
Θ_{bb}	1.3(4)	8.9(83)	1.02(3)	+1.71	10^{-26}esu.cm^2
Θ_{cc}	4.0(6)	-2.3(76)	3.86(6)	+5.17	10^{-26}esu.cm^2

Table 5.7 Molecular constants for SO_2

5.7 HYDROGEN PEROXIDE

The internal rotor H_2O_2 is the simplest molecule that posesses internal rotation. It is therefore that in the past ten years many theoretical papers on this molecule were reported.

The first ab-initio calculations on H_2O_2 (on the barriers to internal rotation) were reported by Kaldor and Shavitt (KAL 66). The results agreed rather poorly with the experimental barriers. Since the theory has been improved considerably and the values for V_{cis} and especially V_{trans} (see Chap. 3 and Fig. 3.3 for definition) obtained by Dunning and Winter (DUN 75) using Hartree-Fock type basis functions are in good agreement with the experimental values.

Until now only gross features as the total electronic energy and the internal rotor potential were examined. It is known that molecular constants such as the electronic dipole moment and the molecular quadrupole moment are more sensitive to the electronic wavefunctions than the energy. Consequently these one electron properties will lead to a better understanding of the internal rotation in the molecule.

For these reasons Zeeman measurements on hydrogen peroxide were performed to obtain the molecular quadrupole moment. From the studied transitions both the values of $g_{JK\tau}$ and $\chi_{JK\tau}$ could be observed, as can be seen in Table 4.16.

In zeroth order the rotational wavefunction is the symmetric rotor function as is shown by Hunt et al (HUN 64). This approximation is good to within 1% or better. The error in the $\chi_{JK\tau}$ constants is of the order of 5% and hence we can safely use this approximation to obtain the expectation values $\langle\tau|\chi_{aa} - \chi_{av}|\tau\rangle$ and $\langle\tau|\chi_{bb} - \chi_{av}|\tau\rangle$. It is seen from Table 5.8 that within the experimental error

molecular constant	observed value	units	
g_{aa}	-0.053197	nm	
g_{bb}	-0.082813	nm	
g_{cc}	0.646553	nm	
$\chi_{aa}-\chi_{av}$	2.80(12)	$10^{-6}cm^3$/mole	$\tau=2$
$\chi_{bb}-\chi_{av}$	3.84(22)	$10^{-6}cm^3$/mole	$\tau=2$
$\chi_{aa}+\chi_{bb}-2\chi_{av}$	6.42(16)	$10^{-6}cm^3$/mole	$\tau=4$
Θ_{aa}	-5.64(30)	$10^{-26}esu.cm^2$	
Θ_{bb}	-5.39(35)	$10^{-26}esu.cm^2$	
Θ_{cc}	11.02(46)	$10^{-26}esu.cm^2$	

Table 5.8 Molecular constants for H_2O_2

$$\langle\tau = 2|\chi_{aa} + \chi_{bb} - 2\chi_{av}|\tau = 2\rangle = \langle\tau=4|\chi_{aa}+\chi_{bb}-2\chi_{av}|\tau=4\rangle \tag{5.17}$$

In order to obtain the values for Θ it is necessary to know the components of the magnetic moment tensor. The error in the observed magnetic moment coupling constant is less than 1 part in 10^4, so that to obtain the tensor components to the same accuracy we are no longer allowed to use the symmetric rotor approximation for the wavefunction, but higher order corrections are needed. However to obtain the components of the molecular quadrupole tensor we are allowed to calculate g_{aa},g_{bb} and g_{cc} in the symmetric rotor approximation, because the error in the components of Θ are determined by the (5%) error in the components of χ. In addition to the symmetric rotor approximation we have to assume that the G-tensor is not very sensitive to the internal rotor state. This implies that we took $\langle\tau=2|g_{\alpha\alpha}|\tau=2\rangle = \langle\tau=4|g_{\alpha\alpha}|\tau=4\rangle$ for α=a,b and c respectively. The values obtained in this way are given in Table 5.8. Because of the approximations used no errors are given in the components. It should be mentioned that for the components of the magnetic moment tensor only relative signs can be obtained. The sign of g_{cc} is assumed to be the same as the sign of g_{cc} in water.

The rotational constants needed in the calculation of the molecular quadrupole moment using Eq(5.3) are taken from Oelfke and Gordy (OEL 69). In spite of the approximations we necessarily had to make, because no more data were available, we assume that the values for Θ_{aa}, Θ_{bb} and Θ_{cc} in Table 5.8 are reliable subject to the error given there. This assumption is based upon the fact that for the other molecular constants, which are independent in first order of the internal rotation angle, the internal rotation effect is less than 10^{-3} (OEL 69).

A comparison of the molecular quadrupole moment with the quadrupole moment of H_2O as obtained by Verhoeven, points out that the values in hydrogen peroxide are somewhat larger, which is mainly due to the difference in the anisotropic susceptibility, in water (VER 69)

$$\chi_{aa} - \chi_{av} = -0.066(16)\times10^{-6}\ \text{ergG}^{-2}\text{mole}^{-1}$$
$$\chi_{bb} - \chi_{av} = +0.154(8)\ \times10^{-6}\ \text{ergG}^{-2}\text{mole}^{-1}$$

which are considerably lower than the values obtained for H_2O_2.

We expect that a dependence of $\underline{\underline{G}}$ on the internal rotation state should be observable in the present apparatus, because the accuracy of the coupling constants is in the order of 10^{-4}. A dependence can, however only be obtained when g_{JK} values for a variety of J,K and τ are available. In spite of the fact that the hydrogen peroxide is very rich of lines, other interesting transitions (for low J-values) occur only at frequencies of 67 GHz and higher. Transitions at these frequencies can be measured in a polar magnet using flat resonators instead of the common cylindrical cavities.

Another possibility is to study the isotopic forms D_2O_2 and HOOD. One disadvantage of these molecules is that the rotational spectrum is not very well known. For HOOD the observed microwave rotation-inversion spectrum has not been understood yet (MAS 60), while the interesting transitions (with low J) for D_2O_2 occur all at high frequencies (above 50 GHz (OEL 69)).

5.8 METHYL ALCOHOL

In Chap. 4 we mentioned the fact that for the studied E-type transitions (J,K=2) → (J,K=1) the linewidth was much larger in zero field than in a magnetic field. We shall now explain these broad features.

Let $\underline{I}_4$ be the angular momentum operator associated with the proton in the OH group and $\underline{I}_T$ the total spin of the protons in the methyl group. Let further the coupling scheme be $\underline{F}_1=\underline{J}+\underline{I}_4$ and $\underline{F}=\underline{F}_1+\underline{I}_T$. As discussed by Heuvel (HEU 72) this coupling scheme is the most likely one.

The E-type levels have $I_T=1/2$. So every rotational E-state with J>0 consists out of four hyperfine levels, (F=J+1,J,J,J-1 respectively), each level is doubly degenerated (K-degeneracy). Intensity calculations for the E-type transitions show that the hyperfine spectrum should consist of four strong lines with $\Delta F=\Delta F_1=0$ and a number of weaker lines. The relative intensity of the weaker lines is such that they disappear in the noise (ELL 74). The observed "line" especially for J=2 is so broad that four lines distributed arbitrarily within the frequency range of the line shape should clearly give structure to the "line".

This reasoning is correct if both rotational J,K-states consist of four hyperfine levels, all doubly degenerated. For K=1, however, the degeneracy is lifted by the δ_{K1}-terms (HEU 72). Hence instead of four lines the $J_2 \rightarrow J_1$ transition consists out of eight $\Delta F=\Delta F_1=0$ lines. Eight lines with a linewidth of about 6-8 kHz each can give a line shape, which corresponds to the observed "line".

Because of the lack of any structure in the observed spectra, combined with the fact that each spectrum consists of eight single lines, it is not possible to draw conclusions about the coupling constants that constitute the spectrum.

Zeeman measurements on these transitions show that the motional Stark effect is the most important interaction in these states, because E-type levels with $K\neq 0$ have first order Stark effect similar to that in symmetric rotors. The Stark energy in

methyl alcohol is given in Eq.(4.2).

The transitions discussed in this section have been observed in interstellar space (BAR 73). The astronomical observations showed structure on the transitions, which is clearly not observed in the zero field laboratory measurements. Therefore it was suggested that the splittings could be due to a magnetic field.

The present observation indicates that, since the most important magnetic interaction is the motional Stark effect, a magnetic splitting is quite improbable. Typical velocities of 10-100 km/s, which are present in interstellar clouds, would require a magnetic field of several gauss in order to observe a shift of only 4-40 kHz. Observations on interstellar OH, which has a magnetic moment of about one Bohr magneton point out that the magnetic fields in interstellar clouds are always in the order of mG. Consequently the splitting of the spectral lines in methyl alcohol lines is not due to the Zeeman effect. A more reasonable explanation for the splitting is that the different lines are due to different parts of the cloud, moving with a different radial velocity, so that the observed lines are in fact lines shifted by the Doppler effect.

5.9 DISCUSSION

In closing it is worthwhile to evaluate the possibilities and shortcomings of our spectrometer for studying weak magnetic interactions by beam maser spectroscopy. This section is divided into two parts. The first describes the machine effects and the second part discusses the molecular properties that can be obtained.

5.9.1 Machine effects

The frequency range of the machine is from 8-45 GHz. The low frequency limit (8 GHz) is caused by the geometry. The diameter of the bore in the superconducting magnet determines the maximum diameter of (cylindrical) cavities. Although measurements on fluoroform at 41.3 GHz proved to be successful, we believe that the upper limit for beam maser experiments using cylindrical cavities is about 45 GHz. At higher frequencies the cavity diameter becomes so small that the accompanying loss in intensity of the beam passing through it and hence in the sensitivity makes detection of maser signals impossible. A way out is to use a parallel disk resonator. This type of resonator is not suitable for the superconducting magnet for two reasons. First of all the useful space in the present magnet is only about 4 cm, while for a reasonable Q-factor the diameter of the resonator disks should be 8-10 cm. The other reason is that the field is homogeneous over a region of 17 cm along the axis and 12 mm in diameter. So the beam width should not exceed 12 mm resulting in a low filling factor of the resonator.

Most of the measurements at high field were performed as $\Delta M=0$ transitions. A complication in this type of transitions is that usually many hyperfine lines overlap. Without any knowledge of the spectrum a determination of the coupling constants becomes then difficult as is illustrated in Sect.5.3.2 for the $2_1 \rightarrow 1_1$ transition in CF_3H. The usually larger splittings of the $\Delta M=\pm 1$ transitions cause another problem. As the molecular g-factor can produce a considerable Zeeman effect at a field of 70 kG, the line broadening due to the field inhomogeneity may become a serious problem. In the measurements on ammonia (Sect. 4.1.1) it turned out to be so large that a

determination of the nitrogen nuclear shielding was not possible.

In several experiments the state scrambler proved to be a powerful tool to repopulate Zeeman levels depleted by the action of the state selector. The occupation of the repopulated levels, however, depends on the type of transitions that have to be induced in the scrambler. When $|\Delta M|>1$ transitions are necessary the repopulation has to occur in more than one step, which makes the transition more difficult to take place.

Calculations on molecular orbits in a state selector show that the gain in (S/N)-ratio stems from an increase of the number of molecules of the focussed levels rather than a decrease of the number of molecules of the defocussed levels. In all of the studied transitions, where scrambling was necessary all levels of the lowest state had negative Stark effect. Using a selector with $\partial E/\partial r<0$ all these levels are focussed and consequently all hyperfine transitions can be measured in the cavity. However, also the levels of the upper state with negative Stark effect are focussed, but in general the Stark effect of these levels differs from the Stark effect of the lower levels resulting in different focussation properties, so that by adjusting the selector voltage the S/N-ratio of a hyperfine transition can be optimized as in the case of fluoroform (Sect. 4.1.2).

5.9.2 Molecular effects

The high field measurements have proved that various weak magnetic interactions in diamagnetic molecules become evident at fields of 70 kG, which are unobservable at fields of 10 kG. In the first place we succeeded to measure the nuclear shielding for fluorine in CF_3H, for chlorine in CH_3Cl and for hydrogen in

NH_3. The proton shielding for CF_3H and CH_3Cl was not observed, because its effect was too small, such that only an upper limit could be obtained. We have seen in Sect. 5.1 that the spin-rotation constant and paramagnetic shielding are related. From many molecules containing methyl groups it is known that the proton spin-rotation interaction is small. Consequently the proton shielding is also expected to be weak, and its effect, even at 70 kG, is only marginal.

The magnetic susceptibility anisotropy is another molecular interaction that can be very well measured even when it is small, as in the case of NH_3 and CF_3H. The susceptibility gives an effect quadratic in the magnetic field, so that its contribution to the energy at 70 kG is about 50 times higher than at 10 kG. From the more accurate value of the susceptibility a more accurate value of the molecular quadrupole moment can be derived. Normally the error in the susceptibility determines completely the error in $\Theta_{\|}$. For symmetric tops the calculation of $\Theta_{\|}$ requires $g_{\|}$, a quantity that can only be measured when $K \neq 0$. Molecules in these states have linear Stark effect as discussed in Sect. 4.1.2 for the $J_K = 1_1 \leftarrow 2_1$ transition in fluoroform. For most of the interesting symmetric rotors the frequency of the rotational transitions involving $K \neq 0$ occur at high frequencies (above 45 GHz). The problems with these high frequencies is discussed in the previous section.

In a review by Flygare and Benson (FLY 71) on measured Zeeman effects in various diamagnetic molecules the authors state that the molecular cubic and quartic susceptibility proportional to H^3 and H^4 respectively are unobservable at fields of 20 kG. We performed a number of measurements in which at various fields the Zeeman effect was observed, and never mea-

sured a contribution of these terms. So we believe that these effects may safely be neglected for the molecules studied. For more complicated molecules a contribution due to these terms might be expected. The components of the tensors responsable for these interactions are complicated functions of the electronic charge distribution and do not give interesting information.

APPENDIX I The coefficients $c^{\Gamma\xi}_{I_{23}}(I_T)$

The coefficients $c^{\Gamma\xi}_{j,I_{23}}(I_T)$ introduced in Sect. 3.1.1 form a transformation matrix from the basis functions $\chi_{I_{23}}(I_T)$ to new basis functions $\chi^{\Gamma\xi}_j(I_T)$ that belong to the irreducible representations of the S_3-group. The transformation of the $\chi^{\Gamma\xi}_j(I_T)$ under the operators of S_3 is given in Eqs(3.13). To obtain the coefficients $c^{\Gamma\xi}_{j,I_{23}}(I_T)$ we must know how the (I_{23},I_T) basis functions transform under the basic operations of S_3. Once we have the transformation matrices we can find out what the coefficients are.

Consider the basisfunctions $|I_{23}I_T\rangle$ for a given value of I_T. Then we have for the (23) operation

$$(23)\ |(I_2I_3)I_{23}I_1I_T\rangle = |(I_3I_2)I_{23}I_1I_T\rangle$$

And from the properties of the Clebsch-Gordan coefficient follows

$$(23)\ |(I_2I_3)I_{23}I_1I_T\rangle = (-1)^{I_2+I_3-I_{23}}|(I_2I_3)I_{23}I_1I_T\rangle \qquad (A\text{-}1)$$

For the other basic operation (132) we get

$$(132)\ |(I_2I_3)I_{23}I_1I_T\rangle = |(I_1I_2)I_{23}I_3I_T\rangle =$$
$$\sum_{I'_{23}} (-1)^{I'_{23}}[(2I_{23}+1)(2I'_{23}+1)]^{\frac{1}{2}} \begin{Bmatrix} I_Y & I_T & I'_{23} \\ I_Y & I_Y & I_{23} \end{Bmatrix} |(I_2I_3)I'_{23}I_1I_T\rangle \qquad (A\text{-}2)$$

The matrix of the (132) operator has the eigenvalues 1 for A_1 and A_2 as we know from Eq(3.13a) and (3.13b), and the eigenvalues $e^{\pm 2\pi i/3}$ for E-type functions. This matrix can be diagonalized and the transformation matrix contains the coefficients $c^{\Gamma\xi}_{I_{23}}(I_T)$. The basis functions for the eigenvalue 1 can be of

A_1 or A_2 type. From Eq.(3.13a) we must have for the A_1 type functions

$$(23)\quad \chi^{A_1}(I_T) = \chi^{A_1}(I_T)$$

For simplicity we have dropped the index j in the equation above.

Substituting the expansion (3.12) and using Eq (A-1) gives

$$\sum_{I_{23}} (-1)^{I_2+I_3-I_{23}} c^{A_1}_{I_{23}}(I_T)\chi_{I_{23}}(I_T) = \sum_{I_{23}} c^{A_1}_{I_{23}}(I_T)\chi_{I_{23}}(I_T)$$

Taking on both sides the inner product with $\chi_{I'_{23}}(I_T)$ gives

$$(-1)^{I_2+I_3-I'_{23}}\, c^{A_1}_{I'_{23}}(I_T) = c^{A_1}_{I'_{23}}(I_T)$$

So $c^{A_1}_{I'_{23}}(I_T) = 0$ unless I'_{23} is chosen such that $I_2+I_3-I'_{23}$ is even. For the A_2 type basis functions $I_2+I_3-I'_{23}$ must be odd. The E type functions belonging to the eigen value $e^{+2\pi i/3}$ are related via (23) as given in Eq(3.13c). We obtain

$$(23)\chi^{E,1}(I_T) = \chi^{E,2}(I_T)$$

Substituting Eq(3.12) and using Eq(A-1) gives

$$c^{E,1}_{I_{23}}(I_T) = (-1)^{I_2+I_3-I_{23}}\, c^{E,2}_{I_{23}}(I_T) \qquad \text{(A-3)}$$

In case that the multiplicity of an irreducible representation for a given I_T is at most one, the functions are uniquely determined by the desired transformation properties in Eq(3.13). If, however the multiplicity of an irreducible representation is two or more, a unique solution is not possible. The coefficients $c^{\Gamma\xi}_{I_{23}}(I_T)$ for I_Y = 1/2, 1 and 3/2 calculated using the method here are given in Table A.1.

I_Y	I_T	Symmetry	I_{23}	$C^{A_1}_{I_{23}}$	$C^{A_2}_{I_{23}}$	$C^{E,1}_{I_{23}}$	$C^{E,2}_{I_{23}}$
1/2	3/2	A_1	1	1			
	1/2	E	1			$\sqrt{\frac{1}{2}}$	$\sqrt{\frac{1}{2}}$
			0			$-i\sqrt{\frac{1}{2}}$	$+i\sqrt{\frac{1}{2}}$
1	3	A_1	2	1			
	2	E	2			$\sqrt{\frac{1}{2}}$	$\sqrt{\frac{1}{2}}$
			1			$-i\sqrt{\frac{1}{2}}$	$i\sqrt{\frac{1}{2}}$
	1	$A_1 + E$	2	$\frac{2}{3}$		$\frac{1}{3}\sqrt{\frac{5}{2}}$	$\frac{1}{3}\sqrt{\frac{5}{2}}$
			1	0		$i\sqrt{\frac{1}{2}}$	$-i\sqrt{\frac{1}{2}}$
			0	$\frac{\sqrt{5}}{3}$		$-\frac{1}{3}\sqrt{2}$	$\frac{1}{3}\sqrt{2}$
	0	A_2	1		1		
3/2	9/2	A_1	3	1			
	7/2	E	3			$\sqrt{\frac{1}{2}}$	$\sqrt{\frac{1}{2}}$
			2			$-i\sqrt{\frac{1}{2}}$	$i\sqrt{\frac{1}{2}}$
	5/2	$A_1 + E$	3	$\sqrt{\frac{7}{15}}$		$\sqrt{\frac{8}{30}}$	$\sqrt{\frac{8}{30}}$
			2	0		$i\sqrt{\frac{1}{2}}$	$-i\sqrt{\frac{1}{2}}$
			1	$\sqrt{\frac{8}{15}}$		$-\sqrt{\frac{7}{30}}$	$-\sqrt{\frac{7}{30}}$
	3/2	$A_1 + A_2 + E$	3	$-\sqrt{\frac{3}{10}}$	0	$\sqrt{\frac{7}{20}}$	$\sqrt{\frac{7}{20}}$
			2	0	$\sqrt{\frac{5}{6}}$	$-i\sqrt{\frac{1}{12}}$	$i\sqrt{\frac{1}{12}}$
			1	$\sqrt{\frac{7}{10}}$	0	$\sqrt{\frac{3}{20}}$	$\sqrt{\frac{3}{20}}$
			0	0	$-\sqrt{\frac{1}{6}}$	$-i\sqrt{\frac{5}{12}}$	$i\sqrt{\frac{5}{12}}$
	1/2	E	2			$i\sqrt{\frac{1}{2}}$	$-i\sqrt{\frac{1}{2}}$
			1			$\sqrt{\frac{1}{2}}$	$\sqrt{\frac{1}{2}}$

Table A-1. The coefficients $C^{\Gamma\xi}_{\backslash}$ for Y nuclear spin 1/2, 1, 3/2.

APPENDIX II The coupling constants for symmetric tops of the form XY_3 for $I_Y=\frac{1}{2}$.

Coupling constant	Symbol	
Spin-rotation X - nucleus	$C^X_{J_K}$	$\frac{1}{2}(M^X_{aa}+M^X_{bb}) + \frac{K^2}{J(J+1)}[M^X_{cc}-\frac{1}{2}(M^X_{aa}+M^X_{bb})]$
Spin-rotation	$C^Y_{J_K}$	$\frac{1}{2}(M^Y_{aa}+M^Y_{bb})+\frac{K^2}{J(J+1)}[M^Y_{cc}-\frac{1}{2}(M^Y_{aa}+M^Y_{bb})] - \frac{(-1)^{J+Y}}{2}\delta_{K,1}(M^Y_{aa}-M^Y_{bb})$
Spin-spin X - Y	$d^{XY}_{J_K}$	$\frac{\mu_o\mu_N^2 g_X g_Y}{4\pi r^3_{XY}}[(1-\frac{3K^2}{J(J+1)})(1-\frac{3}{2}\sin^2\vartheta_o)+\frac{(-1)^{J+Y}}{2}\delta_{K,1}.3\sin^2\vartheta_o]$
Spin-spin Y - Y	$d^{YY}_{J_K}$	$\frac{\mu_o\mu_N^2 g_Y^2}{8\pi r^3_{YY}}(\frac{3K^2}{J(J+1)}-1)$
Quadrupole moment X	$eqQ^X_{J_K}$	$eqQ^X_{J_K}[1-\frac{3K^2}{J(J+1)}]$
Molecular G-tensor	g_{J_K}	$g_\perp + \frac{K^2}{J(J+1)}(g_\parallel - g_\perp)$
Molecular Susceptibility	χ_{J_K}	$[1-\frac{3K^2}{J(J+1)}]\frac{1}{3}(\chi_\perp-\chi_\parallel)$
Isotropic nucl. Shielding -X	σ^X_{aV}	$\frac{2}{3}\sigma^X_\perp + \frac{1}{3}\sigma^X_\parallel$
Anisotropic nucl. Shielding -X	$\sigma^X_{J_K}$	$[1-\frac{3K^2}{J(J+1)}]\frac{1}{3}(\sigma_\perp-\sigma_\parallel)$
Isotropic nucl. Shielding -Y	σ^Y_{aV}	$\frac{1}{3}(\sigma^Y_{aa}+\sigma^Y_{bb}+\sigma^Y_{cc})$
Anisotropic nucl. Shielding Y	$\sigma^Y_{J_K}$	$[1-\frac{3K^2}{J(J+1)}]\frac{1}{6}(\sigma^Y_{aa}+\sigma^Y_{bb}-2\sigma^Y_{cc})-\frac{(-1)^{J+Y}}{2}\delta_{K,1}(\sigma^Y_{aa}-\sigma^Y_{bb})$

APPENDIX III The rotational hamiltonian in H_2O_2

In the coordinate system of Fig. 3.2 the rotational hamiltonian for hydrogen peroxyde in the notation of Sect. 3.3.1 becomes

$$\mathcal{H}_{rot} = \underline{R}.\underline{\underline{A}}^{eff}.R + F\,P^2 + 2FP\rho_a R_a + V(\alpha) \qquad \text{(A-4)}$$

Hunt et al (HUN 64) apply a transformation of the type

$$P = P' - k(\alpha)R'_a$$

$$\begin{pmatrix} R_a \\ R_b \\ R_c \end{pmatrix} = \begin{pmatrix} 1 & 0 & 0 \\ 0 & \cos u(\alpha) & \sin u(\alpha) \\ 0 & -\sin u(\alpha) & \cos u(\alpha) \end{pmatrix} \begin{pmatrix} R'_a \\ R'_b \\ R'_c \end{pmatrix} \qquad \text{(A-5)}$$

with

$$k(\alpha) = \frac{du\ (\alpha)}{d\alpha} = \rho_a$$

in the present notation. As a result on the new basis the coupling between P and R_a is removed, as can easily be seen by substituting Eq.(A-5) into (A-4).

R E F E R E N C E S

ABR 57 A. Abragam, Suppl. Nuovo Cim. VI, Serie X,3 (1957) 1015

AND 66 C.H. Anderson and N.F. Ramsey, Phys. Rev. 149 (1966) 14

ARR 70 G. Arrighini, M. Maestro and R. Moccia, J. Chem. Phys. 52 (1970) 6411

BAR 73 Barret, private communication

BAR 60 C. Barter, R.G. Meisenheimer and D.P. Stevenson, J. Phys. Chem. 64, (1960) 1312

BEN 57 W.S. Benedict, and E.K. Plyler, Can. J. Phys. 21 (1957) 1235

BEN 73 G.L. Bendazolli, D.G. Lister and P. Palmieri, (1973) 791

BHA 69 P. Bhattacharyya and B. Dailey, J. Chem. Phys. 51 (1969) 3051

BLU 68 H. Bluyssen, Thesis (1968), Katholieke Universiteit Nijmegen

COH 73 E.R. Cohen, and B.N. Taylor, J. Phys. Chem. Ref. Data 2 (1973) 663

CON 27 E.U. Conden, Phys. Rev. 30 (1927) 781

COS 58 C.C. Costain, J. Chem. Phys. 29 (1958) 864

DUB 77 A. Dubrulle, D. Boucher, J. Burie and J. Demaison, Chem. Phys. Lett. 45 (1977) 559

DUN 72 T.H. Dunning, R.M. Pitzer and S. Aung, J. Chem. Phys. 57 (1972) 5044

DUN 75 T.H. Dunning and N.W. Winter, J. Chem. Phys. 63 (1975) 1847

DYM 76 A. Dymanus, Int. Rev. of Science, Spectroscopy, Phys. Chem. Series 2, Vol. 3 ed. D.A. Ramsey (Butterworths, London 1976) 127

EDM 57 A.R. Edmonds, Angular momentum in quantum mechanics, (Princeton University Press, Princeton, New Jersey 1957)

ELL 73 A.W. Ellenbroek, Quarterly Report 37 (1973)

ELL 73a A.W. Ellenbroek, Quarterly Report 41 (1973)

ELL 74 A.W. Ellenbroek, Quarterly Report 43 (1974)

ELL 75 A.W. Ellenbroek, Quarterly Report 48 (1975)

ELL 75a A.W. Ellenbroek, Quarterly Report 47 (1975)

ELL 76 A.W. Ellenbroek, and A. Dymanus, Chem. Phys. Lett. 42 (1976) 303

ELL 76a A.W. Ellenbroek, Quarterly Report 51 (1976)

ESH 52 J.R. Eshbach and M.W.P. Strandberg, Phys. Rev. 85 (1952) 24

FAN 59 U. Fano and G. Racah, Irreducible Tensorial Sets, (Academic Press Inc., New York, 1959)

FLY 64 W.H. Flygare, J. Chem. Phys. 41 (1964) 793

FLY 70 W.H. Flygare and R.C. Benson, Mol. Phys. 20 (1971) 225

FOL 70 T.L. Follett, Thesis (1970), Harvard University, Cambridge Massachusetts

FRI 33 R. Frisch and O. Stern, Z. Phys. 85 (1933) 4

GHO 52 S.N. Ghosh, R. Trambarulo and W. Gordy, J. Chem. Phys. 20 (1952) 605

GIE 72 T.D. Gierke and W.H. Flygare, J. Am. Chem. Soc. 94 (1972) 7277

GOR 54 J.P. Gordon, H.J. Zeiger and C.H. Townes, Phys. Rev. 95 (1954) 282

GOR 55 J.P. Gordon, H.J. Zeiger and C.H. Townes, Phys. Rev. 99 (1955) 1264

GUN 54 G.R. Gunther-Mohr, C.H. Townes and J.H. van Vleck, Phys. Rev. 94 (1954) 1191

HEU 72 J.E.M. Heuvel, Thesis (1972), Katholieke Universiteit Nijmegen, The Netherlands

HIN 68 D. Hindermann and C. Cornwell, J. Chem. Phys. 48 (1968) 4148

HOR 76 G. ter Horst, Quarterly Report 51 (1976)

HOU 72 J.T. Hougen, J. Chem. Phys. 57 (1972) 4207

HUI 66 C. Huiszoon, Thesis (1966), Katholieke Universiteit, Nijmegen, The Netherlands

HUN 64 R.H. Hunt, R.A. Leacock, C.W. Peters and K.T. Hecht, J. Chem. Phys. 42 (1964) 1931

HUT 67 W. Huttner and W.H. Flygare, J. Chem. Phys. 47 (1967) 4137

JEN 48 C.K. Jen, Phys. Rev. 74 (1948) 1396

JUD 63 B.R. Judd, Operator techniques in atomic spectroscopy (McGraw-Hill, New York)

KAL 66 U. Kaldor and I. Shavitt, J. Chem. Phys. 44 (1966) 1823

KUK 67 S.G. Kukolich, Phys. Rev. 156 (1967) 83

KUK 70 S.G. Kukolich and S.C. Wofsy, J. Chem. Phys. 52 (1970) 5477

KUK 70a S.G. Kukolich, Chem. Phys. Lett. 5 (1970) 401

KUK 71 S.G. Kukolich, A.C. Nelson and D.J. Ruben, J. Mol. Spectry 40 (1971) 33

KUK 71a S.G. Kukolich, Chem. Phys. Lett. 12 (1971) 215

KUK 72 S.G. Kukolich and A.C. Nelson, J. Chem. Phys. 56 (1972) 4446

KUK 72a S.G. Kukolich and A.C. Nelson, J. Chem. Phys. 57 (1972) 4052

KUK 72b S.G. Kukolich and D.J. Ruben, J. Mol. Spectry. 44 (1972) 607

KUK 73 S.G. Kukolich and K.H. Casleton, Chem. Phys. Lett. 18 (1973) 408

LAW 72 E.A. Laws, R.M. Stevens and W.N. Lipscomb, J. Chem. Phys. 56 (1972) 2029

LEE 71 F.H. de Leeuw, Thesis (1971) Katholieke Universiteit, Nijmegen, The Netherlands

MAJ 32 E. Majorana, Nuovo Cim. 9 (1932) 43

MEE 74 W.L. Meerts, Quarterly Report 44 (1974)

MEU 76 J.J. ter Meulen, Thesis (1976) Katholieke Universiteit, Nijmegen, The Netherlands

OEL 69 W.C. Oelfke and W. Gordy, J. Chem. Phys. 51 (1969) 5336

OZI 68 I. Ozier, L.M. Crapo and S.S. Lee, Phys. Rev. 172 (1968) 63

OZI 76 I. Ozier, S.S. Lee and N.F. Ramsey, J. Chem. Phys. 65 (1976) 3985

POC 69 J. Pochan, R. Stone and W.H. Flygare, J. Chem. Phys. 51 (1969) 4278

POY 75 R.L. Poynter and R.K. Kakar, Astr. J. Suppl. Series 277 29 (1975) 87

RAM 56 N.F. Ramsey, Molecular Beams (Oxford University Press, London 1956)

REI 76 J.M.L.J. Reinartz, Thesis (1976) Katholieke Universiteit, Nijmegen, The Netherlands

REY 71 J.M.H. Reijnders, Quarterly Report 30 (1971)

REY 72 J.M.H. Reijnders, A.W. Ellenbroek and A. Dymanus, Chem. Phys. Lett. 17 (1972) 351

REY 74 J.M.H. Reijnders, A.W. Ellenbroek and A. Dymanus, Chem. Phys. Lett. 26 (1974) 470

ROT 70 S. Rothenberg and H.F. Schaefer, J. Chem. Phys. 53 (1970) 3014

SAI 65 Y. Saito, Can. J. Chem. 43 (1965) 2530

TIG 70 H.L. Tigelaar and W.H. Flygare, Chem. Phys. Lett. 7 (1970) 254

TOW 55 C.H. Townes and A.H. Schawlow, "Microwave Spectroscopy" McGraw Hill Book Company Inc., New York (1955)

VAN 70 D.L. Vanderhart and W.H. Flygare, Mol. Phys. 18 (1970) 77

VER 69 J.A.Th. Verhoeven, Thesis (1969) Katholieke Universiteit, Nijmegen, The Netherlands

VER 70 J.A.Th. Verhoeven, Quarterly Report 27 (1970)

WIC 33 G.C. Wick, Z. Phys. 85 (1933) 25

WOF 70 S.C. Wofsy, J.S. Muenter and W. Klemperer, J. Chem. Phys. 53 (1970) 4005

WOF 71 S.C. Wofsy, J.S. Muenter and W. Klemperer, J. Chem. Phys. 55 (1971) 2014

YI 68 P.N. Yi, I. Ozier and C.H. Anderson, Phys. Rev. 165 (1968) 92

Samenvatting

In dit proefschrift wordt het Zeeman effect onderzocht aan eenvoudige moleculen, zoals gemeten met behulp van een moleculaire bundel maser. Voor de Zeeman metingen stonden twee magneten ter beschikking: een conventionele electromagneet voor metingen bij lage velden (tot 8.7 kG) en een supergeleidende magneet voor metingen bij hoge velden (tot 70 kG).

Daar de sterke magnetische effecten in de meeste interessante moleculen reeds vrij nauwkeurig bekend waren, was het onderzoek hoofdzakelijk gericht op de zwakke magnetische interacties: de moleculaire magnetische susceptibiliteit en de nucleaire afscherming (shielding). Uit de grote hoeveelheid moleculen kozen we voor 1^{o} de interessante en nog weinig onderzochte groep van symmetrische tollen van het C_{3v}-type (n.l. NH_3, CF_3H en CH_3Cl) 2^{o} de asymmetrische "waterachtige" moleculen D_2O en SO_2, als vervolg op de metingen van Verhoeven, en tenslotte 3^{o} de eenvoudigste interne rotatoren, te weten H_2O_2 en CH_3OH, waarvan tot nu toe magnetisch nog niets bekend was.

De gebruikte machine is wezenlijk dezelfde als die welke gebruikt is door Verhoeven. Als bron is nu een nozzle gebruikt, in een enkel geval is gewerkt met een zogeheten seeded beam. In sommige gevallen bleek het noodzakelijk gebruik te maken van een zogenaamde "scrambler" (klutser) om niet bezette hyperfijne niveau's, welke voor de bepaling van de koppelingsconstanten essentieel zijn, te herbezetten.

In het derde hoofdstuk is een algemene theorie gegeven voor de symmetrisatie van de hyperfijn en Zeeman hamiltonian toepasbaar op elk willekeurig C_{3v}-molecuul van het type XY_3. Tevens zijn de matrix elementen van de diverse interacties in deze hamiltoniaan berekend, uitgedrukt in de koppelingsconstanten.

De frequenties van de lijnen van de gemeten overgangen en de daaruit bepaalde waarden voor de koppelingsconstanten zijn gegeven in hoofdstuk vier. Uit deze koppelingsconstanten kunnen, mits voldoende overgangen gemeten zijn de tensorcomponenten van de betreffende interactie worden berekend.

In het laatste hoofdstuk worden de tensoren bediscussieerd. Uit het moleculair magnetisch moment en de susceptibiliteit kan het moleculair quadrupool moment worden bepaald en uit de spin-rotatie tensor en de totale shielding de diamagnetische shielding. Zowel het moleculair quadrupool moment als de diamagnetische shielding zijn grootheden die door theoretici met behulp van ab-initio methoden kunnen worden berekend uit de electronische golffunctie. Beide grootheden zijn aanmerkelijk gevoeliger voor de electronische golffunctie dan de totale energie van het molecuul en vormen daardoor een betere test voor de betrouwbaarheid van deze functie.

Van de onderzochte moleculen kon steeds de susceptibiliteit gemeten worden. De shielding werd met name onderzocht voor symmetrische tollen. Voor zwaardere kernen (fluor, stikstof, chloor) namen we de shielding waar, maar voor waterstof bleek in de meeste gevallen het effect te klein zelfs bij een magneetveld van 70 kG.

Om alle tensorcomponenten te bepalen is het noodzakelijk dat meer dan één rotatieovergang wordt onderzocht. Voor de meeste van de hier bestudeerde moleculen liggen deze overgangen dikwijls bij hoge frequenties (boven 45 GHz). Toekomstige experimenten zullen zich met name hier op moeten richten.

Curriculum vitae

De schrijver van dit proefschrift werd geboren op 24 november 1948 te Apeldoorn. Hij volgde de middelbare schoolopleiding aan het Veluws College in Apeldoorn en behaalde daar in 1966 het diploma H.B.S.-B.

Hij ging daarna natuurkunde studeren aan de Katholieke Universiteit te Nijmegen. Na het kandidaatsexamen werkte hij 1½ jaar in de groep voor atoom- en molecuulfysica van Prof. A. Dymanus. In 1971 volgde het doctoraal examen in de experimentele natuurkunde.

Daarop begon hij een promotie-onderzoek aan bovengenoemde afdeling ter bestudering van het Zeeman effect in eenvoudige moleculen. De resultaten van dit onderzoek zijn in dit proefschrift gegeven.

STELLINGEN

I

De "Infinite Order Sudden Approximation" zoals deze toegepast wordt voor het berekenen van inelastische botsingsdoorsneden dient getest te worden op toestand selectie effecten.

R.T. Pack, J. Chem. Phys. **60** (1974) 633
L.W. Hunter, J. Chem. Phys. **62** (1975) 2855

II

De afwijking tussen de gemeten en berekende antenne patronen zoals geconstateerd door Matarresse en Evensson berust op een onjuiste interpretatie van het gedrag van de diode.

L.M. Mataresse and K.M. Evensson, Appl. Phys. Lett. **17** (1970) 8
Bor-long T.W.U. and S.F. Schwarz, Appl. Phys. Lett. **26** (1975) 672

III

De voorgestelde oplossing van opg. 5.1 (referentie), nl. dat lorentzlijnbreedten additief zijn, is alleen in zeer speciale gevallen waar.

R. Loudon, "The quantum theory of light" Oxford, Clar. Press (1973)

IV

De bewering van Flygare en Benson dat moleculaire bundel experimenten alleen mogelijk zijn voor kleine moleculen behoeft nadere toelichting.

W.H. Flygare and R.C. Benson, Mol. Physics **20** (1971) 225

V

Het "Motional Stark Effect" van symmetrische tollen in een magneetveld geeft bij absorptie metingen aan $K \neq 0$ toestanden niet alleen aanleiding tot lijnverbreding, zoals beweerd door Norris *et al.*, maar ook tot een frequentieverschuiving.

C.L. Norris, E.F. Pearson and W.H. Flygare, J. Chem. Phys. **60** (1974) 1758

VI

De benadering van Miller om glory quenching te berekenen lijkt eenvoudig uitgebreid te kunnen worden om ook de toestandsafhankelijkheid van de totale anisotropie te berekenen. Hierbij moet de verdeling van standen van de moleculaire as evenwel op het moment van dichtste nadering in rekening gebracht worden.

W.H. Miller, J. Chem. Phys. **50** (1969) 3124

VII

In tegenstelling tot de aanname van Williams hangt het hoek oplossend vermogen in de maser niet alleen af van de geometrie, maar ook van de individuele snelheids- en toestandsafhankelijke moleculaire banen in de focussator.

J.R. Williams and S.G. Kukolich, J. Chem. Phys. **66** (1977) 251
U. Borkenhagen, H. Malthan and J.P. Toennies, Chem. Phys. Lett. **41** (1976) 222

VIII

Het overschot aan ecologen in Nederland kan, gezien het te kort aan ongerepte natuur, beschouwd worden als een vorm van structurele werkeloosheid.

IX

Op het gebied van de toepassing van de zwaartekracht bij de geboorte zijn de primitieve volkeren ons ver vooruit.

Nijmegen, 6 oktober 1977 A.W. Ellenbroek